Department of Physics and Astronomy

University of Heidelberg

Master thesis

in Physics

submitted by

Daniel Jiménez Tejero

born in Madrid

2017

Pseudoscalar Inflation, Baryogenesis and Gravitational Waves

This Master thesis has been carried out by Daniel Jiménez Tejero

at the

Max-Planck-Institut für Kernphysik

under the supervision of

Herrn Prof. Dr. Dr. h.c. Manfred Lindner

Pseudoskalarinflation, Baryogenese und Gravitationswellen

Diese Arbeit beschäftigt sich mit einer Klasse von Inflationsmodellen, in der das Inflaton ϕ ein Pseudoskalar ist und an das Hyperladungseichfeld des Standardmodells durch die Wechselwirkung $\mathcal{L} \supset \phi/\left(4\Lambda\right) F\tilde{F}$ koppelt. Diese Kopplung sorgt für eine explosionartige Erzeugung von Eichfeldern maximal helikaler, also einer Polarisation, was Baryogenese durch dessen Zerfall um den Zeitpunkt der elektroschwachen Symmetriebrechung erlaubt. Außerdem beeinflussen diese Eichfelder das Spektrum der Tensorfluktuationen, so dass der durch Inflation erzeugte stochastische Gravitationswellenhintergrund verstärkt wird. Unsere Arbeit wird hier präsentiert, in der wir die neusten Ergebnissen von Baryogenese durch Hypermagnetfeldzerfall um die elektroschwache Symmetriebrechung auf Pseudoskalarinflation anwenden und die Auswirkungen auf das Gravitationswellenspektrum untersuchen. Es zeigt sich, dass, um Baryogenese erfolgreich zu realisieren, die Kopplungsskala circa $\Lambda \sim 3 \times 10^{17}\,\mathrm{GeV}$ betragen muss. Da dies einer kleinen Kopplung entspricht, ist die Eichfeldproduktion bis zum Ende der Inflation nicht relevant, was wiederum zum Folge hat, dass das Gravitationswellenspektrum ein Maximum bei hohen Frequenzen rund um 1 MHz oder höher aufweist. Innerhalb des betrachteten theoretischen Modells ist ein messbares Gravitationswellensignal nur auf Kosten einer Baryonüberproduktion zu erzielen, was nur durch eine Wiedererwärmungstemperatur des Universums unterhalb der elektroschwachen Skala zu erzielen wäre.

Pseudoscalar Inflation, Baryogenesis and Gravitational Waves

In this work we focus on a particular family of inflationary models, pseudoscalar inflation, in which the inflaton ϕ couples to the Standard Model hypercharge gauge field via an anomalous interaction term, $\mathcal{L} \supset \phi/\left(4\Lambda\right) F\tilde{F}$. This coupling results in an explosive production of gauge fields during inflation. These fields are maximally helical, which allows for baryogenesis via decaying hypermagenetic fields at the time of the electroweak crossover. Moreover, the gauge fields backreact on the inflationary dynamics, sourcing tensor perturbations and thereby enhancing the spectrum of the stochastic gravitational wave background coming from inflation. Our latest work is collected here, where we update the study of baryogenesis via decaying hypermagenetic fields produced during inflation and investigate the implication of this on the gravitational wave background. We work in the instant reheating approximation and find that, for successful baryogenesis, the coupling must be weak, with about $\Lambda \sim 3 \times 10^{17}\,\mathrm{GeV}$. The production of gauge fields is therefore only relevant towards the end of inflation, resulting in a peak at high frequencies in the MHz range or above in the gravitational wave spectrum, out of reach of current detectors. A detectable gravitational wave signal at ongoing experiments implies an overproduction of baryon number with this theoretical set up, unless the reheating temperature of the universe is higher than the electroweak scale.

Contents

This work is based on [1].

x

Part I

Foundations

The Big Bang theory is a very successful theory of the formation and evolution of the observable universe as we know it. There are however a few pieces of evidence that cannot be explained by this theory. Inflation comes in as a way of solving some of these mismatches, such as the horizon problem or the flatness problem. In this master thesis, a particular family of models of inflation is investigated, with special focus on the resolution of yet another problem: the baryon asymmetry of the universe. This model presents a minimal way of solving a few cosmological problems at once just by coupling the inflaton field to the U(1) gauge field of the Standard Model.

For this study it will be enough to represent the four forces of nature we know via a minimal coupling of matter to gravity. Matter and its interactions are up to this date best described by the Standard Model (SM) of particle physics. Albeit it is known to be incomplete, is a very successful theory exceptionally describing nature so far, and we take advantage of the tools and principles of which the SM makes use, that is quantum field theory. Gravity on the other hand arises as a consequence of a curved geometry of spacetime, as formulated in General Relativity.

This can be all put together in the context of field theory into one action

$$S = S_{\mathrm{EH}} + S_{\mathrm{matter}} \,, \tag{1}$$

S_{EH} being the Einstein-Hilbert action, responsible for the curvature contributions to the dynamics, and S_{matter} meaning to contain the relevant matter contributions to the universe's dynamics. The action S in (1) contains all the physics and we will make use of the principle of least action to extract it.

This first part will take care of introducing the different terms and conventions used in this work. Chapter 1 takes care of giving an overview of the implications of equation (1), with special attention on the Einstein-Hilbert action S_{EH}; it also gives an insight to the horizon and flatness problems of the conventional Big Bang theory. Chapter 2 motivates the paradigm of inflation, giving a particular value to S_{matter}, and introduces pseudoscalar inflation, i.e. a minimal extension of the standard slow-roll inflation. Chapter 3 then closes this introductory part with a general view of baryogenesis.

Chapter 1

Cosmology

The universe is a complex system formed of complex objects, each of which undergoes its own reactions and processes. But as we zoom out and start averaging small individual objects with their neighbours and observing everything as a whole, it becomes more and more simple. As we zoom out stars get lost in their host galaxies. Zoom out further and galaxies' size and shapes then start losing their importance and just become one more of the components of a cluster. Go to further scales and clusters start difuminating as well within superclusters. In the end the distribution of these objects as a whole seems to be independent of from where and in which direction you look. The universe becomes homogeneous and isotropic. This is a pillar of modern cosmology.

1.1 Coordinates

In order to treat the evolution of the universe as a whole throughout its history, we first need to know its geometry. General relativity is a geometrical theory in which spacetime is nothing but a Lorentzian manifold characterised by its metric tensor. The most general isotropic (and thus homogeneous) metric is the famous Friedman-Lemaître-Robertson-Walker (FLRW) metric (see e.g. [2]), whose components are given by the line element

$$\mathrm{d}s^2 = g_{\mu\nu}\mathrm{d}x^\mu\mathrm{d}x^\nu = -c^2\mathrm{d}t^2 + a^2(t)\mathrm{d}\boldsymbol{r}^2 = -c^2\mathrm{d}t^2 + a^2(t)\left[\frac{\mathrm{d}r^2}{1 - Kr^2} + r^2\mathrm{d}\Omega^2\right]. \quad (1.1)$$

Here, we used spherical coordinates with the usual solid angle element $\mathrm{d}\Omega^2 = \mathrm{d}\theta^2 + \sin^2\theta\,\mathrm{d}\varphi^2$ and the radial coordinate r; c is the speed of light in vacuum.

This metric consists of a static spatial geometry multiplied by a dimensionless, non-negative, time-dependent factor $a(t)$ called *scale factor*. The constant K can take one of three values which defines the curvature of the spatial hypersurfaces: $K = 0$ corresponds to a spatially flat (Euclidean) spacetime, $K = +1$ to a positive

spatial curvature and therefore closed universe (with necessarily finite volume), and $K = -1$ to a negatively-curved 3-geometries and consequently open universe. We keep it mostly general for the remaining of this chapter. From chapter 2 on, however, we mostly limit ourselves to the case $K = 0$ which most faithfully describes our universe[1].

To simplify the metric component g_{rr} and to facilitate the study of light propagation (causality), it is common to transform coordinates

$$\mathrm{d}r \to \mathrm{d}\chi \equiv \frac{\mathrm{d}r}{\sqrt{1 - Kr^2}} \tag{1.2}$$

such that

$$\left[\frac{\mathrm{d}r^2}{1 - Kr^2} + r^2 \mathrm{d}\Omega^2 \right] \to \left[\mathrm{d}\chi^2 + \Sigma_K(\chi) \, \mathrm{d}\Omega^2 \right] \tag{1.3}$$

with

$$r^2 = \Sigma_K(\chi) = \begin{cases} \sinh^2 \chi & K = -1 \\ \chi^2 & K = 0 \\ \sin^2 \chi & K = +1 \,. \end{cases} \tag{1.4}$$

Another common change of coordinates affects the time coordinate

$$\mathrm{d}t \to \mathrm{d}\tau \equiv \frac{\mathrm{d}t}{a(t)} \,, \tag{1.5}$$

defining the *conformal time* τ. This allows us to write the FLRW in a neat (and convenient) form

$$\mathrm{d}s^2 = a^2(\tau) \left(-c^2 \mathrm{d}\tau^2 + \mathrm{d}\chi^2 + \Sigma_K(\chi) \, \mathrm{d}\Omega^2 \right) \,. \tag{1.6}$$

Note that for the case of flat 3-geometries $K = 0$ the metric in this form is conformal to that of Minkowski space. This makes the study of light propagation easier.

1.2   Causal structure of the universe

Light propagation is best studied with the two-dimensional line element

$$\mathrm{d}\tilde{s}^2 = a(\tau) \left(-c^2 \mathrm{d}\tau^2 + \mathrm{d}\chi^2 \right) \tag{1.7}$$

since we are interested in the propagation in the radial direction. Photons travel on null geodesics, that is, trajectories such that $\mathrm{d}\tilde{s}^2 = 0$, which is satisfied as long as

$$\mathrm{d}\chi = c \, \mathrm{d}\tau = \frac{c \, \mathrm{d}t}{a(t)} \,. \tag{1.8}$$

---

[1]The latest experimental results from Planck measuremtnes of the cosmic microwave background (CMB) temperature anisotropies, CMB polarisation, CMB lensing, combined with baryon accoustic oscilations (BAO) measurements, give the constraint $|\Omega_K| < 0.005$ with 95% CL [3]; see eqn. (1.59).

For a given point in spacetime, i.e. an event, it is interesting to find what past events have been in causal contact with it and which future events will potentially be affected by it. That is, what events fall inside the past and future light-cones. For defining the past light-cone, we integrate eqn. (1.8) from a certain "initial" time t_{ini} (or τ_{ini}) to the time coordinate of the event t (or τ),

$$\chi_{\text{PH}}(\tau) = \int_{\tau_{\text{ini}}}^{\tau} c\, \mathrm{d}\tau = c\,(\tau - \tau_{\text{ini}}) = \int_{t_{\text{ini}}}^{t} \frac{c\, \mathrm{d}t}{a(t)} = \int_{a_{\text{ini}}}^{a} \frac{c\, \mathrm{d}a}{\dot{a}\, a} = \int_{\ln a_{\text{ini}}}^{\ln a} c\,(aH)^{-1}\, \mathrm{d}\ln a \quad (1.9)$$

which defines the *particle horizon* χ_{PH}. We introduced the Hubble parameter $H(t) \equiv \dot{a}(t)/a(t)$ and the shorthand notation $\dot{} \equiv \mathrm{d}/\mathrm{d}t$ for the time derivative. Only events at a comoving distance $\chi \leq \chi_{\text{PH}}$ fall inside the past light-cone and can exchange information. For the future light-cone, we analogously define the event horizon

$$\chi_{\text{EH}}(\tau) = \int_{\tau}^{\tau_{\text{max}}} c\, \mathrm{d}\tau = c\,(\tau_{\text{max}} - \tau) \quad (1.10)$$

by integrating from the time of the event τ to a "maximum" conformal time τ_{max} in the far future which could be finite or infinite (the end of the universe so to say). Observers at $\chi > \chi_{\text{EH}}(\tau)$ will never receive a signal sent at τ.

Hubble Law

Another quantity relevant to causality in cosmology is the *Hubble radius* or *Hubble length*. Think of a physical radial distance d (e.g., the distance between two galaxy superclusters, or from us to a far enough galaxy) at a given time t. It is given by the radial line element $\mathrm{d}l = g_{\chi\chi}\mathrm{d}\chi^2$,

$$d(t) = \int \mathrm{d}\chi \sqrt{g_{\chi\chi}} = a(t)\,\chi\,. \quad (1.11)$$

The expansion rate of that distance, or, in other words, the relative speed of the two objects separated by d is then given by the Hubble law

$$\dot{d}(t) = \dot{a}(t)\,\chi = H(t)\,d(t)\,. \quad (1.12)$$

This speed is an expansion speed and it does not involve any information transmission, that is to say it can easily bigger than the speed of light if, e.g., the distance is big enough. This condition is given by

$$\dot{d}(t) > c \quad \Rightarrow \quad d(t) > \frac{c}{H(t)} \quad \Leftrightarrow \quad \chi > \frac{c}{a(t)H(t)} \equiv \chi_{\text{H}}(t)\,. \quad (1.13)$$

We therefore define $c\,(aH)^{-1}\ [cH^{-1}]$ as the comoving [physical] Hubble radius at a given time t. Given an observer, the light emitted from a distance greater than the Hubble radius is slower than the expansion itself and thus never reaches the observer. Therefore, we talk about a *Hubble sphere* of the size of the Hubble radius, which defines the observable universe.

The main difference between the particle horizon $\chi_{\mathrm{PH}}(t)$ and the Hubble radius $\chi_{\mathrm{H}}(t)$ is that the particle horizon defines a comoving distance out of which an event would *never* reach the observer (placed at some coordinates $(t, \boldsymbol{x})$), while the Hubble radius defines the causally-connected region around the observer at any given moment t. In more practical terms, consider two events separated by a comoving distance χ:

- $\chi > \chi_{\mathrm{PH}}$ means they *never* were in causal contact,

- $\chi > \chi_{\mathrm{H}}$ means they are not in causal contact *now*.

Note, however, that in the context of inflation (see chapter 2) it is common to refer to the Hubble sphere as horizon.

In the following, we derive some expression for $a(t)$, such that we can compute χ_{PH}. From now on we switch to natural units such that $c = 1 = \hbar$, while explicitly keeping track of mass dimensions using the reduced Planck mass $M_{\mathrm{Pl}} = 4.341 \times 10^{-9}\,\mathrm{kg} = 2.435 \times 10^{18}\,\mathrm{GeV}$ (see next paragraph for its definition).

1.3   The action

Retrieving equation (1) we look further into its different elements

$$S = S_{\mathrm{EH}} + S_{\mathrm{matter}} = \int \mathrm{d}^4 x \sqrt{-g} \left\{ \frac{M_{\mathrm{Pl}}^2}{2} R + \mathcal{L}_{\mathrm{matter}} \right\}. \tag{1.14}$$

We will define the different symbols below but let us first have a look at the equation itself. It tells us that matter is coupled to gravity by the explicit product $\sqrt{-g}\,\mathcal{L}_{\mathrm{matter}}$, and that geometry couples to itself in a similar way $\sqrt{-g}\,R$ (R is nothing but a collection of first and second derivatives of the metric components $g_{\mu\nu}$) with a coupling constant characterised by the reduced Planck mass $M_{\mathrm{Pl}}^2 = \hbar c/(8\pi G)$ which is just a rescaling of the universal constant of gravity G. When computing the equations of motion of the different fields (geometry and matter fields) upon applying the principle of least action we will see how all the different terms affect the dynamics of each other.

Now, let us define the different symbols.

- $g \equiv \det g_{\mu\nu}$ is a short-hand notation for the determinant of the metric. For example, in the case of the metric in eqn. (1.1), $g = -a^6$.

- R is the Ricci scalar, defined as the contraction of the two indices of the Ricci tensor $R_{\mu\nu}$

$$R = \sum_{\alpha} R^{\alpha}{}_{\alpha} \equiv R^{\alpha}{}_{\alpha} = g^{\alpha\beta} R_{\beta\alpha} \tag{1.15}$$

$$R_{\mu\nu} = \partial_{\alpha} \Gamma^{\alpha}{}_{\mu\nu} - \partial_{\nu} \Gamma^{\alpha}{}_{\mu\alpha} + \Gamma^{\alpha}{}_{\beta\alpha} \Gamma^{\beta}{}_{\mu\nu} - \Gamma^{\alpha}{}_{\beta\nu} \Gamma^{\beta}{}_{\mu\alpha} \tag{1.16}$$

being $\Gamma^\mu{}_{\nu\sigma}$ the Christoffel symbols

$$\Gamma^\mu{}_{\nu\sigma} = \frac{1}{2}\, g^{\mu\alpha}\big(\partial_\sigma g_{\alpha\nu} + \partial_\nu g_{\alpha\sigma} - \partial_\alpha g_{\nu\sigma}\big)\,. \tag{1.17}$$

Note that we use Einstein summation convention, that $\partial_\mu \equiv \frac{\partial}{\partial x^\mu}$ and that $g^{\mu\nu}$ are the components of the inverse of the metric such that $g_{\mu\alpha}g^{\alpha\nu} = \delta_\mu^\nu$ (where $\delta_\mu^\nu = 1$ if $\mu = \nu$, and 0 otherwise, is the Kronecker delta).

- Finally, the Lagrangian density $\mathcal{L}_{\text{matter}} = \mathcal{L}_{\text{matter}}(\Phi_i)$ refers to the matter contribution to the evolution of the universe. Φ_i is just a generic representation of the N_{fields} matter fields, with $i = 1, \ldots, N_{\text{fields}}$. In different stages it is dominated by some certain species such as photons (radiation) during the most part of the conventional Big Bang cosmology; the rest of the matter components are then neglected. In this chapter we only make a general approach assuming only that the universe can be treated as a perfect fluid, that is a fluid with no shear stress, viscosity nor heat conduction. In the next chapter we will give it a definite form for the period of inflation.

1.4 Principle of least action

A system evolves accordingly such that the action is minimised. This is mathematically summarised as

$$\delta S = 0 \tag{1.18}$$

or, in more detail,

$$\frac{M_{\text{Pl}}^2}{2}\int \mathrm{d}^4 x\, \delta[(-g)^{1/2}R] + \int \mathrm{d}^4 x\, \delta[(-g)^{1/2}\mathcal{L}_{\text{matter}}] = 0\,. \tag{1.19}$$

Since we are interested in the dynamics inferred by geometry, in this section we focus on the variation of the action with respect to the metric components $g_{\mu\nu}$. For the dynamics of a given field Φ_i, i.e., for its equations of motion, we need to perform the variation w.r.t. Φ_i. Now, on one hand, the variation of the geometry term can be written as

$$\delta[(-g)^{1/2}R] = \big(\delta(-g)^{1/2}\big)R + (-g)^{1/2}\big(\delta g^{\mu\nu}\big)R_{\mu\nu} + (-g)^{1/2}g^{\mu\nu}\big(\delta R_{\mu\nu}\big)$$
$$= (-g)^{1/2}\left(-\frac{1}{2}\,R\,g_{\mu\nu} + R_{\mu\nu}\right)\delta g^{\mu\nu} + (-g)^{1/2}g^{\mu\nu}\big(\delta R_{\mu\nu}\big) \tag{1.20}$$

using the identity $\delta g = -g\, g_{\mu\nu}\, \delta g^{\mu\nu}$, coming from the derivative of the determinant. For a Riemannian geometry, for which equation (1.17) holds, the term proportional to $\delta R_{\mu\nu}$ gives no contribution to δS_{EH} [4]. On the other hand, the variation of the matter Lagrangian turns to be

$$\delta[(-g)^{1/2}\mathcal{L}] = \left(-\frac{1}{2}(-g)^{1/2}g_{\mu\nu}\mathcal{L} + (-g)^{1/2}\frac{\partial \mathcal{L}}{\partial g^{\mu\nu}}\right)\delta g^{\mu\nu} \tag{1.21}$$

assuming that $\mathcal{L}$ contains only the metric components $g_{\mu\nu}$ themselves and no derivatives of those. We drop the subscript 'matter' for brevity.

This allows us to write eqn. (1.19) as

$$\int \mathrm{d}^4 x \, (-g)^{1/2} \left\{ \frac{M_{\mathrm{Pl}}^2}{2} \left(R_{\mu\nu} - \frac{1}{2} \, R \, g_{\mu\nu} \right) - \frac{1}{2} g_{\mu\nu} \mathcal{L} + \frac{\partial \mathcal{L}}{\partial g^{\mu\nu}} \right\} \delta g^{\mu\nu} = 0 \qquad (1.22)$$

which must hold for all $\delta g^{\mu\nu}$, hence

$$R_{\mu\nu} - \frac{1}{2} \, R \, g_{\mu\nu} = \frac{1}{M_{\mathrm{Pl}}^2} \left(g_{\mu\nu} \mathcal{L} - 2 \frac{\partial \mathcal{L}}{\partial g^{\mu\nu}} \right) \qquad (1.23)$$

or, equivalently,

$$G_{\mu\nu} = \frac{1}{M_{\mathrm{Pl}}^2} \, T_{\mu\nu} \qquad (1.24)$$

where we defined the Einstein $G_{\mu\nu}$ and energy-momentum $T_{\mu\nu}$ tensors. Equations (1.24) are the so-called *Einstein field equations* which describe the non-trivial interactions between geometry and matter. Note that for each tensor component $\{\mu, \nu\}$ we obtain an equation. Of all the ten differential equations in (1.24) (both tensors are symmetric, by definition), only up to six are independent in the most general case once a coordinate system $\{x^\mu\}$ is chosen.

1.5   Energy-momentum tensor

In order to be able to write the energy-momentum tensor components we first need to choose a frame of reference (observer). In the perfect fluid approximation, the energy-momentum tensor can be fully described by its proper energy density ρ and its pressure p in the fluid's rest frame

$$T_{\mu\nu} = \rho \, u_\mu u_\nu + p \left(g_{\mu\nu} + u_\mu u_\nu \right) \qquad (1.25)$$

where $u_\mu = g_{\mu\nu} u^\nu$ is the four-velocity of a given observer, which must satisfy $g_{\alpha\beta} u^\alpha u^\beta = u_\alpha u^\alpha = -1$. We choose an observer comoving with the fluid such that $u^i = 0$. The value of u^0 is given by the metric component g_{00}, according the normalisation condition of u^μ, i.e. $u^0 = \pm(-g_{00})^{-1/2}$. We choose the positive solution. It can be brought to the the convenient form $T^\mu{}_\nu = g^{\mu\alpha} T_{\alpha\nu}$, for which for any metric $g_{\mu\nu}$ its non-zero components are

$$T^0{}_0 = -\rho \qquad \text{and} \qquad T^i{}_j = p \, \delta^i_j \,. \qquad (1.26)$$

In this form, the energy-moment tensor of a perfect fluid is diagonal and independent of the metric.

This parametrisation of $T_{\mu\nu}$ allows us to study the dynamics of the universe without giving any particular form to the Lagrangian $\mathcal{L}$. As soon as we have it in terms of the matter fields Φ_i, we will be able to derive ρ and p in terms of Φ_i and, through

Einstein field equations (1.24), relate geometry and matter fields and study the combined dynamics in that particular case. For the rest of this chapter we will forget about the Lagrangian $\mathcal{L}$ and the fields Φ_i, and work exclusively with energy density ρ and pressure p.

Furthermore, we can think of the universe as composed of different species, each of which have their density ρ_i and pressure p_i, related through an *equation of state*

$$p_i = w_i \, \rho_i \,, \tag{1.27}$$

where in general the equation of state parameter w_i is considered to be constant. In general we assume the interaction among different species to be negligible and treat the dynamics of each individually. This is actually true for most of the evolution of the universe except for the period around matter-radiation equality, moment in which the energy contribution of matter and radiation is of the same order. With this picture $\rho = \sum_i \rho_i$ ($p = \sum_i p_i$) is the total *background* energy density (pressure) of the universe.

1.6 Friedman equations

Now, it is time to derive the dynamical equations describing the evolution of the geometry of the universe. If we plug in the metric (1.1) into the definition of the Einstein tensor $G_{\mu\nu}$ we find[2]

$$G^0{}_0 = -3 \left[\left(\frac{\dot{a}}{a} \right)^2 + \frac{K}{a^2} \right] \tag{1.28}$$

$$G^i{}_j = - \left[2 \, \frac{\ddot{a}}{a} + \left(\frac{\dot{a}}{a} \right)^2 + \frac{K}{a^2} \right] \delta^i_j \tag{1.29}$$

while all other components vanish. We see that as well as with $T^\mu{}_\nu$, this tensor consists of essentially two independent components. This is due to the symmetry of the metric because of the imposed homogeneity and isotropy in space. Thus, the Einstein field equations (1.24) give in this case only two independent equations. These are the *Friedman equations*:

$$\left(\frac{\dot{a}}{a} \right)^2 = H^2 = \frac{1}{3M_{\text{Pl}}^2} \rho - \frac{K}{a^2} \,, \tag{1.30}$$

$$\frac{\ddot{a}}{a} = \dot{H} + H^2 = -\frac{1}{6M_{\text{Pl}}^2} \left(\rho + 3p \right) . \tag{1.31}$$

Combining (1.31) with (1.30), one obtains the continuity equation

$$\dot{\rho} + 3H(\rho + p) = 0 \,, \tag{1.32}$$

---

[2]We used $G^\mu{}_\nu = g^{\mu\alpha} G_{\alpha\nu}$ to make the expressions simpler; $G_{\mu\nu} = M_{\text{Pl}}^{-2} \, T_{\mu\nu}$ and $G^\mu{}_\nu = M_{\text{Pl}}^{-2} \, T^\mu{}_\nu$ are of course completely equivalent.

which must hold component-wise as well

$$\dot{\rho}_i + 3H(\rho_i + p_i) = \dot{\rho}_i + 3\,\frac{\dot{a}}{a}\,\rho_i\,(1 + w_i) = 0\,, \tag{1.33}$$

since it also follows from the energy-momentum conservation

$$\nabla_\mu\,T^\mu{}_\nu = \sum_i \nabla_\mu\,T^{(i)\mu}{}_\nu = 0\,, \qquad \text{with} \quad \nabla_\mu\,T^{(i)\mu}{}_\nu = 0\,. \tag{1.34}$$

Together with the fact that $\nabla_\mu G^\mu{}_\nu = 0$, we see that the continuity equation (1.32) already drops from the Einstein field equations (1.24). Here ∇_μ denotes the covariant derivative on the FLRW manifold, which applied on a scalar is just the coordinate derivative, $\nabla_\mu\varphi \equiv \partial_\mu\varphi$, but applied on tensors the curvature sneaks in in the form of Christoffel symbols

$$\nabla_\mu S^{\nu\rho\cdots}{}_{\sigma\cdots} = \partial_\mu S^{\nu\rho\cdots}{}_{\sigma\cdots} + S^{\alpha\rho\cdots}{}_{\sigma\cdots}\Gamma^\nu{}_{\alpha\mu} + S^{\nu\alpha\cdots}{}_{\sigma\cdots}\Gamma^\rho{}_{\alpha\mu} + \ldots - S^{\nu\rho\cdots}{}_{\alpha\cdots}\Gamma^\alpha{}_{\sigma\mu} - \ldots \tag{1.35}$$

Solving equation (1.33) we find a relation between the background energy density and the scale factor

$$\rho_i(a) = \text{const.} \times a^{-3(1+w_i)}\,. \tag{1.36}$$

1.7   Thermodynamics of an expanding universe

Let us have an overview of the thermal evolution of the energy density (and, indirectly, of the pressure) throughout the expansion of the universe. If the expansion of the universe is slow enough, the different components of the universe (particles) can settle close to local thermal equilibrium. Since the universe is homogeneous, local is also global. This allows us to use statistical mechanics and describe the universe as a whole (macroscopic universe) in terms of the particle behaviour (microscopic universe). In this section we tune again our units such that the Boltzmann constant is set to one, $k_{\mathrm{B}} = 1$, and thus temperature is given in units of energy.

We can imagine the universe as a thermal plasma or thermal bath at a temperature T, composed of different particles with a given mass m_i. As the universe expands it cools down, and some reactions stop having place since the reaction rate decreases as temperature drops such that it becomes of a comparable size of the expansion rate $\sim H$. Particles do not encounter each other any more and so reactions among them shut down. When this happens to a certain species and interactions with the thermal bath cease, we say the species is *decoupled*. They will therefore have a different temperature $T_i \neq T$, while coupled species have $T_i = T$ (and $T \equiv T_\gamma$ since photons are the dominant species).

If $m_i \gg T_i$ the particles are non-relativistic, which in cosmology is usually called *matter*. Both baryonic matter (in late times) and dark matter fall into this category. Their energy density is simply given by the number of particles N_i, their mass m_i and

the (proper) volume they occupy V. From these three quantities, only the volume changes with the expansion as $V \propto a^3$.

$$\rho_{\rm m} = \sum_{\text{non-rel}} \rho_i = \sum_{\text{non-rel}} \frac{m_i N_i}{V} \equiv \sum_{\text{non-rel}} m_i n_i \qquad \text{with} \quad \rho_i \propto a^{-3}, \tag{1.37}$$

where we defined the number density of the i-th species, n_i ($\propto a^{-3}$). Note that since they share the same volume V, and N_i and m_i do not change with expansion, also the total energy density $\rho_{\rm m}$ scales as a^{-3}

$$\rho_{\rm m} = \frac{1}{V} \sum_{\text{non-rel}} m_i N_i \propto a^{-3}. \tag{1.38}$$

Comparing this to eqn. (1.36), we find

$$p_{\rm m} = \sum_{\text{non-rel}} p_i = 0 \qquad \left(w_i^{\text{non-rel}} = 0 = w_{\rm m}\right). \tag{1.39}$$

If $m_i \ll T_i$ then we deal with ultra-relativistic particles, which one refers to as *radiation* in cosmology. As a first approximation, let us make a rough estimate to find out the equation of state parameter. For simplicity, consider N_γ photons, each with an energy $\hbar\omega$, again, in a proper volume V. This time also the frequency ω is redshifted by expansion by $\omega \propto a^{-1}$, such that, ignoring all interactions with other particles,

$$\rho_\gamma \sim \frac{N_\gamma \hbar\omega}{V} \sim n_\gamma \hbar\omega \propto a^{-4}. \tag{1.40}$$

This provides together with eqn. (1.36) the equation of state for photons, which holds for any relativistic species too[3],

$$p_\gamma = \frac{1}{3} \rho_\gamma \qquad \left(w_\gamma = \frac{1}{3}\right). \tag{1.41}$$

Yet all species with $m_i \ll T_i$ contribute to the radiation energy density at a given T, each in a particular way. In a more quantitative study using statistical mechanics one finds[4]

$$\rho_{\rm r} = \sum_{\text{rel}} \rho_i = \frac{\pi^2}{30} g_*(T) T^4. \tag{1.42}$$

$g_*(T)$ is the *effective number of relativistic degrees of freedom* at a given temperatrue T and is nothing but precisely a count of species that participate in $\rho_{\rm r}$, weighted with their internal degrees of freedom (DOFs) g_i (and their temperature T_i relative to that of the thermal plasma $T \equiv T_\gamma$, in case they are decoupled)

$$g_*(T) = \sum_{\text{bosons}} g_i \left(\frac{T_i}{T}\right)^4 + \frac{7}{8} \sum_{\text{fermions}} g_i \left(\frac{T_i}{T}\right)^4. \tag{1.43}$$

---

[3]See e.g. equation (3.2.43) in [2] and the discussion therein.
[4]See e.g. equation (3.2.54) in [2] and the discussion therein.

At $T \gtrsim 100\,\text{GeV}$ all particles in the Standard Model are relativistic:

$$g_*^{\text{TOT}} = (1 + 3 + 8) \times 2 + 4 + \frac{7}{8} \times 2 \times 3 \times (3 \times 2 \times 2 + 2 + 1) = \frac{427}{4} = 106.75\,. \quad (1.44)$$

This corresponds to the unbroken phase, i.e., before the electroweak symmetry breaking (EWSB), when all vector bosons B_Y, W^a, G^a are massless and therefore have $g = 2$ internal DOFs, and the Higgs boson is still a doublet with four scalar DOFs $g = 4$. We do not include right-handed neutrinos in the SM. Today, on the other hand, only photons are relativistic[5]

$$g_*(T_0) \equiv g_*^0 = 2\,. \quad (1.46)$$

The subscript $_0$ (or superscript ^{0}) denotes quantities evaluated today (at $t = t_0$).

Another thermodynamic quantity of interest to track the evolution of the universe is the entropy density $s \equiv S/V$. As stated by the second law of thermodynamics, the total entropy of the universe S either increases or stays constant $\mathrm{d}S \geq 0$, with $\mathrm{d}S = 0$ corresponding to equilibrium. The entropy is dominated by the thermal bath of relativistic particles, since photons are much more numerous than baryons. All processes out of equilibrium induce a negligible change to the total entropy S, such that the expansion of the universe can be considered adiabatic to a good approximation. This translates to

$$S = \text{const.} \quad \Rightarrow \quad s \propto a^{-3} \quad (1.47)$$

during the *whole* evolution of the universe. Moreover, from the second law of thermodynamics

$$s = \frac{\rho + p}{T} = \sum_{\text{rel}} \frac{\rho_i + p_i}{T_i} = \frac{4}{3} \sum_{\text{rel}} \frac{\rho_i}{T_i} = \frac{2\pi^2}{45}\, g_{*S}(T)\, T^3 \quad (1.48)$$

with

$$g_{*S}(T) = \sum_{\text{bosons}} g_i \left(\frac{T_i}{T}\right)^3 + \frac{7}{8} \sum_{\text{fermions}} g_i \left(\frac{T_i}{T}\right)^3 \quad (1.49)$$

defined as the *effective number of relativistic degrees of freedom contributing to the entropy*. This shows that for the entire course of evolution of the universe,

$$g_{*S}(T)\, a^3\, T^3 = \text{const.}\,, \quad (1.50)$$

is required by conservation of entropy. This is a key result in cosmology, essential to relate temperature and scale factors at different times.

---

[5]It is possible that one of the neutrinos is still relativistic today, which together with the photon would provide

$$g_*^0 = 2 + \frac{7}{8}\,(2 \times 1) \left(\frac{T_{\nu 0}}{T_0}\right)^4 = 2 + \frac{7}{8} \times 2 \times \left(\frac{4}{11}\right)^{4/3} \simeq 2.45 \quad (1.45)$$

(see below for the computation of T_ν/T_γ). However, for simplicity, we consider all neutrinos relativistic today.

Again for $T \gtrsim 100\,\text{GeV}$, the Standard Model yields

$$g_{*S}^{\text{TOT}} = g_*^{\text{TOT}} = 106.75 \,, \tag{1.51}$$

and for today

$$g_{*S}^0 = 2 + \frac{7}{8} \times 2 \times N_{\text{eff}} \times \frac{4}{11} = \frac{43}{11} \simeq 3.94 \,. \tag{1.52}$$

Here, the neutrinos contributed[6] as a decoupled species to g_{*S}^0 with a temperature $T_{\nu 0}$ different from the thermal bath (today only photons). We also replaced the 3 relativistic neutrinos by an effective $N_{\text{eff}} = 3.046$ given by the Standard Model, which takes into account the fact that neutrino decoupling is not instantaneous.

At around $T \sim 1\,\text{MeV}$ the rate of the weak interactions that kept neutrinos in thermal equilibrium with the plasma drops below the Hubble rate and neutrinos decoupled. T_ν decreases parallel to T_γ until electron-positron annihilation at around $T_\gamma \sim m_e \sim 0.5\,\text{MeV}$, when the thermal production of electrons and positrons stops and their annihilation transfers all their energy into that of the photons, putting the decline of T_γ on hold briefly, and effectively lowering T_ν relative to T_γ.

Now, let us compute some numbers. In this process, the effective number of degrees of freedom in entropy of the thermal bath of coupled species changed

$$\text{from} \quad g_{*S} = 2 + \frac{7}{8} \times 2 \times 2 = \frac{11}{2} \quad \text{at } T \gtrsim m_e \qquad \text{to} \quad g_{*S} = 2 \quad \text{at } T < m_e \,.$$

According to eqn. (1.50)[7] this implies an increase of aT_γ overall

$$\left(aT_\gamma\right)_{T<m_e} = \left(\frac{11/2}{2}\right)^{1/3} \left(aT_\gamma\right)_{T \gtrsim m_e} \tag{1.53}$$

while aT_ν remains constant—the entropy of neutrinos is also conserved $a^3 s_\nu = \text{const.}$ Additionally, the gas of neutrinos and that of photons went through the same evolution up to this point, hence $T_\nu = \left(T_\gamma\right)_{T \gtrsim m_e}$. Consequently,

$$\left(\frac{4}{11}\right)^{1/3} \left(aT_\gamma\right)_{T<m_e} = \left(aT_\gamma\right)_{T \gtrsim m_e} = \left(aT_\nu\right)_{T \gtrsim m_e} = \left(aT_\nu\right)_{T<m_e} \,, \tag{1.54}$$

i.e., after e^+e^--annihilation,

$$\frac{T_\nu}{T_\gamma} = \left(\frac{4}{11}\right)^{1/3} \tag{1.55}$$

---

[6]Even though we assumed all three neutrinos to be non-relativistic today, they still contribute to the total entropy (density) of the universe: They were relativistic at the time of decoupling and since then no interaction changed their entropy significantly. Thus, they still count as relativistic degrees of freedom in entropy. Their energy density, however, is affected by expansion and eventually reaching $m_{\nu_i} n_{\nu_i}$ as $T_\nu \gg m_{\nu_i}$.

[7]Strictly speaking eqn. (1.50) was derived for the *total* entropy, of all species. However, it also holds separately for the coupled and for each of the decoupled contributions, since decoupled means precisely (almost) non-interacting and therefore no (significant) entropy transfer.
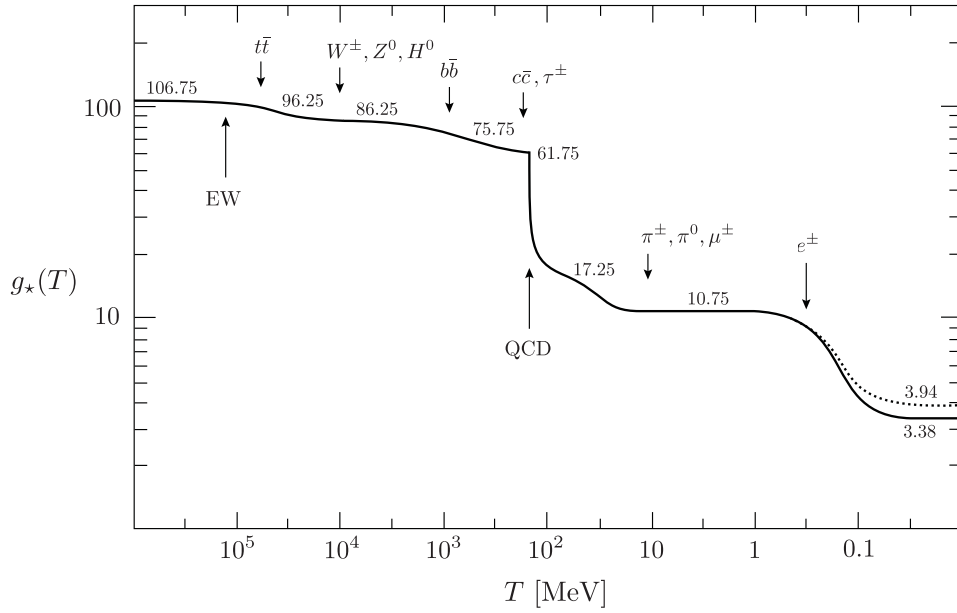
Figure 1.1: Temperature dependence of the effective number of relativistic degrees of freedom in energy density g_* and entropy density g_{*S} (dotted line). They are identical up to the point of $e^- e^+$-annihilation, when the temperature of decoupled relativistic neutrinos starts differing from that of photons. They decrease as the particles in the Standard Model become non-relativistic. Taken from [2], where they use the SM with three massless neutrinos, and therefore they contribute to g_*^0 (numbers on the right), even though the plot only shows up to $T = 10 \, \mathrm{keV}$, temperature at which neutrinos are still relativistic. Moreover, instead of using 3 massless neutrinos they use the Standard Model's effective number of relativistic neutrinos N_{eff}.

This is exact for massless neutrinos. For massive neutrinos it is a good approximation justified but the small masses and the temperatures of the process.

Figure 1.1 shows the evolution of g_* and g_{*S} from the total value in the early universe till today's value.

1.8   Solving the Friedman equations

The principle of least action provided us with two independent equations (1.30) and (1.31), from which we derived the continuity equation (1.32), with solution (1.36) for each species. Now there is one equation left, whose solution should describe the fullevolution of the scale factor $a(t)$.

First, we rewrite the first Friedman equation (1.30) to a more meaningful form, in terms of quantities accessible today by experiments, i.e. Ω_i, (see discussion and eqn. (1.58) below). We then extract all evolution information of the energy density ρ in terms of a and the effective number of DOFs with help of eqns. (1.39), (1.42) and

(1.50).

From the first Friedman equation we see that the value of the Gaussian curvature K depends on the energy density ρ of the background, in particular

$$K = a^2 \left(\frac{1}{3M_{\mathrm{Pl}}^2} \rho - H^2 \right) . \tag{1.56}$$

This means that for a particular value of ρ the universe is (spatially) flat (i.e. $K = 0$). Since observables cannot be measured for an arbitrary time in the universe's evolution, in cosmology one takes today's values as reference. Therefore, we define the *critical density* ρ_{crit}^0 as the density the universe would need to have today to make $K = 0$

$$\rho_{\mathrm{crit}}^0 \equiv 3M_{\mathrm{Pl}}^2 H_0^2 . \tag{1.57}$$

ρ_{crit}^0 is commonly used as unit to express today's energy densities, such that we get a dimensionless, constant *density parameter*

$$\Omega_i \equiv \frac{\rho_i^0}{\rho_{\mathrm{crit}}^0} . \tag{1.58}$$

Evaluating the first Friedman equation (1.30) today and rewriting it in terms of Ω_i, we find

$$1 = \sum_i \Omega_i - \frac{K}{(a_0 H_0)^2} \equiv \sum_i \Omega_i + \Omega_K , \tag{1.59}$$

i.e., deviations from $\sum_i \Omega_i = 1$ means deviations from a flat universe. This is essentially how the constraint $\left| \Omega_K \right| < 0.005$ in footnote 1 was obtained by the Planck Collaboration [3]. Talking about experiments, one usually finds the quantities $\Omega_i h^2$ as a given experimental result. This is meant to track and in some way exclude the errors that today's Hubble rate (or Hubble constant) H_0 introduces on such a quantity, since it usually carried quite sizeable uncertainties. Therefore, it is conventional to define a dimensionless *rescaled Hubble constant h*,

$$H_0 = 100h \, \mathrm{km \, s^{-1} \, Mpc^{-1}} . \tag{1.60}$$

Planck results [3] claim $H_0 = (67.8 \pm 0.9) \, \mathrm{km \, s^{-1} \, Mpc^{-1}}$, that is to say $h = 0.678 \pm 0.009$.

Let us proceed with the decomposition of the total energy density ρ of the universe relative to the critical density today ρ_{crit}^0, first component by component. For non-relativistic species, we simply have

$$\frac{\rho_{\mathrm{m}}(a)}{\rho_{\mathrm{crit}}^0} = \frac{\rho_{\mathrm{m}}(a)}{\rho_{\mathrm{m}}^0} \frac{\rho_{\mathrm{m}}^0}{\rho_{\mathrm{crit}}^0} = \left(\frac{a_0}{a} \right)^3 \Omega_{\mathrm{m}} , \tag{1.61}$$

since all contribute equally. For relativistic species, though, the weight of each species contained in g_* plays a role such that

$$\frac{\rho_{\mathrm{r}}(a)}{\rho_{\mathrm{crit}}^0} = \frac{\rho_{\mathrm{r}}(a)}{\rho_{\mathrm{r}}^0} \frac{\rho_{\mathrm{r}}^0}{\rho_{\mathrm{crit}}^0} = \frac{g_*(T) \, T^4}{g_*^0 \, T_0^4} \Omega_{\mathrm{r}} = \frac{g_*(a)}{g_*^0} \left(\frac{g_{*S}^0}{g_{*S}(a)} \right)^{4/3} \left(\frac{a_0}{a} \right)^4 \Omega_{\mathrm{r}} , \tag{1.62}$$

where we expressed the ratio of temperatures in terms of the scale factor from the entropy conservation condition (1.50). There is finally one last possibility we did not discuss so far. There might be some type of energy density which remains constant during all the evolution, $\rho_\Lambda = \text{const.}$ or $\Omega_\Lambda = \text{const.}$ From the continuity equation (1.33) it is evident that $p_\Lambda = -\rho_\Lambda$, i.e., that $w_\Lambda = -1$. This is called *vacuum energy* in cosmology, and it is part of the standard model of cosmology ΛCDM with which e.g. the Planck Collaboration performs most of the CMB data analysis. It is not only important because of that, but also because it dominates our universe today (see eqn. (1.64)).

Finally, take eqn. (1.30), divide by today's Hubble rate H_0, consider the general case $\rho = \rho_\text{r} + \rho_\text{m} + \rho_\Lambda$ and find

$$\left(\frac{H}{H_0}\right)^2 = \Omega_\text{r}\,\frac{g_*}{g_*^0}\left(\frac{g_{*S}^0}{g_{*S}}\right)^{4/3}\left(\frac{a_0}{a}\right)^4 + \Omega_\text{m}\left(\frac{a_0}{a}\right)^3 + \Omega_\Lambda + \Omega_K\left(\frac{a_0}{a}\right)^2 \tag{1.63}$$

which is eqn. (1.59) generalised to any time. The density parameters according to [3,5] are

$$\Omega_\text{r} \simeq 5.4 \times 10^{-5}\,, \quad \Omega_\text{m} \simeq 0.31\,, \quad \Omega_\Lambda \simeq 0.69\,, \quad |\Omega_K| < 5 \times 10^{-3}\,. \tag{1.64}$$

Looking at this, we realise that at early times radiation dominates the expansion when the scale factor is the smallest relative to today, $a/a_0 \lesssim 10^{-6}$, and that the vacuum energy dominates at late times (today). Note that the factor in front of Ω_r taking care of the changes in degrees of freedom are important quantitatively, since it can vary between

$$0.65 \simeq \frac{g_*^\text{TOT}}{g_*^0}\left(\frac{g_{*S}^0}{g_{*S}^\text{TOT}}\right)^{4/3} \leq \frac{g_*}{g_*^0}\left(\frac{g_{*S}^0}{g_{*S}}\right)^{4/3} \leq \frac{g_*^0}{g_*^0}\left(\frac{g_{*S}^0}{g_{*S}^0}\right)^{4/3} = 1 \tag{1.65}$$

Qualitatively, however, it does not have so much impact on the evolution of ρ_r.

As we can clearly see from figure 1.2, there are three distinct phases in the evolution of the universe: the radiation domination (RD), matter domination (MD) and the dark energy domination (ΛD). For each of these, we can simply neglect all other contributions in equation (1.63), and simply solve the one-component Friedman equation:

$$H(a) = H_0\sqrt{\frac{\rho_i(a)}{\rho_\text{crit}^0}} = H_0\sqrt{\Omega_i}\left(\frac{a_0}{a}\right)^{\frac{3}{2}(1+w_i)} \tag{1.66}$$

or, equivalently, solving for $a(t)$ (recall $H = \dot{a}/a$),

$$a(t) = a_0\left[1 - \frac{3}{2}(1+w_i)\,H_0\sqrt{\Omega_i}\,(t_0 - t)\right]^{\frac{2}{3(1+w_i)}} \sim t^{\frac{2}{3(1+w_i)}} \qquad \text{for} \quad w_i > -1 \tag{1.67}$$

$$a(t) = a_0\,e^{H(t-t_0)} \qquad \text{with} \quad H = H_0\sqrt{\Omega_\Lambda} = \text{const.} \qquad\qquad \text{for} \quad w_i = -1 \tag{1.68}$$

where in the case of RD $i = \text{r}$ we ignore the change of degrees of freedom, since it is not relevant for the qualitative discussion here. The latter case for which $w_i = -1$ and
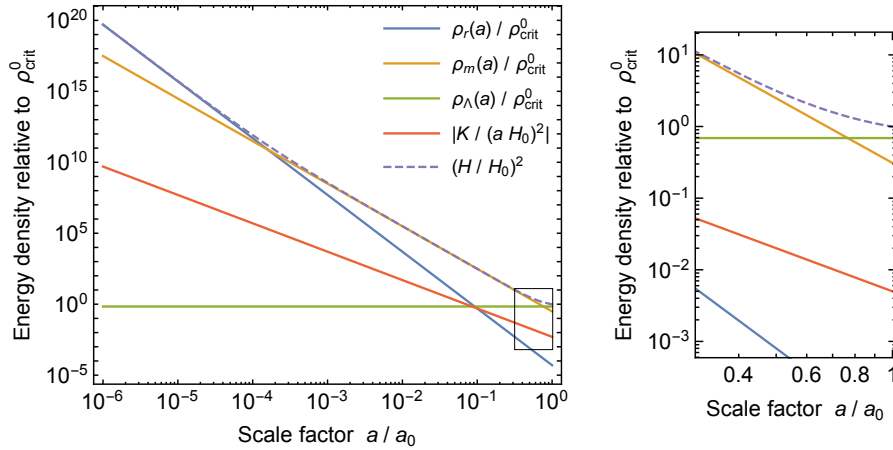
Figure 1.2: Evolution of each of the terms in the Friedman equation (1.63). It reflects the respective contribution to the Hubble rate $H(a)/H_0$ of the different components $\rho_{\rm r}$, $\rho_{\rm m}$ and ρ_Λ, as well as of curvature. The curvature contribution $\left|\frac{K}{a^2 H_0^2}\right| = \left|\left(\frac{a_0}{a}\right)^2 \Omega_K\right|$ is depicted with $\Omega_K = -0.005$, to show the biggest possible contribution allowed by the CMB constraints. We see that radiation dominates at early times, until the non-relativistic matter takes over and finally dark energy took control of the expansion recently. Curvature never dominates the dynamics of the expansion. The right panel is a zoomed-in region highlighted in the left panel for the latest times, when the transition from matter to dark energy takes place.

$H = \text{const.}$ (with the metric (1.1)) is the so-called *de Sitter space*. For completeness, we solve eqn. (1.66) for conformal time as well (recall $\dot{a} = \mathrm{d}a/(a\mathrm{d}\tau) \equiv a'/a$, see eqn. (1.5)),

$$a(\tau) = a_0 \left[1 - \frac{1}{2}(1 + 3w_i) H_0 \sqrt{\Omega_i}\, (\tau_0 - \tau)\right]^{\frac{2}{1+3w_i}} \sim \text{sgn}\,(1 + 3w_i)\, \tau^{\frac{2}{1+3w_i}} \,. \quad (1.69)$$

1.9 Cosmological Problems

The conventional Big Bang theory brought a unique explanation to the universe as we observe it today. However, there are also observations that are not fully explained. This section collects some of them, for which we will explore a solution in the next two remaining chapters of this part.

1.9.1 Horizon Problem

The cosmic microwave background (CMB) is relic radiation from the evolution of the universe. As the hot plasma of particles cools down, nuclei start forming (essentially hydrogen, some helium and a bit of other slightly heavier nucleus) and eventually (some hundred thousand years or a billion of degrees later) electrons start attaching

to them, forming neutral atoms. This period is called *recombination*. At this point, 380 000 years after the Big Bang, when the hot plasma has a temperature of around $T \sim 0.25 \, \text{eV} \sim 2900 \, \text{K}$ [2], photons can finally freely travel without being scattered by electrons or protons, usually referred to as *photon decoupling*. This is the radiation we observe today as the CMB, expanded and therefore cooled down to today's $T_0 \simeq 0.235 \, \text{meV} \simeq 2.73 \, \text{K}$ [5]. This radiation is the oldest light we have from the early universe, and its discovery and observation opened a new chapter in cosmology.

Remarkably, the CMB is isotropic, after removing the dipole anisotropy due to our relative motion w.r.t. the CMB photons. It is mostly uniform, with temperature anisotropies smaller than a few parts in one hundred thousand [6]. Which means that any two photons of the last scattering surface (the set of points from where the CMB photons we observe today that were emitted after photon decoupling) must have been in causal contact. One finds out that the math does not add up, as there was simply not enough time for that to happen. In other words, the comoving distance of two CMB photons is smaller than the particle horizon at the time of photon decoupling—according to the conventional Big Bang, with conventional matter governing the dynamics.

In view of figure 1.2, it seems sensible to assume that the early universe always expanded dominated by "conventional" matter, i.e., matter that satisfies the strong energy condition (SEC)

$$\text{tr}\, T^{(i)\mu}{}_\nu = \rho_i + 3p_i = \rho_i \left(1 + 3w_i\right) > 0 \qquad \text{or simply} \qquad w_i > \frac{1}{3} \,. \tag{1.70}$$

Under this condition the comoving Hubble radius is (see eqns. (1.13) and (1.66))

$$(aH)^{-1} = \frac{(a_0 H_0)^{-1}}{\sqrt{\Omega_i}} \left(\frac{a}{a_0}\right)^{\frac{1}{2}(1+3w_i)} \tag{1.71}$$

which implies an always-growing Hubble sphere. The particle horizon, in turn, takes the form (see eqn. (1.9))

$$\chi_{\text{PH}} = \frac{2\,(a_0 H_0)^{-1}}{(1 + 3w_i)\sqrt{\Omega_i}} \left[\left(\frac{a}{a_0}\right)^{\frac{1}{2}(1+3w_i)} - \left(\frac{a_{\text{ini}}}{a_0}\right)^{\frac{1}{2}(1+3w_i)} \right] \equiv \tau - \tau_{\text{ini}} \,. \tag{1.72}$$

τ_{ini} corresponds to the Big Bang singularity $a_{\text{ini}} \to 0$ such that, for an expansion always dominated by a fluid with $w_i > -1/3$,

$$\tau_{\text{ini}} \xrightarrow{a_{\text{ini}} \to 0} 0 \tag{1.73}$$

and thus χ_{PH} is finite and gets its main contribution from late times

$$\chi_{\text{PH}} = \frac{2\,(a_0 H_0)^{-1}}{(1 + 3w_i)\sqrt{\Omega_i}} \left(\frac{a}{a_0}\right)^{\frac{1}{2}(1+3w_i)} = \frac{2}{1 + 3w_i}(aH)^{-1} \,, \qquad \text{for} \quad w_i > -\frac{1}{3} \,, \tag{1.74}$$

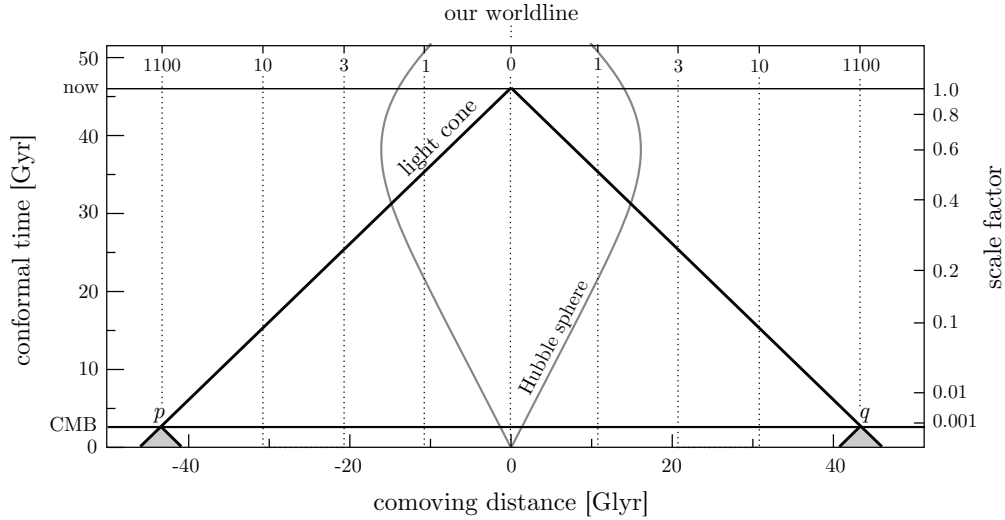which implies a finite particle horizon.

Figure 1.3: Our past lightcone tracking back to the origin of CMB. The past lightcones of points p and q on the last scattering surface in opposite directions in the sky do not overlap, meaning they were never in casual contact. In other words, the comoving distance between them is bigger than the comoving time $\tau_{\mathrm{CMB}} - \tau_{\mathrm{ini}} = \tau_{\mathrm{CMB}}$. Figure from [2].

This shows a problem, because photons at decoupling $\tau = \tau_{\mathrm{dec}}$ are only causally connected with finitely far neighbours, not being able to communicate with all CMB photons. Figure 1.3 shows how, if the Big Bang singularity occurred at $\tau_{\mathrm{ini}} \to 0$, the past lightcones of two CMB photons opposite in the sky do not overlap. However, all CMB photons show the same temperature, so either the initial conditions of the universe are very specific—what in physics is called a *fine-tuning problem*—or the dynamics were different such that all CMB photons have in fact been in causal contact at some point. In section 2.1 we introduce inflation as a mechanism that gives an explanation to the isotropy as well as to the anisotropies of the CMB.

1.9.2 Flatness Problem

A monotonically growing Hubble sphere also involves some issues with flatness. As already mentioned (e.g. in footnote 1), experiments suggest the universe is essentially flat. However, flatness is an unstable point in the dynamics of the universe, and if it expanded just with matter satisfying the SEC (up to the dark energy-matter equality) then the initial conditions would have needed to be oddly particular, namely $K = 0$ or extremely close to zero. This is another fine-tuning problem, for which inflation gives an elegant solution.

Chapter 2

Inflation

2.1 General features of inflation

As we saw in the previous section, there are some problems associated with a universe in which the Hubble sphere has always been growing. What about adding a period in the universe history in which the Hubble sphere shrinks? We retrieve eqn. (1.71)

$$(aH)^{-1} \propto a^{\frac{1}{2}(1+3w_i)} \quad \Rightarrow \quad \frac{\mathrm{d}(aH)^{-1}}{\mathrm{d}a} \propto \frac{1}{2}(1+3w_i)a^{\frac{1}{2}(3w_i-1)} \tag{2.1}$$

to see that in order to have a shrinking Hubble sphere we need

$$\frac{\mathrm{d}(aH)^{-1}}{\mathrm{d}a} < 0 \quad \Leftrightarrow \quad 1 + 3w_i < 0 \quad \Leftrightarrow \quad w_i = \frac{p_i}{\rho_i} < -\frac{1}{3}. \tag{2.2}$$

Indeed, the particle horizon $\chi_{\mathrm{PH}}(\tau) = \tau - \tau_{\mathrm{ini}}$ (see eqn. (1.72)) is now dominated by the initial contribution

$$\tau_{\mathrm{ini}} \propto a_{\mathrm{ini}}^{\frac{1}{2}(1+3w_i)} \xrightarrow{a_{\mathrm{ini}} \to 0} -\infty \quad \Leftrightarrow \quad w_i < -\frac{1}{3}. \tag{2.3}$$

Now CMB photons have plenty of time (infinite) to get into causal contact, meaning that no matter at what comoving distance they are from each other their past lightcones are due to overlap inevitably. This is illustrated in figure 2.1.

Furthermore, in a universe dominated by a fluid with $w_i < -1/3$, the universe undergoes an accelerated expansion. Take the equation of state (1.27) and the second Friedmann equation (1.31), and assume this fluid is the only component in the universe. Then,

$$\frac{\ddot{a}}{a} = -\frac{1}{6M_{\mathrm{Pl}}^2}\rho_i\left(1 + 3\frac{p_i}{\rho_i}\right) = -\frac{H^2}{2}\left(1 + 3\frac{p_i}{\rho_i}\right) > 0 \quad \Leftrightarrow \quad \frac{p_i}{\rho_i} < -\frac{1}{3}. \tag{2.4}$$
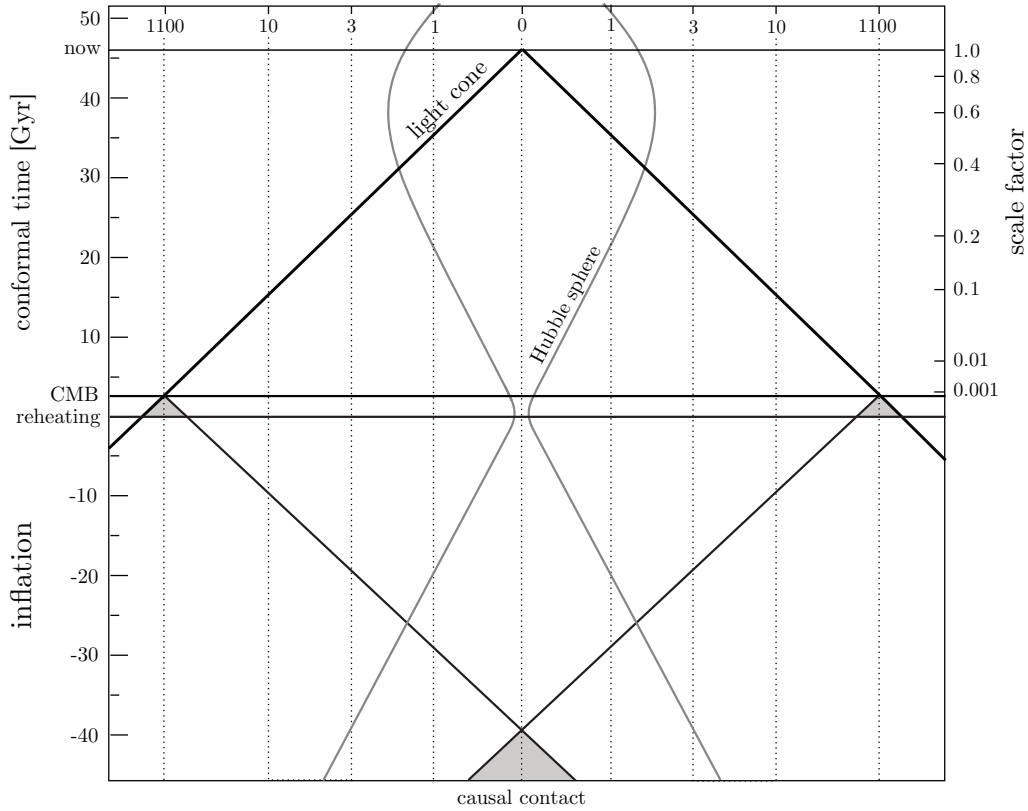
Figure 2.1: Diagram showing the new picture after introducing a period of accelerated expansion (see eqn. (2.4)), called *inflation*. Where previously (see fig. 1.3) the origin of conformal time was at $\tau_{\mathrm{ini}} = 0$ and corresponded to the Big Bang singularity, now it corresponds to the epoch of reheating $\tau_{\mathrm{rh}} = 0$. Past lightcones from the last scattering surface at τ_{CMB} now overlap, meaning CMB photons are in fact in casual contact. Of course the vertical axis continues downwards towards minus infinity, when the Big Bang singularity occurs $\tau_{\mathrm{ini}} \to -\infty$, or up to the regime where new physics are expected to arise. The evolution of the Hubble radius is also shown for reference. Figure from [2].

We can also rewrite the second derivative of the scale factor in terms of the Hubble parameter

$$\frac{\ddot{a}}{a} = H^2 + \dot{H} \equiv H^2(1 - \varepsilon) > 0 \quad \Leftrightarrow \quad \varepsilon \equiv -\frac{\dot{H}}{H^2} = \frac{3}{2}\left(1 + \frac{p_i}{\rho_i}\right) < 1 \qquad (2.5)$$

where we defined the non-negative parameter ε as the variation rate of the Hubble parameter. Its smallness remarks $H(t)$ must not vary too quickly.

This period in the history of the universe is called *inflation*. It is nothing but a period of accelerated expansion, so rapid it rips apart patches of the universe, away from each other, leaving them causally disconnected, and expands—or *inflates*—quantum fluctuations of the primordial universe to macroscopic sizes, some of which are imprinted in the spectrum of the CMB photons. It does not only successfully predict the

isotropy of the CMB as well as the presence of anisotropies, but also provides seeds for structure formation, i.e., provides a spectrum of density inhomogeneities which with time turn into large scale structures of the universe we observe today. To sum up, when talking about inflation, we talk about a period

- of accelerated expansion $\ddot{a} > 0$

- with a slowly-varying Hubble rate $\varepsilon = -\dot{H}/H^2 < 1$,

- modelled by a fluid that violates the SEC, $\operatorname{tr} T^{(i)\mu}{}_\nu < 0$, and has a negative enough pressure $p_i < -\rho_i/3$,

- during which the (comoving) size of the "instantaneous" observable universe shrinks $\mathrm{d}(aH)^{-1}/\mathrm{d}a < 0$

- which therefore extends the particle horizon of any event to infinity $\chi_{\mathrm{PH}} \to \infty$, or at least to a size big enough to solve the horizon problem.

All statements are equivalent.

Some first models of inflation [7,8] were based on the idea of a de Sitter expansion, for which $p = -\rho$ and therefore $H = \text{const.}$ as discussed in section 1.8. Solving $H = \dot{a}/a$ for $a(t)$ during inflation $t \leq t_{\mathrm{end}}$,

$$\int_a^{a_{\mathrm{end}}} \frac{\mathrm{d}a}{a} = \int_t^{t_{\mathrm{end}}} \mathrm{d}t\, H \quad \Rightarrow \quad \frac{a(t)}{a_{\mathrm{end}}} = \mathrm{e}^{-H(t_{\mathrm{end}}-t)} \equiv \mathrm{e}^{N_{\mathrm{end}}-N} \tag{2.6}$$

where we defined the *number of* e-*folds N* before the end of inflation[1],

$$\mathrm{d}N \equiv -H\mathrm{d}t\,, \tag{2.7}$$

as just another measure of time which counts the number factors of the natural number e by which the scale factor varied. We set $N_{\mathrm{end}} = 0$ at the end of inflation, such that $a(N) = a_{\mathrm{end}}\mathrm{e}^{-N}$. Note that (2.6) is just a redefinition of (1.68) with more convenient integration limits. During de Sitter expansion, the conformal time is

$$\tau_{\mathrm{end}} - \tau = \int_t^{t_{\mathrm{end}}} \frac{\mathrm{d}t}{a(t)} = \frac{1}{a_{\mathrm{end}}} \left(-\frac{1}{H}\right) \left[1 - \mathrm{e}^{H(t_{\mathrm{end}}-t)}\right] = -\frac{1}{Ha_{\mathrm{end}}} + \frac{1}{Ha}\,. \tag{2.8}$$

Shrinking the Hubble radius to a small enough size would mean

$$(a_{\mathrm{end}}H)^{-1} \to 0 \quad \Rightarrow \quad \tau_{\mathrm{end}} \to 0\,, \tag{2.9}$$

defining a zero point in conformal time. In standard cosmology without inflation the origin of conformal corresponded to the Big Bang singularity $t_{\mathrm{ini}} = 0$. However, an inflationary period effectively pushes it back to negative conformal time (towards

---

[1]When we say, for example, $N = 60$, we mean '60 e-folds before the end of inflation.'

$\tau_{\text{ini}} \to -\infty$ in the extreme case). $\tau = 0$ now corresponds to *reheating*, a transition phase between inflation and the radiation-dominated early universe (the hot Big Bang). The energy of inflation must therefore decay into Standard Model particles during this phase. We can, moreover, identify the conformal time $\tau < 0$ during de Sitter expansion as

$$\tau = -(aH)^{-1}\,. \tag{2.10}$$

Such early models, however had some problems such as they would not reheat properly or they would last for too long. These became then the "old" inflation and new models [9, 10] of "new" inflation appeared. They feature a quasi-de Sitter expansion in which H is not completely constant. We generally call these models *single-field slow-roll inflation*.

2.2   Single-field slow-roll inflation

The most common way of describe inflation is with a homogeneous scalar field $\phi = \phi(t)$ (or $\phi(\tau)$), named the *inflaton*. It is coupled to gravity as in equation (1.14), with its dynamics given by the Lagrangian density

$$\mathcal{L}_\phi = -\frac{1}{2}\, g^{\alpha\beta}\, \partial_\alpha \phi\, \partial_\beta \phi - V(\phi) = -\frac{1}{2}\, g^{00}(\partial_0 \phi)^2 - V(\phi)\,, \tag{2.11}$$

where $V(\phi)$ is the inflaton potential density. Different models of inflation give different forms to the potential V, each of which shows different features in different observables, such as the spectrum of the CMB photons or stochastic gravitational waves.

Even if it seems that the inflaton is just another component of the matter content of the universe, the scalar field ϕ is just a modellisation of the mechanism. One of the first models of inflation, in fact, was originally proposed as some correction of gravity for high energies via an extra term $\propto R^2$ in the Einstein-Hilbert action. This is called *Starobinski inflation* [11]. It can be modelled through a scalar field and written as $\mathcal{L}_\phi$ in eqn. (2.11), with the potential

$$V_{\text{Starobinsky}}(\phi) = V_0 \left(1 - e^{\gamma_s \phi}\right)^2\,, \quad \phi < 0\,, \tag{2.12}$$

with some parameters V_0 and γ_s. For the following, however, we will keep $V(\phi)$ unspecified and do a model-independent study of inflation via scalar fields.

2.2.1   Equations of motion for the inflaton

The equation of motion of the inflaton field is the Klein-Gordon equation in a curved spacetime, with the FLRW metric (1.1) (or (1.6))[2]

$$\ddot{\phi} + 3H\dot{\phi} + \frac{\mathrm{d}V}{\mathrm{d}\phi} = 0 \qquad \left(\phi'' + 2\frac{a'}{a}\phi' + a^2\frac{\mathrm{d}V}{\mathrm{d}\phi} = 0\right) \tag{2.13}$$

---

[2]Eqn. (2.13) is derived imposing the action in eqn. (1.14) to be an extremum for any field configuration $\phi(z)$, i.e. $\delta S/\delta\phi(z) \overset{!}{=} 0$.

with H given by the Friedman equations derived in section 1.6 and computed for inflation in the following subsection. Eqn. (2.13) differs from the Klein-Gordon equation in Minkowski space in the friction term $3H\dot{\phi}$ introduced by the expansion of the universe.

2.2.2 Friedman Equations during inflation

We shall now compute the energy and pressure of the inflaton in order to study the dynamics derived in the previous chapter. We know from section 1.4 that the energy-momentum tensor can be obtained from the Lagrangian

$$T^\mu{}_\nu = \delta^\mu_\nu \mathcal{L} - 2g^{\mu\sigma}\frac{\partial \mathcal{L}}{\partial g^{\sigma\nu}}\,. \tag{2.14}$$

In this case,

$$\frac{\partial \mathcal{L}_\phi}{\partial g^{\sigma\nu}} = -\frac{1}{2}\,\partial_\sigma\phi\,\partial_\nu\phi = -\frac{1}{2}\,(\partial_0\phi)^2\delta^0_\sigma\delta^0_\nu \tag{2.15}$$

and

$$T^{(\phi)\mu}{}_\nu = \delta^\mu_\nu \mathcal{L}_\phi + g^{00}(\partial_0\phi)^2\delta^{\mu 0}\delta^0_\nu\,. \tag{2.16}$$

Therefore, the energy density and pressure are given by

$$\rho_\phi = -T^0{}_0 = \frac{1}{2}g^{00}(\partial_0\phi)^2 + V(\phi) - g^{00}(\partial_0\phi)^2\,, \tag{2.17a}$$

$$p_\phi = \frac{1}{3}T^i{}_i = \frac{\delta^i_i}{3}\left(-\frac{1}{2}g^{00}(\partial_0\phi)^2 - V(\phi)\right) \equiv \mathcal{L}_\phi \tag{2.17b}$$

for which after specifying some coordinates we get

$$\rho_\phi = \frac{1}{2}\dot{\phi}^2 + V(\phi) = \frac{1}{2}\left(\frac{\phi'}{a}\right)^2 + V(\phi)\,, \tag{2.18a}$$

$$p_\phi = \frac{1}{2}\dot{\phi}^2 - V(\phi) = \frac{1}{2}\left(\frac{\phi'}{a}\right)^2 - V(\phi)\,, \tag{2.18b}$$

in cosmic time t and conformal time τ, respectively, and with the short-hand notations $\dot{} \equiv \frac{\mathrm{d}}{\mathrm{d}t}$ and $' \equiv \frac{\mathrm{d}}{\mathrm{d}\tau}$ for the time derivatives. For the rest of this section we work exclusively with cosmic time t.

This gives a equation of state parameter w_ϕ

$$w_\phi = \frac{p_\phi}{\rho_\phi} = \frac{\frac{1}{2}\dot{\phi}^2 - V}{\frac{1}{2}\dot{\phi}^2 + V} < -\frac{1}{3} \quad \Rightarrow \quad \frac{1}{2}\dot{\phi}^2 < \frac{1}{2}V \tag{2.19}$$

which implies that the potential energy must be at least twice as big as the kinetic energy.

The first Friedman equations is

$$3M_{\mathrm{Pl}}^2 H^2 = \rho_\phi = \frac{1}{2}\dot{\phi}^2 + V(\phi)\,, \tag{2.20}$$

while the second is simply eqn. (2.5), from where we can find

$$\varepsilon = \frac{1}{2M_{\mathrm{Pl}}^2}\left(\frac{\dot{\phi}}{H}\right)^2.$$

(2.21)

In other words, inflation, i.e., $\varepsilon < 1$, only takes place if the kinetic energy $\frac{1}{2}\dot{\phi}^2$ contribution to the total energy ρ_ϕ is less than a third.

2.2.3   The slow roll approximation

One usually takes a de Sitter limit, in which

$$p_\phi \to -\rho_\phi \quad \Leftrightarrow \quad \frac{1}{2}\dot{\phi}^2 \ll V.$$

(2.22)

That is, the potential energy dominates over the kinetic energy, such that we can rewrite the first Friedman equation (2.20) as

$$H^2 \simeq \frac{V(\phi)}{3M_{\mathrm{Pl}}^2}$$

(2.23)

in this limit. $\varepsilon \to 0$ is equivalent to the de Sitter limit.

Furthermore, it is also often considered the case

$$\ddot{\phi} \ll 3H\dot{\phi}$$

(2.24)

such that the friction term dominates in the Klein-Gordon equation (2.13), which now takes the form

$$3H\dot{\phi} + \frac{\mathrm{d}V}{\mathrm{d}\phi} \simeq 0.$$

(2.25)

To parametrise this approximation, we define a second dimensionless parameter η

$$\eta \equiv -\frac{\ddot{\phi}}{\dot{\phi}H} = \varepsilon + \frac{1}{2\varepsilon}\frac{\mathrm{d}\varepsilon}{\mathrm{d}N},$$

(2.26)

where for the second step we used the time derivative of eqn. (2.21),

$$\frac{\dot{\varepsilon}}{\varepsilon} = 2\,\frac{H}{\dot{\phi}}\left(\frac{\ddot{\phi}}{H} - \frac{\dot{H}}{H^2}\dot{\phi}\right),$$

(2.27)

and $\mathrm{d}N = -H\mathrm{d}t$.

These approximations are what is called *the slow roll approximation* and is valid as long as the *slow roll parameters* ε and η are small, $\varepsilon, |\eta| \ll 1$. Inflation will take place as long as $\varepsilon < 1$, regardless of the value of η, but this approximation holds for certain choices of the potential [6] and makes the computations easier. η gives information about how ε evolves during inflation, relevant for quantifying how long ε stays under 1, i.e., how long the inflationary period is.

We can rewrite the slow roll parameters in terms of the potential and its derivatives using eqns. (2.23) and (2.25),

$$\varepsilon \simeq \frac{1}{2M_{\text{Pl}}^2 H^2} \left(\frac{\mathrm{d}V}{\mathrm{d}\phi} \right)^2 \frac{1}{9H^2} \simeq \frac{1}{2M_{\text{Pl}}^2} \left(\frac{\mathrm{d}V}{\mathrm{d}\phi} \right)^2 \left(\frac{M_{\text{Pl}}^2}{V} \right)^2 = \frac{M_{\text{Pl}}^2}{2} \left(\frac{1}{V} \frac{\mathrm{d}V}{\mathrm{d}\phi} \right)^2 \equiv \varepsilon_V \quad (2.28)$$

and, since

$$3\dot{H}\dot{\phi} + 3H\ddot{\phi} + \dot{\phi}\frac{\mathrm{d}^2 V}{\mathrm{d}\phi^2} \simeq 0 \,, \tag{2.29}$$

$$\eta = -\frac{\ddot{\phi}}{\dot{\phi}H} \simeq \frac{1}{3H^2}\frac{\mathrm{d}V}{\mathrm{d}\phi} + \frac{\dot{H}}{H^2} \simeq M_{\text{Pl}}^2 \frac{1}{V}\frac{\mathrm{d}^2 V}{\mathrm{d}\phi^2} - \frac{M_{\text{Pl}}^2}{2} \left(\frac{1}{V}\frac{\mathrm{d}V}{\mathrm{d}\phi} \right)^2 \equiv \eta_V - \varepsilon_V \,. \tag{2.30}$$

We see ε_V is some measure of the steepness of the potential relative to its magnitude, while η_V indicates its curvature. The slow roll conditions $\varepsilon_V, |\eta_V| \ll 1$ are equivalent to $\varepsilon, |\eta| \ll 1$. Slow roll does not necessarily mean a potential which is flat for a period long enough, but also a steep potential with high enough values V satisfies these conditions. In any case, the picture is still quite straight forward: the field ϕ rolls slowly down the potential, till its speed is too big and inflation stops. As soon as ε reaches 1, inflation finishes and reheating starts.

The advantage of the slow roll parameters in terms of the potential, ε_V and η_V, is that once the potential $V(\phi)$ is specified, ε_V and η_V can be directly computed. This is useful, for example, to compute the value of the field at the end of inflation ϕ_{end} from the condition

$$\varepsilon_V(\phi_{\text{end}}) = 1 \,, \tag{2.31}$$

which is then helpful to compute the number of e-foldsremaining,

$$N = -\int_t^{t_{\text{end}}} H\mathrm{d}t = -\int_\phi^{\phi_{\text{end}}} \frac{H}{\dot{\phi}}\mathrm{d}\phi = -\frac{1}{\sqrt{2}M_{\text{Pl}}^2} \int_\phi^{\phi_{\text{end}}} \frac{\mathrm{d}\phi}{\sqrt{\varepsilon_V(\phi)}} \,. \tag{2.32}$$

Quantities predicted by inflation that will be introduced in the next section will also be computable from these parameters.

In order to solve the horizon and flatness problems, inflation has to last for long enough. From a thermodynamic argument, using entropy conservation, one finds [6] that the universe must inflate for a minimum of

$$N_{\text{min}} \sim 60 \tag{2.33}$$

or, more precisely, assuming a realistic range of reheating temperatures T_{rh} between 10^3 GeV and 10^{16} GeV, we obtain [12, 13]

$$46 \lesssim N_{\text{min}} \lesssim 60 \,. \tag{2.34}$$

Note that there are no upper limits on the number of e-folds inflation must last.
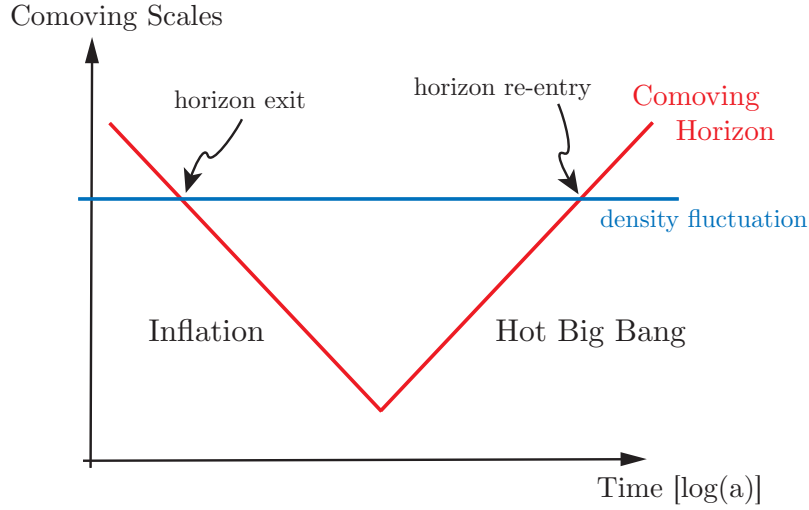
Figure 2.2: Evolution of perturbations in an inflationary universe. Fluctuations exit the horizon, staying causally disconnected and "frozen" till re-entry. In a universe without infla- tion the comoving horizon would be strictly increasing, and therefore we could not speak of horizon exit nor re-entry. Here comoving horizon refers to the comoving Hubble sphere. Note that it is equivalent to figure 2.1 rotated 90°. Figure from [21].

2.3   Quantum fluctuations during inflation

The universe is not homogeneous at small scales. It is full of galaxies, stars, planets. They grew from initial inhomogeneities in the early universe, seeds that through gravitational interaction evolved into complex structures we observe today. They are initial conditions for which the Big Bang cosmology does not have an explanation but inflation provides a mechanism to generate fluctuations in even larger scales than the horizon [14–20].

The general idea behind the mechanism is that a certain inhomogeneity of a certain (physical) scale[3] grows with expansion. During inflation, the physical Hubble sphere does not grow as fast, and the perturbation is left outside of the horizon, being causally disconnected from then on. Until during the Big Bang cosmology the Hubble sphere grows again faster than the scale factor and thus the perturbation falls again inside or *re-enters* the horizon. If we switch to comoving distances, then the comoving scale of a certain perturbation (the comoving wavelength) will remain always constant along expansion and the comoving Hubble radius shrinks and grows again when inflation comes to an end. This can be seen in figure 2.2. Note that if the perturbations are larger than today's Hubble sphere, are (and will probably always be) inaccessible to us, since they are still outside of the horizon (and we currently live in a de Sitter universe, dominated by dark energy, with a shrinking Hubble sphere). That limits

---

[3]Think of an inhomogeneity as a wave or perturbation in the cosmic fluid and its scale as its wavelength λ.

the observational information we can get from the early universe. Namely, we can only see up to the last 60 e-folds of inflation: From the smallest scales that re-entered the horizon just at the end of inflation $N = 0$, to the biggest scales, corresponding to perturbations re-entering the horizon today.

But inflation also predicts how the inhomogeneities are produced in the first place. In the following we will make a brief overview of how these perturbations are computed and how they translate into observables. For that, we follow the treatment done in [21], which is in turn based on [20, 22–29].

In the scalar field picture, ϕ evolves classically on its potential $V(\phi)$, but it is also subject to quantum fluctuations $\delta\phi$ about the classical trajectory $\phi(t)$. Formally,

$$\delta\phi(t, \boldsymbol{x}) = \phi(t, \boldsymbol{x}) - \bar{\phi}(t) \,, \tag{2.35}$$

where we explicitly write a bar on the classical field $\bar{\phi}(t)$ in order to highlight the fact that it is a classical background field, and $\phi(t, \boldsymbol{x})$ is simply the total field. One expects as well perturbations around the background (spatially flat) FLRW metric

$$\delta g_{\mu\nu}(t, \boldsymbol{x}) = g_{\mu\nu}(t, \boldsymbol{x}) - \bar{g}_{\mu\nu}(t) \,. \tag{2.36}$$

Fluctuations are considered to be small, $\delta\phi \ll \bar{\phi}$, $\delta g_{\mu\nu} \ll \bar{g}_{\mu\nu}$, such that the linear order of the Einstein equations expansion in perturbations

$$\delta G_{\mu\nu} = M_{\mathrm{Pl}}^{-2} \, \delta T_{\mu\nu} \tag{2.37}$$

determine the evolution of these to very high accuracy. Since the scalar field dominates the energy-momentum tensor during inflation, its fluctuations $\delta\phi$ will directly affect those of the metric $\delta g_{\mu\nu}$ and viceversa. This is called *backreaction*.

We can decompose the perturbations into independent scalar, vector and tensor components. Inflation does not generate vector fluctuations and they are diluted with expansion, thus we will ignore them here. We focus on scalar and tensor perturbations, which are observed today as density (and thus temperature) fluctuations and gravitational waves, respectively. On one hand, we obtain from the field fluctuations $\delta\phi$ scalar perturbations in the energy density $\delta\rho$ and pressure δp[4]. On the other hand, metric fluctuations $\delta g_{\mu\nu}$ present both scalar Φ, $\mathcal{B}$, Ψ and $\mathcal{E}$, and tensor h_{ij} fluctuations,

$$\mathrm{d}s^2 = -(1 + 2\Phi)\mathrm{d}t^2 + 2\, a\, \partial_i \mathcal{B}\, \mathrm{d}t\mathrm{d}x^i + a^2\big[(1 - 2\Psi)\delta_{ij} + (2\, \partial_i\partial_j\mathcal{E} + h_{ij})\big]\mathrm{d}x^i\mathrm{d}x^j \,, \tag{2.38}$$

with h_{ij} transverse ($\nabla_i h^{ij} = 0$) and traceless ($h_i^i = 0$).

2.3.1 Scalar perturbations

The tensor perturbations are automatically gauge-invariant but the scalar ones are not. In other words, if we change our coordinates the perturbations $\delta\phi$ will in general change as well. Hence the importance of defining gauge-invariant quantities to

---

[4]There is also a tensor contribution to δT_{ij} from the anisotropic stress Σ_{ij}, with $\partial^i \Sigma_{ij} = 0 = \Sigma_i^i$, but it is negligible to a good approximation.

study the evolution of these. The most relevant gauge-invariant quantity for us is the *comoving curvature perturbation*

$$\mathcal{R} \equiv \Psi - \frac{H}{\bar{\rho} + \bar{p}}(\delta\rho + \delta p) = \Psi + \frac{H}{\dot{\bar{\phi}}}\delta\phi \,, \tag{2.39}$$

where we replaced the matter perturbations by those of the scalar field during inflation.

In general, we will work in Fourier space

$$\mathcal{R}(t, \boldsymbol{x}) = \int \frac{\mathrm{d}^3 \boldsymbol{k}}{(2\pi)^{3/2}} \, \mathcal{R}_{\boldsymbol{k}}(t) \, \mathrm{e}^{\mathrm{i}\boldsymbol{k}\cdot\boldsymbol{x}} \,, \tag{2.40}$$

with Fourier modes $\mathcal{R}_{\boldsymbol{k}}(t)$, which represent the fluctuations at a comoving scale $\lambda = 2\pi k^{-1}$. Fourier modes do not interact with each other since the linear equations of motion (2.37) are translation invariant[5]. Thus we can study them independently. The evolution of $\mathcal{R}_{\boldsymbol{k}}$ is given by the perturbed Einstein equations (2.37) as

$$\dot{\mathcal{R}}_{\boldsymbol{k}} = -\frac{H}{\bar{\rho} + \bar{p}} \, \delta p_{\mathrm{en}} + \frac{k^2}{(aH)^2}\left(\dots \right) , \tag{2.41}$$

where

$$\delta p_{\mathrm{en}} \equiv \delta p - \frac{\dot{\bar{p}}}{\dot{\bar{\rho}}}\delta\rho \tag{2.42}$$

is the non-adiabatic component of the pressure perturbation and is a gauge-invariant quantity. Therefore, for adiabatic matter perturbations ($\delta p_{\mathrm{en}} = 0$), $\mathcal{R}$ is conserved on superhorizon scales $k^{-1} \gg (aH)^{-1}$, where $k = 2\pi\lambda^{-1}$ is the comoving wavenumber of a perturbation—with λ a comoving wavelength. This means that computing $\mathcal{R}_{\boldsymbol{k}}$ at horizon exit automatically gives the perturbation mode at horizon re-entry. Figure 2.3 illustrates this.

Fluctuations, however, are quantum during inflation. That means, they have to be treated as such. In order to do that we proceed as follows:

1. Start with the action (1.14) with $\mathcal{L} = \mathcal{L}_\phi$, for a (non-homogeneous) scalar field $\phi(t, \boldsymbol{x})$ (or $\phi(\tau, \boldsymbol{x})$). Expand it to first order in perturbations. This will provide us with the right normalisation.

2. Derive the equations of motion, redefine the fields in terms of the Mukhanov variable v and go to Fourier space to get the *Mukhanov-Sasaki equation* of the Fourier modes $v_{\boldsymbol{k}}$,

$$v_{\boldsymbol{k}}'' + \left(k^2 - \frac{z''}{z} \right) v_{\boldsymbol{k}} = 0 \,. \tag{2.43}$$

3. Perform the mode expansion of the modes $v_{\boldsymbol{k}}$ to promote them to quantum operators, imposing canonical commutation relations.
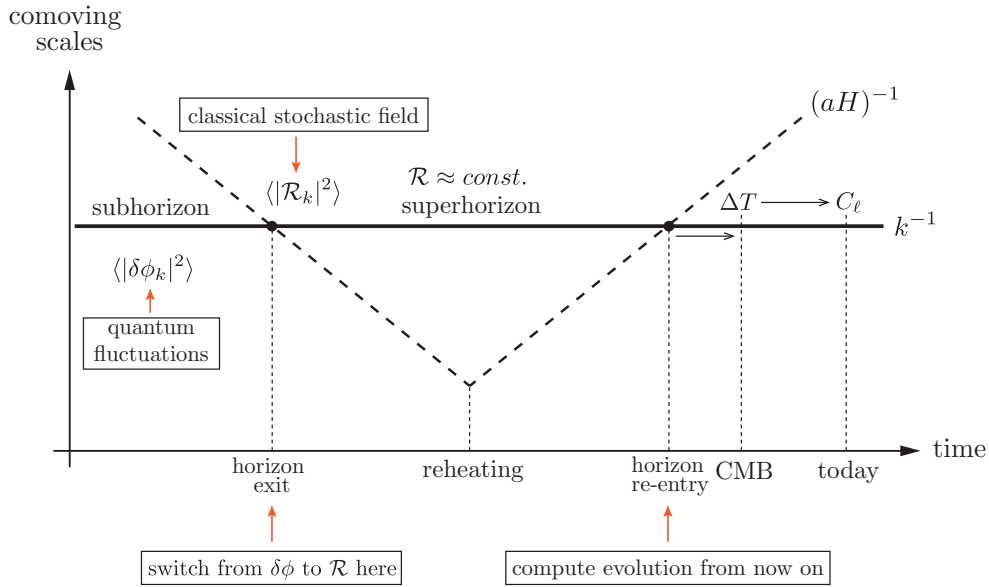
---

[5]Proof in Appendix A of [21].

Figure 2.3: Evolution of a scalar perturbation of a comoving size k^{-1} during and after inflation, quantified by the quantities $\delta\phi$ and $\mathcal{R}$. At the time of recombination the perturbation induces a fluctuation in the temperature ΔT of the CMB spectrum, which can be measured in the primordial spectrum given in a multipole expansion with coefficients C_ℓ. From [2].

4. Choose a vacuum. A known result of quantum field theory in curved spacetimes is that there is no unique vacuum. Each observer may have a different one. Therefore, match the solutions to that of a Minkowski (flat) vacuum of a comoving observer in the infinite (far) past, $\tau \to -\infty$, or, equivalently, when the mode is deep inside the horizon $k \gg aH$. That is the so-called *Bunch-Davies vacuum*.

5. Finally, express the Mukhanov-Sasaki equation in the limit of de Sitter expansion, $\varepsilon \to 0$, where we can solve it exactly using the constraints obtained via quantisation and the initial conditions. We then obtain unique *Bunch-Davies mode functions*, with which we can compute the two-point correlation functions, that is to say the *power spectrum* of perturbations.

Note that procedure is the same for both scalar and tensor perturbations. They will just differ on the action[6] and thus in the equations of motion, but they can be both brought to the same form of the Mukhanov-Sasaki equation through the corresponding field redefinition.

If one follows this procedure for computing $\mathcal{R}_{\boldsymbol{k}}$, one arrives to the Bunch-Davies mode functions

$$v_k(\tau) = \frac{\mathrm{e}^{-\mathrm{i}k\tau}}{\sqrt{2k}}\left(1 - \frac{\mathrm{i}}{k\tau}\right) \tag{2.44}$$

---

[6]For instance, the scalar perturbations are sourced by both field and metric fluctuations, while tensor perturbations are just those from the metric (neglecting anisotropic stress).

which are the coefficients of the Fourier expansion of the (already-quantised) *Mukhanov variable* $\hat{v}$, or

$$\hat{v}_{\boldsymbol{k}}(\tau) = v_k(\tau)\,\hat{a}_{\boldsymbol{k}} + v_k^*(\tau)\,\hat{a}_{-\boldsymbol{k}}^\dagger \equiv \int \frac{\mathrm{d}^3\boldsymbol{x}}{(2\pi)^{3/2}}\, v(\tau, \boldsymbol{x})\,\mathrm{e}^{-\mathrm{i}\boldsymbol{k}\cdot\boldsymbol{x}}\,, \qquad (2.45)$$

for the modes, with the creation $\hat{a}_{-\boldsymbol{k}}^\dagger$ and annihilation $\hat{a}_{\boldsymbol{k}}$ operators satisfying the canonical commutation relation

$$\big[\hat{a}_{\boldsymbol{k}}, \hat{a}_{\boldsymbol{k}'}^\dagger\big] = \delta^{(3)}\big(\boldsymbol{k} - \boldsymbol{k}'\big) \qquad (2.46)$$

if and only if the mode functions are normalised as

$$\langle v_k, v_k \rangle \equiv \frac{\mathrm{i}}{\hbar}\big(v_k^* v_k' - v_k^{*\prime} v_k\big) = 1\,. \qquad (2.47)$$

The Mukhanov variable is related to $\mathcal{R}_{\boldsymbol{k}}$ via

$$v \equiv z\mathcal{R} \qquad \text{with} \quad z^2 \equiv a^2 \frac{\dot{\phi}^2}{H^2} = 2M_{\mathrm{Pl}}^2 a^2 \varepsilon\,. \qquad (2.48)$$

Scalar power spectrum

The quantisation allows us to properly compute the two-point correlation functions in de Sitter space,

$$\langle \hat{v}_{\boldsymbol{k}} \hat{v}_{\boldsymbol{k}'} \rangle = \langle 0|\hat{v}_{\boldsymbol{k}} \hat{v}_{\boldsymbol{k}'}|0\rangle = v_k v_k^* \langle 0|\hat{a}_{\boldsymbol{k}} \hat{a}_{-\boldsymbol{k}'}^\dagger|0\rangle = |v_k|^2 \delta^{(3)}\big(\boldsymbol{k} + \boldsymbol{k}'\big) \equiv P_v(k)\,\delta^{(3)}\big(\boldsymbol{k} + \boldsymbol{k}'\big)\,, \qquad (2.49)$$

where we used eqns. (2.45) and (2.46). The *power spectrum* $P_v(k)$ is the quantity of interest, so we shall evaluate it at superhorizon scales $k^{-1} \gg (aH)^{-1}$, where the scalar perturbations do not evolve anymore. Recalling (2.10) that in de Sitter space $\tau = -(aH)^{-1}$, and making use of eqn. (2.44),

$$P_v(k) = \lim_{k\tau \to 0} |v_k(\tau)|^2 = \lim_{k\tau \to 0} \frac{1}{2k}\left(1 - \frac{1}{(k\tau)^2}\right) = \frac{(aH)^2}{2k^3}\,. \qquad (2.50)$$

This power spectrum was derived for any field satisfying the Mukhanov-Sasaki equation in de Sitter space. One just needs to rescale the Mukhanov variable correspondingly to obtain the power spectrum of any field.

In perfect de Sitter space, $\varepsilon = 0$, and therefore $z = 0$, so that the curvature perturbation $\mathcal{R} = v/z$ would be ill-defined. In a perfect de Sitter universe expansion is eternal, and perturbations make little sense. However, we know inflation will eventually end and therefore perturbations will become meaningful, while the spacetime during inflation departs slightly from the idealised de Sitter spacetime. Therefore, we take this deviation as a expansion on the small slow roll parameter ε.

Considered that, we can compute now the power spectrum of the comoving curvarture perturbations

$$P_{\mathcal{R}}(k) = \frac{1}{z^2} P_v(k) = \frac{1}{4M_{\text{Pl}}^2 k^3} \frac{H^2}{\varepsilon} = \frac{1}{2k^3} \frac{H^4}{\dot{\phi}^2} \tag{2.51}$$

which remains constant (for a fixed k) once the k-mode exited the horizon, i.e., when $k = aH$. That means, we can evaluate H and $\dot{\phi}$ at the time when $aH = k$, and therefore all quantities in $P_{\mathcal{R}}(k)$ will depend only on k. This will also be the spectrum of perturbations at horizon re-entry. It is also conventional to express the power spectrum in its dimensionless form

$$\Delta_s^2(k) \equiv \frac{k^3}{2\pi^2} P_{\mathcal{R}}(k) = \frac{1}{8\pi^2 M_{\text{Pl}}^2} \frac{H^2}{\varepsilon}\bigg|_{k=aH}. \tag{2.52}$$

H and ε are still expected to evolve slightly with time, therefore the amplitude of the spectrum will not be the same for all scales, since bigger scales exit the horizon at early stages of inflation, while the smallest exit the horizon just before reheating. To measure the (small) scale dependence of the spectrum, one defines the *scalar spectral index n_s*

$$n_s - 1 \equiv \frac{\mathrm{d}\ln\Delta_s^2}{\mathrm{d}\ln k}, \tag{2.53}$$

with $n_s = 1$ corresponding to scale invariance. Usually the spectrum is expressed as a power law, simply integrating eqn. (2.53),

$$\Delta_s^2(k) = A_s(k_\star) \left(\frac{k}{k_\star}\right)^{n_s(k_\star)-1} \tag{2.54}$$

where $k_\star$ is the *pivot scale* or reference scale (one of the integration limits). This pivot scale is usually taken to be the CMB scales, since it is for that scale for which we can measure the amplitude A_s and the spectral index n_s. Think of it as some kind of Taylor expansion around a value accessible by experiments, valid to a good approximation for slowly varying H and ε.

We can split the right hand side of eqn. (2.53) into two factors

$$\frac{\mathrm{d}\ln\Delta_s^2}{\mathrm{d}\ln k} = \frac{\mathrm{d}\ln\Delta_s^2}{\mathrm{d}N} \times \frac{\mathrm{d}N}{\mathrm{d}\ln k}. \tag{2.55}$$

The first one is[7]

$$\frac{\mathrm{d}\ln\Delta_s^2}{\mathrm{d}N} = \frac{\mathrm{d}}{\mathrm{d}N}\left[2\ln H - \ln(8\pi^2) - \ln\varepsilon\right] = \frac{2}{H}\frac{\mathrm{d}H}{\mathrm{d}N} - \frac{1}{\varepsilon}\frac{\mathrm{d}\varepsilon}{\mathrm{d}N} = 2\varepsilon - 2(\eta - \varepsilon) = 4\varepsilon - 2\eta \tag{2.56}$$

---

[7]We recover the definitions of the slow roll parameters in eqns. (2.5) and (2.26). In the case of the first one

$$\varepsilon = -\frac{\dot{H}}{H^2} = -\frac{1}{H}\frac{\mathrm{d}H}{H\mathrm{d}t} = \frac{1}{H}\frac{\mathrm{d}H}{\mathrm{d}N}.$$

while for the second we use the fact that $k = aH$ and retrieve $a(N)$ from (2.6)

$$\mathrm{d}\ln k = \mathrm{d}\ln a + \mathrm{d}\ln H = -N + \mathrm{d}\ln H \tag{2.57}$$

and so

$$\frac{\mathrm{d}N}{\mathrm{d}\ln k} = \left[\frac{\mathrm{d}\ln k}{\mathrm{d}N}\right]^{-1} = \left[-1 + \frac{\mathrm{d}\ln H}{\mathrm{d}N}\right]^{-1} = [-1 + \varepsilon]^{-1} = -1 - \varepsilon + \mathcal{O}(\varepsilon^2). \tag{2.58}$$

We can therefore express the spectral index exclusively in terms of the slow roll parameters as

$$n_s = 1 + (4\varepsilon - 2\eta)\left(-1 - \varepsilon + \mathcal{O}(\varepsilon^2)\right) = 1 - 4\varepsilon + 2\eta + \mathcal{O}(\varepsilon^2, \varepsilon\eta) \simeq 1 - 6\varepsilon_V + 2\eta_V \tag{2.59}$$

as well as in terms of the potential slow roll parameters defined in eqns. (2.28) and (2.30). Note that all these quantities must be evaluated at the time when the mode exits the horizon, $aH = k$, to give $n_s(k)$ as just a function of k.

2.3.2   Tensor perturbations

The only tensor perturbation was that of the metric of the 3-hypersurfaces h_{ij}, whose Fourier decomposition is

$$h_{ij}(\tau, \boldsymbol{x}) = \sum_{\varkappa} \int \frac{\mathrm{d}^3\boldsymbol{k}}{(2\pi)^{3/2}}\, h_{\boldsymbol{k}}^{\varkappa}(\tau)\, \epsilon_{ij}^{\varkappa}(k)\, \mathrm{e}^{\mathrm{i}\boldsymbol{k}\cdot\boldsymbol{x}}\,, \tag{2.60}$$

where $h_{\boldsymbol{k}}^{\varkappa}(\tau)$ are the Fourier or polarisation modes, $\epsilon_{ij}^{\varkappa}(k)$ the polarisation tensors, and $\varkappa = +$ or $\times$ the plus or cross polarisations. The polarisation tensors form an orthogonal basis for each k, such that $k^i \epsilon_{ij} = 0$ and $\varepsilon_{ij}^{\varkappa}(k)\varepsilon_{ij}^{\varkappa'}(k) = 2\delta_{\varkappa\varkappa'}$. As h_{ij}, the $\epsilon_{ij}(k)$ are traceless: $\epsilon_i^i = 0$.

As discussed before, the quantisation procedure works analogously for the scalar ones, with the difference that now we have two Mukhanov fields $v_{\boldsymbol{k}}^{\varkappa}(\tau)$, one for each polarisation, related to the Fourier modes $h_{\boldsymbol{k}}^{\varkappa}(\tau)$ through

$$v_{\boldsymbol{k}}^{\varkappa} = \frac{M_{\mathrm{Pl}}}{2}\, a\, h_{\boldsymbol{k}}^{\varkappa}\,. \tag{2.61}$$

Tensor power spectrum

The power spectrum of tensor perturbations $P_t(k)$ is given by the sum of both polarisations, each of which contributes equally

$$P_t(k) = 2\, P_h(k) = 2\left(\frac{2}{aM_{\mathrm{Pl}}}\right)^2 P_v(k) = \frac{4}{k^3}\frac{H^2}{M_{\mathrm{Pl}}^2}\bigg|_{k=aH}\,, \tag{2.62}$$

or in its dimensionless version

$$\Delta_t^2(k) = \frac{2}{\pi^2} \frac{H^2}{M_{\text{Pl}}^2} \bigg|_{k=aH}. \tag{2.63}$$

Analogously to the scalar spectral index, we can define a *tensor spectral index* n_t, again, with all quantities evaluated at the time when $k = aH$,

$$n_t(k) \equiv \frac{\text{d}\ln\Delta_t^2}{\text{d}\ln k} = \frac{\text{d}\ln\Delta_t^2}{\text{d}N} \times \frac{\text{d}N}{\text{d}\ln k} = 2\varepsilon \times \left(-1 - \varepsilon + \mathcal{O}(\varepsilon^2)\right) = -2\varepsilon + \mathcal{O}(\varepsilon^2) \simeq -2\varepsilon_V. \tag{2.64}$$

A conventional way of normalising the amplitude of tensor perturbations is with respect to the scalar perturbations,

$$r \equiv \frac{\Delta_t^2}{\Delta_s^2} = 16\varepsilon \simeq -8n_t. \tag{2.65}$$

2.4 Pseudoscalar Inflation

Let us now study a particular family of inflationary models: pseudoscalar inflation. It is a minimal modification of the standard single-field slow-roll inflation, by just adding a coupling of the inflaton field ϕ to a gauge field, described by the Lagrangian

$$\mathcal{L} = -\frac{1}{2} g^{\mu\nu} \partial_\mu\phi \, \partial_\nu\phi - V(\phi) - \frac{1}{4} F_{\mu\nu} F^{\mu\nu} - \frac{1}{4\Lambda} \phi \, F_{\mu\nu} \tilde{F}^{\mu\nu}, \tag{2.66}$$

where

$$F_{\mu\nu} \equiv \nabla_\mu A_\nu - \nabla_\nu A_\mu = \partial_\mu A_\nu - \partial_\nu A_\mu \tag{2.67}$$

is the field strength tensor of the gauge field A_μ, $\tilde{F}^{\mu\nu} \equiv \frac{1}{2}\tilde{\varepsilon}^{\mu\nu\rho\sigma} F_{\rho\sigma}$ is its dual, and $\tilde{\varepsilon}_{\alpha\beta\gamma\delta} = (-g)^{1/2}[\alpha\beta\gamma\delta]$ and $\tilde{\varepsilon}^{\alpha\beta\gamma\delta} = g^{-1}\tilde{\varepsilon}_{\alpha\beta\gamma\delta}$ are the generalised totally antisymmetric Levi-Civita tensors in curved spacetimes [4]. Since we will mostly work with the metric (1.6) conformal to flat space, we will usually work with the flat Levi-Civita tensors $\varepsilon^{\alpha\beta\gamma\delta}$ and factor out the determinant, such that $\tilde{\varepsilon}^{\alpha\beta\gamma\delta} = (-g)^{-1/2}\varepsilon^{\alpha\beta\gamma\delta}$, with $\varepsilon^{0123} = +1$.

In this work we will identify the gauge group with the hypercharge sector U(1) of the Standard Model. This will allow generate baryons as we will see in the next chapters.

In the next part, we change notation. Given the pseudoscalar nature of the coupling, we identify it with an pseudo-Nambu-Goldstone boson. Therefore, we label the inflaton with a. We then accordingly relabel the scale factor as $R(t)$ or $R(\tau)$.

Chapter 3

Baryogenesis

Antimatter exists and is a direct consequence of combining two very fundamental theories in physics: quantum mechanics and the theory of relativity. In a universe with a thermal expansion, such as one ours, there is a point in time at which the temperatures are high enough to have both matter and antimatter, in pair-creation and annihilation processes in thermal equilibrium. When the temperature drops enough, the pair-creation processes stop and particles and antiparticles annihilate each other until only photons are left[1]. Or at least that would be the case in a symmetric universe. But here we are. So our universe cannot be a symmetric one.

Let us call ourselves matter, as it is conventional; more precisely, we are made of baryons. Then, there must have been an asymmetric initial condition before the baryon-antibaryon—or, rather, quark-antiquark—annihilation, at temperatures $T \gtrsim 1\,\mathrm{GeV}$, with more baryons than antibaryons. Let us measure that asymmetry as the difference in number of baryons and antibaryons relative to the total number

$$\frac{N_B - N_{\bar{B}}}{N_B + N_{\bar{B}}}\bigg|_{T \gtrsim 1\,\mathrm{GeV}} . \tag{3.1}$$

This would be the *baryon asymmetry of the universe* (BAU) in the primordial plasma.

However, the sum of baryons and antibaryons $N_B + N_{\bar{B}}$ is not directly accessible to us, so we need a better quantity to measure the BAU. Particles and antiparticles annihilate into photons, and, in a universe with just expansion, the ratio

$$\frac{N_B - N_{\bar{B}}}{N_\gamma} \tag{3.2}$$

would be of the same order than that in eqn. (3.1), with expansion just diluting the density (not the number) of (anti)baryons and photons with expansion. However, processes such as electron-positron annihilation and the annihilation of baryons and

---

[1]And a few lonely particles and antiparticles which could not find each other because of the expansion of the universe.

antibaryons itself changes N_γ all the way from $T \sim 1\,\text{GeV}$ till today $T_0 \sim 0.2\,\text{meV}$. Despite that, the change is altogether not so relevant and we can still define

$$\eta_B^0 \equiv \left.\frac{N_B - N_{\bar{B}}}{N_\gamma}\right|_{T_0} \simeq \left.\frac{N_B - N_{\bar{B}}}{N_\gamma}\right|_{T_0} \sim \left.\frac{N_B - N_{\bar{B}}}{N_B + N_{\bar{B}}}\right|_{T \gtrsim 1\,\text{GeV}} . \tag{3.3}$$

Typically, the number of baryons and photons is divided by the volume, such that η_B is given in terms of number densities instead

$$\eta_B^0 = \frac{n_B - n_{\bar{B}}}{n_\gamma} . \tag{3.4}$$

At the time in the evolution of the universe in which the lightest nuclei are formed, called the *Big Bang nucleosynthesis* (BBN) at temperatures $T_{\text{BBN}} \sim 1\,\text{MeV}$, the abundance of baryons (more precisely, nucleons), is a key parameter of the thermonuclear reactions. From the measured present-day abundance of primordial nuclei, mostly from that of deuterium, we find some bounds for this baryon asymmetry of [5]

$$5.8 \times 10^{-10} \leq \eta_B^{\text{BBN}} \leq 6.6 \times 10^{-10} \qquad (95\% \text{ CL}) . \tag{3.5}$$

On the other hand, the baryon asymmetry also affects the power spectrum of temperature fluctuations in the CMB. Seeded in principle by inflation, inhomogeneities in density create certain gravitational potential wells of dark matter around which the baryon-photon plasma oscillates, what is called *baryon acoustic oscillations*. These oscillations can be measured through the relative hight of the peaks of the CMB temperature spectrum. The latest CMB observations give a density parameter for baryons $\Omega_b h^2 = 0.0223 \pm 0.0002$ [3] which corresponds to [5]

$$\eta_B^{\text{CMB}} = (6.09 \pm 0.06) \times 10^{-10} . \tag{3.6}$$

This shows a nice agreement in this quantity at two different epochs (energy scales), which points out the reliability of these values.

3.1   General conditions for baryogenesis

So now we are sure there is an asymmetry, let us have a look at how it must be originated. There are three necessary conditions for producing more baryons than antibaryons, i.e., for successful baryogenesis. These are the so-called *Sakharov conditions* [30]:

(i) baryon number B violation,

(ii) C and CP violation,

(iii) deviation from thermal equilibrium.

The first condition is straightforward—without a baryon number violating process, it is not possible for a system to go from a $B = 0$ to a $B \neq 0$ state. Second, if C (or CP) hold, then all process involving the creation of particles would have a C (or CP) conjugate which creates antiparticles with the same probability. And third, thermal equilibrium correspond to time translation invariance and therefore the expectation values do not change; if we want B to change, we need to depart from equilibrium.

The Sakharov conditions can be fulfilled within the Standard Model and cosmology [31]. The baryon number is violated by non-perturbative effects. C and CP violating interactions are present: the weak interactions violate parity, and the complex phase of the Cabibbo-Kobayashi-Maskawa violates CP. The expansion of the universe, finally is a deviation from thermal equilibrium itself.

However, given the nature of these couplings and the thermal evolution of our universe[2], the Standard Model (and cosmology) fail to produce enough baryon asymmetry.

In section 4.2 a mechanism is presented which uses physics of the Standard Model only, but succeeds producing the right amount of baryons. It relies on the chiral anomaly of the standard model as well as on an particular initial condition: maximally helical hypermagnetic fields at the time of electroweak symmetry breaking. This initial condition is automatically given by models of pseudoscalar inflation coupled to the Standard Model U(1) gauge group.

---

[2]Here we refer to the second order phase transition that undergoes our universe, instead of first transition which would allow successful baryogenesis via sphaleron processes.

Part II

Our work

Chapter 4

Introduction

In this paper, we are going to study general models of pseudoscalar inflation and their implications for the present-day spectrum of gravitational waves as well as for baryogenesis via primordial hypermagnetic fields around the time of electroweak symmetry breaking (EWSB). In the following, we will review the status of gravitational waves from pseudoscalar inflation in Sec. 4.1 and baryogenesis after primordial magnetogenesis in Sec. 4.2. Readers familiar with both subjects may directly skip to Sec. 4.3, where we outline the philosophy behind our analysis.

4.1 Gravitational waves from an anomalous inflaton coupling to gauge fields

The celebrated detection of gravitational waves (GWs) from a binary black hole merger by the LIGO/Virgo collaboration [32] (see also [33,34]) has literally ringed in the era of gravitational-wave astronomy. In the near future, GW experiments will develop into standard observational tools, allowing us to routinely observe — or better: listen to — a variety of astrophysical phenomena. But also from the perspective of particle physics and cosmology, the observation of GWs bears a huge potential. In particular, the stochastic background of cosmological GWs emitted during the early universe carries invaluable information on physical processes at extremely high energies that are hard or even impossible to access by other means [35]. Among the different possible mechanisms to generate GWs in the early universe, a prime example is cosmic inflation [7–11], which unavoidably results in the amplification of the quantum vacuum fluctuations of the gravitational field [14, 36, 37]. In fact, the direct observation of relic GWs from the epoch of inflation would represent a powerful probe of the earliest moments of our Universe, complementary to other observables that are sensitive to the dynamics of inflation, such as, e.g., the temperature anisotropies of the cosmic microwave background (CMB). Standard single-field slow-roll inflation, however, predicts a present-day GW spectral energy density, $\Omega_{\mathrm{GW}}^0 h^2 (f)$, that falls short of the

current experimental sensitivity by many orders of magnitude,[1]

$$\Omega_{\rm GW}^0 h^2 (f) \sim 10^{-16} \left(\frac{r}{0.1} \right) , \tag{4.1}$$

where the primordial tensor-to-scalar ratio r is bounded from above by the CMB observations of the PLANCK satellite, $r < 0.11$ (95 % C. L.) [40]. This estimate needs to be contrasted with the sensitivity of the Advanced LIGO detector after its first run, $\Omega_{\rm GW}^0 h^2 (f) \sim 10^{-7}$ (95 % C. L., at its most sensitive frequencies, $f \simeq 20 \cdots 86\,{\rm Hz}$) [41]. This sensitivity is certainly an achievement, but still at least nine orders of magnitude away from the expected signal from inflation. Meanwhile, future satellite experiments such as DECIGO [42, 43] and BBO [44, 45] promise to reach sensitivities that might suffice to detect GWs from inflation at $\mathcal{O}(0.1 \cdots 1)$ Hz. But the realization of these experiments is still uncertain and possibly several decades away.

In view of this situation, one is tempted to ask what mechanism could potentially enhance the GW signal from inflation. Here, an interesting possibility — that has recently received renewed attention in the literature [46, 47] — is the boosted production of GWs in models of pseudoscalar inflation [48, 49]. This class of inflationary models is built upon the idea that inflation is driven by the dynamics of a pseudoscalar pseudo-Nambu-Goldstone boson (PNGB) [50, 51].[2] Such fields correspond to pseudoflat directions in field space, the flatness of which is protected against radiative corrections by an approximate shift symmetry. For this reason, axion-like directions provide a *natural* opportunity to realize slow-roll inflation. The axionic shift symmetry in models of pseudoscalar inflation may, in particular, correspond to the nonlinear realization of an approximate, Peccei-Quinn-like global symmetry $G_{\rm global}$. Furthermore, if this global symmetry is anomalous under some local gauge symmetry $G_{\rm gauge}$, the inflaton, a, will couple to the field strength tensor of the corresponding gauge field via an effective Chern-Simons term,

$$\mathcal{L}_{\rm eff} \supset -\frac{a}{4\,\Lambda} \, F_{\mu\nu} \tilde{F}^{\mu\nu} , \tag{4.2}$$

where $\tilde{F}^{\mu\nu}$ denotes the dual field strength tensor, $\tilde{F}^{\mu\nu} = \frac{1}{2} \left(-g\right)^{-1/2} \epsilon^{\mu\nu\sigma\tau} F_{\sigma\tau}$, and where the suppression scale Λ is related to the spontaneous symmetry breaking scale of $G_{\rm global}$. Similarly, an effective coupling such as in Eq. (4.2) may arise in compactifications of string theory [56]. In heterotic string theory, e.g., the Green-Schwarz mechanism of anomaly cancellation [57] gives rise to several (model-dependent as well as model-independent) axions that couple to the gauge fields of the theory as in Eq. (4.2); see [58] for a discussion in the context of pseudoscalar inflation.

---

[1]This estimate depends on the reheating temperature, $T_{\rm rh}$, after inflation. For $T_{\rm rh} \lesssim \mathcal{O}\left(10^9\right)$ GeV, one expects that the GW energy density at frequencies in the $\mathcal{O}(10 \cdots 100)$ Hz range is further diluted — and hence suppressed w.r.t. Eq. (4.1) — during the stage of expansion dominated by the coherent oscillations of the inflaton field [38, 39].

[2]The typical example for a PNGB in physics beyond the standard model is the QCD axion [52, 53] in the Peccei-Quinn solution to the strong CP problem [54, 55]. PNGBs in extensions of the standard model are, therefore, also often referred to as axion-like particles or simply axions. In the following, we will use these terms interchangeably.

The anomalous coupling in Eq. (4.2) now has important implications for the dynamics of inflation and, eventually, for the present-day spectrum of GWs. To see this, one first has to note that the axion-gauge-field coupling in Eq. (4.2) results in the explosive production of gauge quanta during inflation [59–61] (see also [62, 63]). Depending on the sign of the inflaton velocity, $\dot{a}$, one of the two helicity modes of the gauge field is exponentially amplified, such that the resulting field configuration is maximally helical. This is a direct consequence of the fact that the time-dependent vacuum expectation value (VEV) of the inflaton field breaks parity invariance during inflation, $\langle \dot{a} \rangle \neq 0$. As the energy transmitted to the gauge field increases, the gauge field begins to back-react on the evolution of the inflaton, effectively contributing another friction term (next to the Hubble friction term) to its equation of motion [64–66]. At the same time, fluctuations in the gauge field configuration result in additional source terms for the primordial scalar and tensor perturbations. Together, these effects have a variety of phenomenological consequences, ranging from modified predictions for various CMB observables [58, 67–69], over the production of primordial black holes [69–72], to — and here we finally are — an enhanced spectrum of GWs [46–49].

Recently, it has been pointed out that the GW signal from pseudoscalar inflation may be even amplified to such an extent that it falls into the sensitivity reach of upcoming GW interferometer experiments [46, 47]. Here, a particularly promising inflation model appears to be Starobinsky inflation [11], which could potentially lead to observable GWs over a vast range of frequencies. This prediction, however, relies on the assumption of a strong axion coupling, $M_{\rm Pl}/\Lambda \sim \mathcal{O}\,(100)$, such that the energy stored in the gauge field begins to dominate the total energy budget towards the end of inflation. As long as the backreaction from the gauge field on the inflationary dynamics remains at a perturbative level at all times, a significantly weaker GW signal is expected.

4.2 Baryogenesis from decaying (hyper)magnetic helicity

The prospect of a sizable GW signal from pseudoscalar inflation entails the question as to what other observable signatures one might hope for. Thanks to the rich phenomenology of this inflationary scenario, it should be possible to correlate the strength of the expected GW signal to other observables. In particular, one would like to know in which case one should either expect a strong or only a rather weak signal in GWs. In this context, an interesting feature of pseudoscalar inflation supplemented by a coupling to gauge fields is the production of primordial gauge fields towards the end of inflation [59–61]. In fact, if the gauge symmetry $G_{\rm gauge}$ is identified with the standard model hypercharge gauge group, $U(1)_Y$, the primordial hypermagnetic fields generated during inflation might act as seeds for the ubiquitous, intergalactic magnetic fields that permeate our Universe today [73, 74]. Interestingly enough, deficits of secondary cascade photons from TeV blazars have recently been identified, which can be explained by intergalactic magnetic fields [75–81]. Pseudoscalar inflation coupled

to the standard model hypercharge sector, therefore, offers an exciting opportunity for *primordial magnetogenesis* [82], which can in principle be tested by more detailed observations of intergalactic magnetic fields.

Moreover, the primordial (hyper)magnetic fields generated during pseudoscalar inflation allow to generate a primordial baryon asymmetry around the time of EWSB [83–85]. The key ingredient in this scenario of baryogenesis is the chiral triangle anomaly in the standard model, which relates changes in the global baryon number B as well as in the global lepton number L to changes in the Chern-Simons numbers in the electroweak sector,[3]

$$\Delta B = \Delta L = N_g \left(\Delta N_{\mathrm{CS}}^W - \Delta N_{\mathrm{CS}}^Y \right) , \quad \Delta N_{\mathrm{CS}}^Y = \frac{g_Y^2}{16\pi^2} \Delta \mathcal{H} . \tag{4.3}$$

Here, $N_g = 3$ denotes the number of fermion generations in the standard model, while N_{CS}^W and N_{CS}^Y stand for the Chern-Simons numbers associated with the $SU(2)_W$ and $U(1)_Y$ gauge fields, respectively.[4] Eq. (4.3) illustrates the well-known fact that $SU(2)_W$ instanton and sphaleron transitions, which correspond to jumps in the non-Abelian Chern-Simons number N_{CS}^W, violate both B and L. But at the same time, Eq. (4.3) also indicates that both B and L can be generated (or destroyed) by changes in the hypermagnetic helicity $\mathcal{H}$. And in fact, in the presence of a maximally helical hypermagnetic field generated during pseudoscalar inflation, this is exactly what happens at temperatures around the electroweak scale: The hypermagnetic field is converted into the electromagnetic (EM) field and, as a consequence, the helicity carried by the hypermagnetic field is transferred to the one carried by the EM field. This corresponds to the decay of the net hypermagnetic helicity $\mathcal{H}$, which, in turn, generates a nonzero baryon number according to the relation in Eq. (4.3). This mechanism of *baryogenesis via primordial (hyper)magnetic fields* has recently received quite some attention in the literature [88–92] (see also [93, 94]).

In the following, we will adopt the results of [91], which represents the most comprehensive study of this scenario of baryogenesis at the electroweak scale so far. The authors of [91] use recent results from magnetohydrodynamic (MHD) simulations [74, 95] to model the evolution of the magnetic field. In particular, they account for the inverse cascade behavior of the magnetic field below a certain critical temperature, which is characterized by the transfer of power from small scales to large scales [96–98]. Moreover, they include all of the standard model Yukawa interactions as well as the chiral magnetic effect [61, 99]. This is essential to correctly assess the efficiency of $SU(2)_W$ sphaleron processes in washing out the previously generated baryon number.

---

[3]Both baryon and lepton number also exhibit a gravitational anomaly, which can likewise be used to construct scenarios of baryogenesis [86, 87]. In our analysis, the gravitational anomaly will, however, play no role.

[4]Of course, only N_{CS}^W represents a Chern-Simons number in the actual sense, for only the weak isospin gauge sector with non-Abelian gauge group $SU(2)_W$ possesses a topologically nontrivial vacuum structure. In the hypercharge gauge sector, the Chern-Simons number N_{CS}^Y is, by contrast, understood to be related to the hypermagnetic helicity $\mathcal{H}$, which accounts for topologically nontrivial configurations (knots) of the hypermagnetic gauge field.

Finally, the authors of [91] model the gradual conversion of the hypermagnetic field into an EM field during EWSB, i.e., during the electroweak crossover, $\boldsymbol{B}_Y \to \boldsymbol{B}_{\mathrm{EM}}$, in terms of a temperature-dependent weak mixing angle $\theta_W(T)$. In this respect, the analysis in [91] differs drastically from related works, which simply assume that both the generation of baryon number as well as the $SU(2)_W$ sphalerons shut off simultaneously at temperatures around the electroweak scale. As shown in [91], this assumption turns out to be an oversimplification, which basically corresponds to treating the electroweak crossover as a first-order phase transition. In actual fact, the conversion of the hypermagnetic field into the EM field is accompanied by a strong variation in the hypermagnetic helicity and, thus, responsible for an enhanced generation of baryon number. Likewise, one must take into account that also the emerging EM field still participates in redistributing the total baryon number, as it communicates B violation in the left-handed fermions to the right-handed fermions. Taken all together, the authors of [91] find that successful baryogenesis is feasible, as long as the present-day magnetic field exhibits a certain physical strength, B_p^0, as well as a certain physical correlation length, λ_p^0,

$$B_p^0 \sim 10^{-17} \cdots 10^{-16}\,\mathrm{G}\,, \quad \lambda_p^0 \sim 10^{-3} \cdots 10^{-2}\,\mathrm{pc}\,, \tag{4.4}$$

and a positive maximal helicity. Note that these values satisfy the relation one expects for magnetic fields that undergo the direct/inverse cascade process, $B_p^0 = 10^{-14}\,\mathrm{G}\left(\lambda_p^0/0.3\,\mathrm{pc}\right)$ [100].[5] At the same time, they, however, come with an uncertainty of at least one order of magnitude because of the current theoretical uncertainties in modeling the exact evolution of the electroweak crossover. In the following, we will use the numbers in Eq. (4.4) as a benchmark, keeping in mind that they merely convey an idea of the correct orders of magnitude. Besides that, our final results can be readily carried over to other values of B_p^0.

4.3 Correlation between gravitational waves and successful baryogenesis

As outlined in Sec. 4.1, pseudoscalar inflation anomalously coupled to the gauge fields of some gauge group G_{gauge} results in the enhanced production of primordial GWs. Here, the identification of G_{gauge} with some non-Abelian group results in the scenario of chromo-natural inflation [101–104] (see also Ref. [105]). The description of an inflaton coupling to non-Abelian fields is, however, slightly more challenging; and hence we shall focus on the Abelian case in this work, for simplicity. Furthermore,

---

[5]In this paper, we are going to work in *natural Lorentz-Heaviside units*, in which $\hbar = c_0 = \epsilon_0 = 1$. These are the typical units of particle physics, where the electrical charge e is supposed to be related to the fine structure constant α as $e = \sqrt{4\pi\alpha}$. This means that $1\,\mathrm{G} = 6.91 \times 10^{-20}\,\mathrm{GeV}^2\,(4\pi\epsilon_0)^{-1/2}\,(\hbar c_0)^{-3/2} = 1.95 \times 10^{-20}\,\mathrm{GeV}^2$. In *natural Gaussian CGS units*, one has by contrast $\hbar = c_0 = 4\pi\epsilon_0 = 1$, such that $e = \sqrt{\alpha}$ and $1\,\mathrm{G} = 6.91 \times 10^{-20}\,\mathrm{GeV}^2$. To convert from our units to CGS units, one simply has to replace $1\,\mathrm{G} \to (4\pi)^{-1/2}\,\mathrm{G}$. Meanwhile, the conversion from parsec to inverse GeV is unambiguous and identical in both unit systems, $1\,\mathrm{pc} = 1.56 \times 10^{32}\,\mathrm{GeV}^{-1}$.

among all conceivable Abelian gauge groups that the inflaton could couple to, the standard model hypercharge, $U(1)_Y$, certainly plays a preeminent role. With $U(1)_Y$ being the only Abelian gauge group in the standard model, an inflaton coupling to the hypercharge sector may be regarded as a *most minimal* departure from the standard model. A coupling to any other gauge symmetry, such as, e.g., $U(1)_{B-L}$, would by contrast require the introduction of new gauge degrees of freedom (DOFs). Moreover, coupling pseudoscalar inflation to the hypercharge sector also offers an intriguing possibility for primordial magnetogenesis, which can be tested by the observations of the present intergalactic magnetic fields, as well as for baryogenesis from the decay of (hyper)magnetic helicity; see the discussion in Sec. 4.2. For these reasons, we deem the identification $G_{\mathrm{gauge}} \to U(1)_Y$ the most interesting choice. In contrast to any hidden gauge symmetries beyond the standard model, an inflaton coupling to $U(1)_Y$ is slightly less speculative and, at the same time, more predictive in terms of observable consequences.

In this paper, we are, therefore, going to focus on general models of pseudoscalar inflation supplemented by a Chern-Simons-type interaction between the inflaton and the hypermagnetic gauge field. In particular, we are going to address the following two questions:

(1) Under what conditions does pseudoscalar inflation result in a (hyper)magnetic field of just the right magnitude, such that primordial magnetogenesis at the end of inflation sets the stage for successful baryogenesis at the electroweak scale? That is, how does one need to choose the parameters of pseudoscalar inflation in order to satisfy the two conditions in Eq. (4.4)? In this part of our analysis, we are basically going to update previous studies of *baryogenesis from pseudoscalar inflation* [88, 92] (see also [106]). By employing the results presented in [91], we make sure to include several important effects that had been neglected up to this point (such as, e.g., the inverse cascade regime, the chiral magnetic effect, and the role of the standard model Yukawa interactions). In doing so, we will work in the approximation of instant reheating, for simplicity. In principle, both magnetic fields and gravitational waves are also produced during the stage of reheating [106–108]. The correct description of this phase, however, requires a dedicated numerical simulation that includes both nonperturbative particle production and MHD. In particular, one should take into account the backreaction on the gauge field production from the hypercharged particles in the emerging plasma. Such a study is not yet available, which is why we will ignore the details of the reheating phase altogether. On the one hand, the approximation of instant reheating introduces some (perhaps very large) uncertainties into our analysis.[6] On the other

---

[6]The lattice simulation in [106], e.g., indicates a large enhancement of hypermagnetic fields at the stage of reheating. On the contrary, the authors of [108] point out the necessity of a relatively low reheating temperature in order to avoid high electric conductivity, which would otherwise prevent hypermagnetic helicity from developing during reheating. However, a low reheating temperature automatically comes with a large dilution of the hypermagnetic field. From this perspective, one would therefore rather expect a suppression than an enhancement from reheating. In the following, we will evade the (still on-going) debate which of these conclusions is correct and simply neglect any contributions to the hypermagnetic field from reheating. Instead, we will simply focus on the gauge

hand, it allows us to remain absolutely model-independent, as far as the concrete dynamics of inflation and reheating are concerned. Against this background, we hope that our analysis may motivate further studies of reheating after pseudoscalar inflation that account for the complicated interplay between gauge field production and the properties of the emerging charged plasma.

(2) What are the implications of successful baryogenesis for the present-day GW spectrum? Assuming that primordial magnetogenesis results in magnetic fields in accord with Eq. (4.4), is there still a chance to obtain GWs that could be detected in GW experiments in the near future?

To answer these questions, we will now proceed as follows: In Sec. 5, we will first review the production of hypermagnetic fields in models of pseudoscalar inflation. We will discuss in particular the dependence on the suppression scale Λ as well as the backreaction on the inflationary dynamics. In Sec. 6, we will then study the evolution of the primordial hypermagnetic fields from the time of their production all the way to the present epoch. In Sec. 7, we will in turn study the implications for baryogenesis as well as for the GW spectrum. Here, our main interest will be to establish a connection between successful baryogenesis and the expected strength of the GW signal from inflation. In Sec. 8, we will finally illustrate some of our main results numerically by means of a concrete example, based on the original model of natural inflation [50, 51]. Sec. 9 contains our conclusions as well as a brief outlook on how our work could be continued.

---

field production during inflation. In this sense, our estimate is a quantitatively conservative one.

Chapter 5

Gauge field production during inflation

We begin by reviewing the mechanism of gauge field production in models of pseudoscalar inflation [59–61]. This will also serve the purpose to establish our notation and conventions.

5.1 Equations of motion for the inflaton and gauge fields

For an arbitrary model of pseudoscalar inflation coupled to the standard model hypercharge sector via an effective Chern-Simons term, the relevant Lagrangian takes the following form,

$$\mathcal{L} \supset -\frac{1}{2}\partial_\mu a\,\partial^\mu a - \frac{1}{4}F_{\mu\nu}F^{\mu\nu} - V(a) - \frac{a}{4\Lambda}F_{\mu\nu}\tilde{F}^{\mu\nu}\,. \tag{5.1}$$

Here, the field a denotes the axion-like pseudoscalar inflaton; $F_{\mu\nu} = \partial_\mu A_\nu - \partial_\nu A_\mu$ is the field strength tensor belonging to the hypercharge gauge field A_μ; and $\tilde{F}^{\mu\nu}$ is the dual field strength tensor, $\tilde{F}^{\mu\nu} = \frac{1}{2}\left(-g\right)^{-1/2}\epsilon^{\mu\nu\sigma\tau}F_{\sigma\tau}$. For the time being, we remain as model-independent as possible and do not specify the concrete form of the inflaton potential $V(a)$. Only in Sec. 8, we will become more explicit and identify $V(a)$ with the scalar potential of particular models of inflation. The last term in Eq. (5.1) represents the anomalous Chern-Simons interaction between the inflaton and the hypercharge gauge field. The parameter Λ denotes an effective suppression scale, the magnitude of which is related to the energy scale at which the anomalous coupling is generated. In the following, we will treat it as a free parameter. The combination a/Λ, i.e., the prefactor of the topological term $\frac{1}{4}F_{\mu\nu}\tilde{F}^{\mu\nu}$, may be regarded as an effective, field-dependent vacuum angle in the hypercharge sector, $\theta = a/\Lambda$. If we replaced a by a constant, θ would become unphysical and could be transformed away by a fermion rotation. However, with a being a dynamical field, the vacuum angle θ is physically meaningful; see also [109].

Given the Lagrangian in Eq. (5.1), one obtains for the homogeneous Friedmann equation,

$$H^2 = \left(\frac{\dot{R}}{R}\right)^2 = \frac{\rho}{3M_{\mathrm{Pl}}^2}\,, \quad \rho = \frac{1}{2}\dot{a}^2 + V(a) + \frac{1}{2}\left\langle \boldsymbol{E}^2\right\rangle + \frac{1}{2}\left\langle \boldsymbol{B}^2\right\rangle. \tag{5.2}$$

Here, H is the Hubble rate; R denotes the scale factor in the Friedmann-Lemaître-Robertson-Walker metric, $ds^2 = -dt^2 + R^2(t)\,d\boldsymbol{x}^2 = -R^2(t)\left(d\tau^2 - d\boldsymbol{x}^2\right)$; ρ represents the total energy density; and $M_{\mathrm{Pl}} = (8\pi G)^{-1/2} = 2.44 \times 10^{18}\,\mathrm{GeV}$ is the reduced Planck mass. $\dot{R}$ stands for the derivative of the scale factor w.r.t. physical time t. Below, we will also encounter derivatives w.r.t. conformal time τ, which will be denoted by a prime. The total energy density ρ can be obtained from the stress-energy tensor. In addition to the usual contributions from the inflaton field, it now also receives contributions from the hyperelectric and hypermagnetic fields $\boldsymbol{E}$ and $\boldsymbol{B}$. We are going to work in radiation gauge, which combines the gauge fixing conditions of Coulomb (or transverse) gauge, $\boldsymbol{\nabla} \cdot \boldsymbol{A} = 0$, and Weyl (or temporal) gauge, $A_0 = 0$. The fields $\boldsymbol{E}$ and $\boldsymbol{B}$ are then related to the components of the hypercharge vector field A_μ as follows,

$$A_\mu = (A_0, \boldsymbol{A})\,, \quad \boldsymbol{E} = -\frac{1}{R^2}\,\partial_\tau \boldsymbol{A} = -\frac{1}{R^2}\,\boldsymbol{A}'\,, \quad \boldsymbol{B} = \frac{1}{R^2}\,\boldsymbol{\nabla} \times \boldsymbol{A}\,. \tag{5.3}$$

$\boldsymbol{E}$ and $\boldsymbol{B}$ are understood to represent *physical* field strengths, whereas A_μ is a *comoving* quantity that needs to be determined in dependence of the comoving coordinates $x^\mu = (\tau, \boldsymbol{x})$. The angle brackets in Eq. (5.2) denote the expectation values of $\boldsymbol{E}^2$ and $\boldsymbol{B}^2$, respectively. During inflation, these expectation values correspond to *quantum mechanical* vacuum expectation values. In order to determine the *classical* field strengths after inflation, we identify these quantum expectation values with the ensemble averages of the classical fields just at the end of inflation,

$$\langle \cdot \rangle_{\text{quantum vacuum}} \quad \overset{\text{end of inflation}}{\longrightarrow} \quad \langle \cdot \rangle_{\text{classical ensemble}}\,. \tag{5.4}$$

Similarly as the Friedmann equation, the equation of motion for the homogeneous inflaton field also turns out to receive corrections in presence of the anomalous axion-gauge-field coupling,

$$\ddot{a} + 3H\dot{a} + \frac{dV}{da} = \frac{1}{\Lambda}\left\langle \boldsymbol{E}\boldsymbol{B}\right\rangle. \tag{5.5}$$

Here, the new source term on the right-hand side may be regarded as an additional friction term (next to the usual Hubble friction term, $3H\dot{a}$). In the case of strong gauge field production, the source term eventually dominates over the Hubble friction term, which alters the inflationary dynamics towards end of inflation [64–66] (see also [46,47]). As we will see later on, this regime will be less relevant for our purposes, i.e., as long as we require successful baryogenesis.

The dynamics of the vector field are governed by the following wave equation,

$$\Box \boldsymbol{A} = -\boldsymbol{A}'' + \boldsymbol{\nabla}^2 \boldsymbol{A} = -\frac{a'}{\Lambda} \boldsymbol{\nabla} \times \boldsymbol{A} \,, \tag{5.6}$$

where the axion-gauge-field coupling induces again a source term on the right-hand side. To find the solution of this equation, it is convenient to perform a Fourier transform and work in momentum space. Upon quantization of the individual Fourier modes, $\boldsymbol{A}$ may be written as

$$\boldsymbol{A}\left(\tau, \boldsymbol{x}\right) = \sum_{\lambda=\pm} \int \frac{d^3 \boldsymbol{k}}{\left(2\pi\right)^{3/2}} \left[A_\lambda\left(\tau, \boldsymbol{k}\right) \boldsymbol{\epsilon}_\lambda\left(\boldsymbol{k}\right) \hat{a}_\lambda\left(\boldsymbol{k}\right) e^{i\boldsymbol{kx}} + \text{h.c.} \right] \,. \tag{5.7}$$

Here, $\lambda = \pm$ labels the two possible helicity states; $A_\pm$ denote the corresponding mode functions; $\boldsymbol{\epsilon}_\pm$ are the two polarization vectors; and $\hat{a}_\pm$ stand for the corresponding annihilation operators, which annihilate states $|\boldsymbol{k}, \lambda\rangle$ with 3-momentum $\boldsymbol{k}$ and polarization λ. The vectors $\boldsymbol{\epsilon}_\pm$ for given momentum $\boldsymbol{k}$ form an orthonormal basis in the complex vector space perpendicular to $\boldsymbol{k}$,

$$\boldsymbol{\epsilon}_\lambda\left(\boldsymbol{k}\right) \cdot \boldsymbol{\epsilon}_{\lambda'}^*\left(\boldsymbol{k}\right) = \delta_{\lambda\lambda'}\,, \quad \boldsymbol{\epsilon}_\lambda\left(\boldsymbol{k}\right) \cdot \boldsymbol{k} = 0\,, \quad i\boldsymbol{k} \times \boldsymbol{\epsilon}_\lambda\left(\boldsymbol{k}\right) = \lambda\,k\,\boldsymbol{\epsilon}_\lambda\left(\boldsymbol{k}\right)\,, \tag{5.8}$$

where $k = |\boldsymbol{k}|$. Meanwhile, the annihilation and creation operators, $\hat{a}_\lambda\left(\boldsymbol{k}\right)$ and $\hat{a}_\lambda^\dagger\left(\boldsymbol{k}\right)$, satisfy the usual canonical commutation relations, $\left[\hat{a}_\lambda\left(\boldsymbol{k}\right), \hat{a}_{\lambda'}^\dagger\left(\boldsymbol{k}'\right)\right] = \delta_{\lambda\lambda'}\,\delta^{(3)}\left(\boldsymbol{k} - \boldsymbol{k}'\right)$. Inserting the Fourier expansion in Eq. (5.7) into the equation of motion in Eq. (5.6) and using the relations in Eq. (5.8), one then obtains the following mode equations in momentum space,

$$\left[\frac{\partial^2}{\partial \tau^2} + k^2 \left(1 - \frac{x_\lambda\left(\xi\right)}{x\left(\tau, k\right)}\right)\right] A_\lambda\left(\tau, \boldsymbol{k}\right) = 0\,, \quad x\left(\tau, k\right) = -k\tau\,, \quad x_\lambda\left(\xi\right) = 2\lambda\,\xi\,, \tag{5.9}$$

where we have defined the *instability parameter* ξ as follows,

$$\xi = \frac{1}{2H} \frac{\dot{a}}{\Lambda}\,. \tag{5.10}$$

The mode equations are isotropic in momentum space, which is why we will label the mode functions only by their absolute momenta from now on, $A_\lambda\left(\tau, \boldsymbol{k}\right) \to A_\lambda^k\left(\tau\right)$. The parameter x in Eq. (5.9) quantifies whether, at a certain conformal time τ, a given mode with wavenumber k has a spatial extent (i.e., physical wavelength $\lambda_p = 2\pi R/k$) larger or smaller than the Hubble radius, H^{-1}. To see this, one simply has to recall that during inflation, i.e., in quasi-de Sitter space, τ is approximately given as $\tau \simeq -1/\left(RH\right)$. This readily implies $x \simeq 2\pi H^{-1}/\lambda_p$. The magnitude of x needs to be compared with x_λ, which is defined in terms of the instability parameter ξ. The parameter $x_\lambda = \lambda\,\dot{\theta}/H$ in Eq. (5.9) hence measures the rate of variation of the effective vacuum angle $\theta = a/\Lambda$ in relation to the Hubble rate H. With the above definitions, one also finds that $x_\lambda/x = \lambda\,k_{\text{crit}}/k$, where $k_{\text{crit}} = R\,\dot{\theta}$ is a certain critical (comoving) momentum scale. From the perspective of gauge field production, the quantities x_λ,

ξ, and k_{crit} vary only slowly with time. This is a direct consequence of the slow-roll motion of the field a during inflation. When solving the mode equations in Eq. (5.9), we will, therefore, treat x_λ at any given moment in time as a constant. This will provide us with solutions for the vector-field modes that are respectively valid during certain periods of inflation, when x_λ takes particular, approximately constant values. Other than that, we will make no further approximations when solving Eq. (5.9).

From Eq. (5.9), it is evident that, for $x < |x_\lambda|$, the helicity modes corresponding to positive x_λ become tachyonically unstable. A positive baryon asymmetry requires a positive (hyper)magnetic helicity [89–91]. In the following, we will therefore consider the case where $\dot{a} > 0$, such that $x_+ > 0$ and $x_- < 0$. In this case, the positive-helicity modes A_+^k will be tachyonically unstable at $x < x_+$.[1] Once x has dropped down to values smaller than x_+, the modes A_+^k begin to exponentially grow. The negative-helicity modes A_-^k experience, by contrast, only a shift in their dispersion relation towards effectively *larger* momenta, $k^2 \to k^2(1 + k_{\mathrm{crit}}/k)$. They, thus, always stay at the quantum level. For constant ξ, the exact solutions for $A_\pm^k$ are given in terms of Whittaker W functions (which are related to confluent hypergeometric functions) [113]. This is because Eq. (5.9) can be brought into a particular form of Whittaker's equation,

$$\left(\frac{d^2}{dz^2} - \frac{1}{4} + \frac{\kappa_\lambda}{z} \right) A_\lambda^k(z) = 0\,, \quad z = -2ix = 2ik\tau\,, \quad \kappa_\lambda = \frac{x_\lambda}{2i} = -i\lambda\xi\,. \quad (5.11)$$

We require that the modes $A_\pm^k$ reduce to the usual Bunch-Davis solution in the asymptotic past,

$$\lim_{-k\tau \to \infty} A_\lambda^k(\tau) = \frac{e^{-ik\tau}}{\sqrt{2k}}\,. \quad (5.12)$$

With this boundary condition, the Whittaker equation in Eq. (5.11) has the following solution,

$$A_\lambda^k(\tau) = \frac{e^{\lambda\pi\xi/2}}{\sqrt{2k}}\, W_{-i\lambda\xi,1/2}(2ik\tau)\,, \quad (5.13)$$

where $W_{-i\lambda\xi,1/2}$ is the Whittaker function $W_{\kappa,\mu}$ with indices $\kappa = \kappa_\lambda = -i\lambda\xi$ and $\mu = 1/2$. This function grows exponentially as a function of τ for $\lambda = +$ and remains oscillatory for $\lambda = -$.

5.2 Backreaction on the inflationary dynamics

In the previous section, we have seen how the axion-induced source term on the right-hand side of Eq. (5.6) manages to excite vector-field modes with positive helicity; see

---

[1]Conversely, in the case of negative inflaton velocity, $\dot{a} < 0$, we would have to deal with $x_- > 0$ and $x_+ < 0$. This would result in a negative helicity and, consequently, in a negative baryon asymmetry. For the inflationary dynamics, the sign of the induced helicity does not matter. Moreover, as long as the inflaton potential is invariant under parity, $a \leftrightarrow -a$, the sign of the inflaton velocity does not affect the inflationary dynamics as well.

Eq. (5.13). We shall now examine the consequence of this nonperturbative gauge field production for the inflationary dynamics. In the presence of a macroscopic gauge field configuration, the Friedmann and Klein-Gordon equations in Eqs. (5.2) and (5.5) need to be supplemented by the following expressions,

$$\rho_{EE} = \frac{1}{2} \left\langle \boldsymbol{E}^2 \right\rangle = \frac{1}{2R^4} \int \frac{d^3 \boldsymbol{k}}{(2\pi)^3} \left| \frac{\partial}{\partial \tau} A_+^k \right|^2 , \tag{5.14}$$

$$\rho_{BB} = \frac{1}{2} \left\langle \boldsymbol{B}^2 \right\rangle = \frac{1}{2R^4} \int \frac{d^3 \boldsymbol{k}}{(2\pi)^3} \, k^2 \left| A_+^k \right|^2 ,$$

$$\rho_{EB} = \frac{1}{2} \left\langle \boldsymbol{E}\boldsymbol{B} \right\rangle + \frac{1}{2} \left\langle \boldsymbol{B}\boldsymbol{E} \right\rangle = -\frac{1}{2R^4} \int \frac{d^3 \boldsymbol{k}}{(2\pi)^3} \, k \frac{\partial}{\partial \tau} \left| A_+^k \right|^2 ,$$

where we neglect the vacuum contributions from the negative-helicity modes. The quantities ρ_{EE} and ρ_{BB} have a direct interpretation in the sense that they correspond to the energy densities stored in the hyperelectric and hypermagnetic fields, respectively. The quantity ρ_{EB} is the corresponding cross term. We note that the $\boldsymbol{E}$ and $\boldsymbol{B}$ fields do *not* commute at the quantum level, which is why ρ_{EB} is defined as the symmetrized version of $\langle \boldsymbol{E}\boldsymbol{B} \rangle$. Technically, the right-hand side of Eq. (5.5) is understood to correspond to ρ_{EB}/Λ. In the classical limit, the commutator $[\boldsymbol{E}, \boldsymbol{B}]$, however, vanishes and ρ_{EB} and $\langle \boldsymbol{E}\boldsymbol{B} \rangle$ become equivalent to each other.

The energy densities in Eq. (5.14) are functions of the inflationary Hubble rate H as well as of the instability parameter ξ; see Eq. (5.10). To extract the dependence on these two parameters, it turns out convenient to rewrite the momentum integrals in Eq. (5.14) as follows,

$$\rho_{EE} = \mathcal{I}_{EE}\left(\xi\right) \frac{e^{2\pi\xi}}{\xi^3} H^4 , \quad \rho_{BB} = \mathcal{I}_{BB}\left(\xi\right) \frac{e^{2\pi\xi}}{\xi^5} H^4 , \quad \rho_{EB} = -\mathcal{I}_{EB}\left(\xi\right) \frac{e^{2\pi\xi}}{\xi^4} H^4 , \tag{5.15}$$

with the integral functions $\mathcal{I}_{EE}$, $\mathcal{I}_{BB}$ and $\mathcal{I}_{EB}$ being defined as

$$\mathcal{I}_{EE}\left(\xi\right) = \frac{\xi^3}{8\pi^2} e^{-\pi\xi} \int_0^{x_{\mathrm{UV}}} dx \, x^3 \left| \frac{\partial}{\partial x} W_{\kappa_+, 1/2}\left(-2ix\right) \right|^2 , \tag{5.16}$$

$$\mathcal{I}_{BB}\left(\xi\right) = \frac{\xi^5}{8\pi^2} e^{-\pi\xi} \int_0^{x_{\mathrm{UV}}} dx \, x^3 \left| W_{\kappa_+, 1/2}\left(-2ix\right) \right|^2 ,$$

$$\mathcal{I}_{EB}\left(\xi\right) = \frac{-\xi^4}{8\pi^2} e^{-\pi\xi} \int_0^{x_{\mathrm{UV}}} dx \, x^3 \frac{\partial}{\partial x} \left| W_{\kappa_+, 1/2}\left(-2ix\right) \right|^2 .$$

Here, we choose a sign convention such that all three functions are positive. The fact that ρ_{EB} actually takes negative values is accounted for by the explicit minus sign in Eq. (5.15). In principle, the momentum integrals in Eq. (5.14) are UV-divergent, as they receive vacuum contributions from an infinite number of high-frequency modes (i.e., modes deep inside the Hubble horizon). To regularize this divergence, we introduce a UV cut-off scale, $x_{\mathrm{UV}} = k_{\mathrm{UV}}/\left(RH\right)$, which allows us to integrate over

only those modes that are excited above the vacuum level. The natural choice for $x_{\rm UV}$ is consequently $x_{\rm UV} = x_+ = 2\xi$, such that the momentum cut-off $k_{\rm UV}$ coincides with $k_{\rm crit}$, i.e., the highest wavenumber that still leads to a tachyonic instability in Eq. (5.9).

In view of Eq. (5.16), it is also interesting to note that we absorbed the *explicit* time dependence of the vector-field modes $A_\pm^k(\tau)$ in Eq. (5.14) into the integration variable $x = -k\tau$. The remaining time dependence is then canceled by the time dependence of R^{-4} in front of the integrals in Eq. (5.14). At first glance, this renders all of the three quantities in Eq. (5.15) constant in time. However, there remains an *implicit* time dependence encoded in the parameters ξ and H, which actually slowly vary during inflation. In the following, we will determine ρ_{EE}, ρ_{BB}, ρ_{EB} at any time t during inflation simply by evaluating Eq. (5.15) for the respective values of $\xi(t)$ and $H(t)$. If we were to treat the time dependence of ξ and H more carefully, we would have to solve Eqs. (5.2), (5.5), and (5.9) simultaneously. Such an analysis is beyond the scope of this paper.

The advantage of the parametrization in Eq. (5.15) is that all of the three functions $\mathcal{I}_{EE}$, $\mathcal{I}_{BB}$, and $\mathcal{I}_{BE}$ asymptotically approach constant values at $\xi \gg 1$. This is depicted in Fig. 5.1, where we also demonstrate the sensitivity of the three integral functions to variations in the UV cut-off. As can be seen from Fig. 5.1, all three functions become insensitive to the exact choice for $x_{\rm UV}$ as soon as they approach their respective asymptotic values. For $\xi \gtrsim 4$, it is, therefore, safe to approximate $\mathcal{I}_{EE}$, $\mathcal{I}_{BB}$, and $\mathcal{I}_{BE}$ by the constant values shown in Fig. 5.1,

$$\rho_{EE} \simeq 1.3 \times 10^{-4} \frac{e^{2\pi\xi}}{\xi^3} H^4, \quad \rho_{BB} \simeq 1.5 \times 10^{-4} \frac{e^{2\pi\xi}}{\xi^5} H^4, \quad \rho_{EB} \simeq -2.6 \times 10^{-4} \frac{e^{2\pi\xi}}{\xi^4} H^4.$$
$$(5.17)$$

These results are consistent with the approximate solution for the excited mode functions, $A_+^k(x) = (2k)^{-1/2} (x/x_+)^{1/4} \exp\left[\pi x_+/2 - 2\sqrt{xx_+}\right]$, which is often employed in the literature.

With Eq. (5.17) at our disposal, we are now able to assess the relative importance of the new terms in Eqs. (5.2) and (5.5). We are mainly interested in the following two ratios,

$$\delta_{\rm F} = \frac{\rho_{EE} + \rho_{BB}}{3H^2 M_{\rm Pl}^2}, \quad \delta_{\rm KG} = \left|\frac{\rho_{EB}/\Lambda}{3H\dot{a}}\right| = \left|\frac{\rho_{EB}}{6\xi\Lambda^2 H^2}\right|. \quad (5.18)$$

Here, $\delta_{\rm F}$ quantifies the hyper-EM contributions to the Friedmann equation, while $\delta_{\rm KG}$ measures the importance of the source term in the Klein-Gordon equation in comparison to the Hubble friction term. For $4 \lesssim \xi \lesssim 10$, these two ratios are well fit by the following numerical expressions,

$$\delta_{\rm F} \simeq 2.8 \times 10^{-4} \exp\left[0.90 \times 2\pi(\xi - 5)\right] \left(\frac{H}{10^{13}\,{\rm GeV}}\right)^2, \quad (5.19)$$

$$\delta_{\rm KG} \simeq 7.6 \times 10^{-4} \exp\left[0.83 \times 2\pi(\xi - 5)\right] \left(\frac{H}{10^{13}\,{\rm GeV}}\right)^2 \left(\frac{3 \times 10^{17}\,{\rm GeV}}{\Lambda}\right)^2.$$
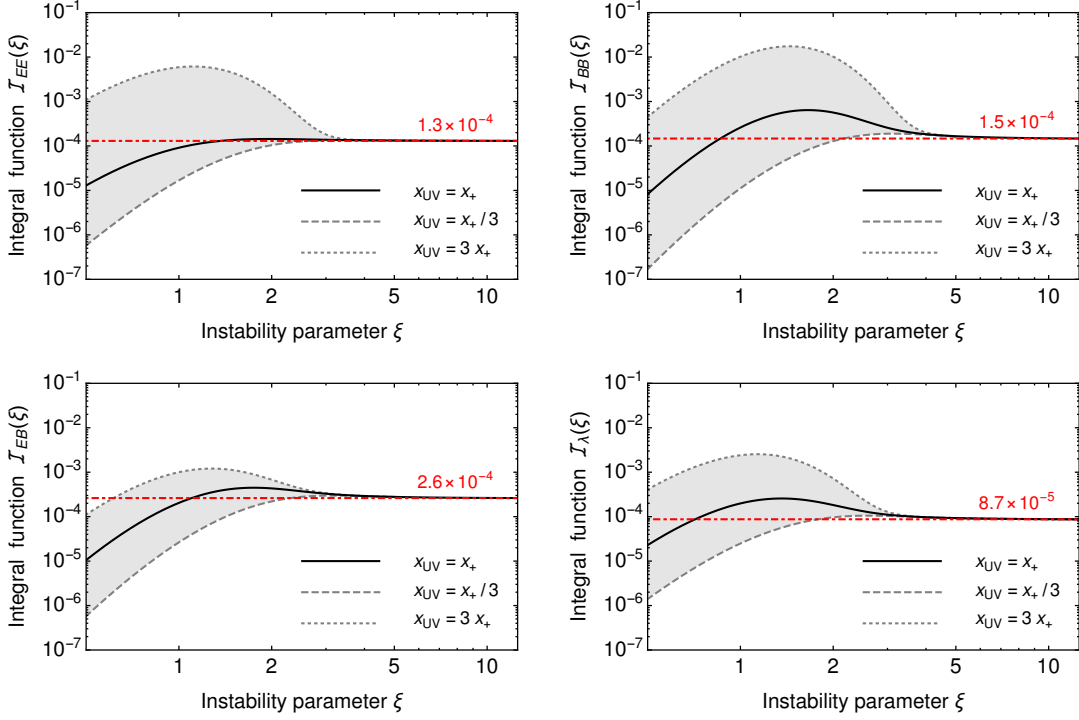
Figure 5.1: Dependence of the integral functions $\mathcal{I}_{EE}$ **(upper left panel)**, $\mathcal{I}_{BB}$ **(upper right panel)**, $\mathcal{I}_{EB}$ **(lower left panel)**, and $\mathcal{I}_\lambda$ **(lower right panel)**, on the instability parameter ξ; see Eqs. (5.10), (5.16), and (5.24). For each function, we illustrate the effect of varying the UV cut-off scale (parametrized in terms of the upper integration boundary x_{UV}) within roughly one order of magnitude. At any given value of ξ, the parameter x_+ corresponds to $x_+ = 2\xi$; see Eq. (5.9). The red numbers and horizontal lines indicate the respective asymptotic values at $\xi \gg 1$.

These relations are the first important results of our analysis. We stress that they represent numerical fit functions, which we obtain by fitting δ_{F} and δ_{KG} as functions of $e^{2\pi\xi}$, H^2, and Λ^{-2}. The factors 0.90 and 0.83 in front of $2\pi\xi$ in Eq. (5.19) account for the competition between the exponentials ($e^{2\pi\xi}$) and the inverse powers (ξ^{-3}, ξ^{-4}, and ξ^{-5}) of ξ in Eq. (5.15). In Fig. 5.2, we compare our fit functions with the corresponding exact expressions for δ_{F} and δ_{KG} in Eq. (5.18).

From Eq. (5.19), we see that the backreaction from the gauge field on the inflationary dynamics is negligible, at least for the chosen reference values. This conclusion drastically changes as soon as we go to larger values of ξ and H as well as to smaller values of Λ. Here, we find in particular an upper bound on ξ, such that the ratio δ_{F} does not take values larger than unity; see Fig. 5.2,

$$\delta_{\mathrm{F}} \leq 1 \quad \Rightarrow \quad \xi \leq \xi_{\max}(H) \simeq 6.4 - 0.82 \log_{10}\left(\frac{H}{10^{13}\,\mathrm{GeV}}\right). \qquad (5.20)$$
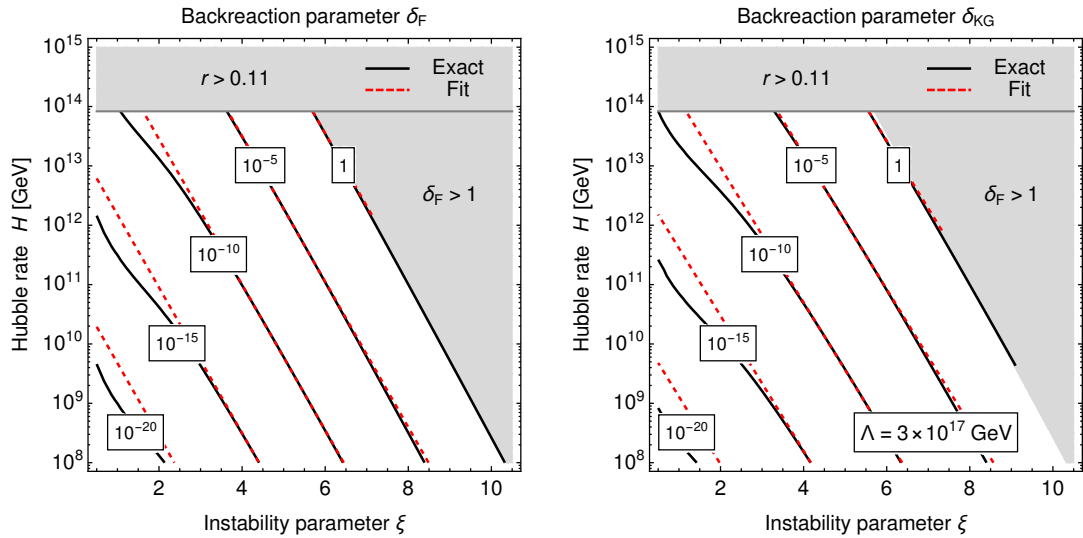
Figure 5.2: Backreaction parameters δ_F **(left panel)** and δ_{KG} **(right panel)** as functions of the instability parameter ξ and the Hubble rate H. The parameter δ_F quantifies the amount of backreaction in the Friedmann equation, while the parameter δ_{KG} quantifies the amount of backreaction in the Klein-Gordon equation; see Eq. (5.18). The black solid contours represent the exact expressions for δ_F and δ_{KG}, including the complicated ξ dependence of the integral functions in Eq. (5.16). The red dashed contours represent the numerical fit functions in Eq. (5.19). In the right panel, the suppression scale Λ is fixed at $\Lambda = 3 \times 10^{17}$ GeV. The scaling of δ_{KG} with Λ is trivial, $\delta_{KG} \propto \Lambda^{-2}$. By definition, values of δ_F larger than unity are unphysical; see Eq. (5.20). For values of the Hubble rate greater than $H \simeq 8 \times 10^{13}$ GeV, the PLANCK constraint on the tensor-to-scalar ratio, $r \lesssim 0.11$, is violated.

This bound is model-independent and needs to be obeyed by any model of pseudoscalar inflation coupled to an Abelian gauge sector. For ξ values beyond this bound, one formally finds that more than $100\,\%$ of the total energy density is stored in the hyper-EM field. This signals that the backreaction from the excited gauge fields is no longer negligible in the Friedmann equation; and hence the above solutions are no longer trustable.[2] Meanwhile, the ratio δ_{KG} can be varied independently, even if ξ satisfies Eq. (5.20), simply by adjusting the strength of the axion-gauge-field coupling. According to Eq. (5.19), lowering the suppression scale Λ by a factor 10 readily increases δ_{KG} by two orders of magnitude. For the same values of ξ and H as in Eq. (5.19), $\xi = 5$ and $H = 10^{13}$ GeV, but with $\Lambda = 3 \times 10^{16}$ GeV, the source term in Eq. (5.5) begins to compete with the Hubble friction term, $\delta_{KG} \sim 0.1$. As we will see in the following, such small values of Λ, however, turn out to be incompatible with the idea of baryogenesis from pseudoscalar inflation.

---

[2]Recently, it is claimed that there are other upper bounds for ξ where the evaluation of the gauge field production in the previous section is valid, coming from the perturbativity [110,111] and possible thermalization [112]. We expect that our analysis is qualitatively correct even taking into account these constraints. Note that in the parameter we are interested in the value of ξ reaches the bound only at the last stage of inflation as we will see in Sec. 8.

5.3 Hypermagnetic field at the end of inflation

As long as we stay sufficiently far away from the maximal ξ value in Eq. (5.20) and as long as the suppression scale Λ is not chosen too small, the effect of gauge field production merely represents a small (and most often completely negligible) perturbation of the inflationary dynamics. In this regime, we can therefore safely trust our analysis in the previous section. In particular, we can use our result for the hypermagnetic field energy density, ρ_{BB}, in Eq. (5.15) to estimate the physical hypermagnetic field strength, B_p, at any given time during inflation,

$$B_p^2 = 2\,\rho_{BB} = \left\langle \boldsymbol{B}^2 \right\rangle = \frac{1}{R^4} \int \frac{d^3\boldsymbol{k}}{(2\pi)^3}\, k^2 \left| A_+^k \right|^2 = 2\,\mathcal{I}_{BB}\left(\xi\right) \frac{e^{2\pi\xi}}{\xi^5}\, H^4\,, \qquad (5.21)$$

where we again neglect the vacuum contributions from the negative-helicity modes. This field strength is the evident manifestation of *primordial magnetogenesis* in models of pseudoscalar inflation coupled to the hypercharge gauge field. For typical values of ξ and H, one finds

$$B_p \simeq 1.1 \times 10^{49}\,\mathrm{G} \left(\frac{f_{BB}\left(\xi\right)}{f_{BB}\left(5\right)} \right)^{1/2} \left(\frac{H}{10^{13}\,\mathrm{GeV}} \right)^2\,, \quad f_{BB}\left(\xi\right) = \mathcal{I}_{BB}\left(\xi\right) \frac{e^{2\pi\xi}}{\xi^5}\,. \quad (5.22)$$

In the next section, we will discuss the postinflationary evolution of this primordial hypermagnetic field, arguing that it is not completely erased during the radiation-dominated era. The primordial hypermagnetic field may, in fact, survive all the way up to the present epoch and contribute to the intergalactic magnetic fields that we observe today.

Another important quantity that characterizes the primordial hypermagnetic field is the physical correlation length, λ_p. To estimate λ_p, we compute the average of all relevant wavelengths, weighted by their respective contributions to the energy density ρ_{BB},

$$\lambda_p = \frac{1}{\rho_{BB}} \frac{1}{2R^4} \int \frac{d^3\boldsymbol{k}}{(2\pi)^3} \frac{2\pi R}{k}\, k^2 \left| A_+^k \right|^2 = \xi\, \frac{\mathcal{I}_\lambda\left(\xi\right)}{\mathcal{I}_{BB}\left(\xi\right)} \frac{2\pi}{H}\,. \qquad (5.23)$$

Here, the integral function $\mathcal{I}_\lambda$ is defined in analogy to the three functions in Eq. (5.16)

$$\mathcal{I}_\lambda\left(\xi\right) = \frac{\xi^4}{8\pi^2}\, e^{-\pi\xi} \int_0^{x_{\mathrm{UV}}} dx\, x^2 \left| W_{\kappa_+,1/2}\left(-2ix\right) \right|^2\,. \qquad (5.24)$$

Similarly as the other integral functions, $\mathcal{I}_\lambda$ becomes insensitive to the exact choice of x_{UV} as soon as it approaches its asymptotic value. For $\xi \gtrsim 4$, it is well approximated by $\mathcal{I}_\lambda \simeq 8.7 \times 10^{-5}$; see Fig. 5.1. Together with the asymptotic value for $\mathcal{I}_{BB}$, this shows that the hypermagnetic fields typically exhibit a correlation length that extends over more than one Hubble radius,

$$\lambda_p \simeq 3.0 \left(\frac{\xi}{5} \right) \lambda_H\,, \quad \lambda_H = \frac{2\pi}{H}\,. \qquad (5.25)$$

More explicitly, we find that λ_p typically takes values of the following order of magnitude,

$$\lambda_p \simeq 1.1 \times 10^{-50}\,\text{Mpc}\left(\frac{f_\lambda\left(\xi\right)}{f_\lambda\left(5\right)}\right)\left(\frac{10^{13}\,\text{GeV}}{H}\right)\,,\quad f_\lambda\left(\xi\right) = \xi\,\frac{\mathcal{I}_\lambda\left(\xi\right)}{\mathcal{I}_{BB}\left(\xi\right)}\,. \tag{5.26}$$

The above expressions for B_p and λ_p in Eqs. (5.21) and (5.23) are valid at any time during inflation. In the following, we are however going to be mostly interested in the values of B_p and λ_p at the end of inflation, i.e., at the onset of reheating. In this paper, we will work in the approximation of instant reheating, such that the end of inflation coincides with the beginning of the radiation-dominated era. To find the values of B_p and λ_p at this time, it is, therefore, sufficient to simply evaluate Eqs. (5.21) and (5.23) for $H = H_{\text{rh}}$ and $\xi = \xi_{\text{rh}}$, where H_{rh} and ξ_{rh} respectively denote the Hubble rate and the instability parameter at the end of inflation. Both quantities are model-dependent, which is why we will treat them as free parameters in the following. At this point it is interesting to note that, for most models of interest, ξ_{rh} is entirely controlled by the strength of the axion-gauge-field coupling. To see this, let us suppose that the end of inflation is triggered by a violation of the first slow-roll condition. That is, inflation ends because the Hubble parameter H is no longer quasi-constant. This condition is conveniently quantified in terms of the slow-roll parameter ε. Let us assume for now that the backreaction from gauge field production is negligible. In the usual slow-roll approximation, one then has

$$\varepsilon = \frac{d\ln H}{dN_e} \approx \frac{M_{\text{Pl}}^2}{2}\left(\frac{d\ln V}{da}\right)^2 \approx \frac{\dot{a}^2}{2\,H^2 M_{\text{Pl}}^2}\,, \tag{5.27}$$

where N_e denotes the number of e-folds until the end of inflation. Next, let us rewrite the condition $\varepsilon \sim 1$ at the end of inflation in terms of ξ_{rh} and Λ. This yields

$$\varepsilon \approx \frac{2\,\xi_{\text{rh}}^2\Lambda^2}{M_{\text{Pl}}^2} \sim 1 \quad\Rightarrow\quad \xi_{\text{rh}} \sim \frac{M_{\text{Pl}}}{\sqrt{2}\,\Lambda} \simeq 5.7\left(\frac{3\times 10^{17}\,\text{GeV}}{\Lambda}\right)\,. \tag{5.28}$$

Together with Eq. (5.19), this result confirms that, for $\Lambda \gtrsim 3 \times 10^{17}\,\text{GeV}$, the backreaction on the inflationary dynamics is mostly negligible at all times. For smaller values of Λ, the ratio δ_{KG} however quickly approaches values of order unity towards the end of inflation.

Chapter 6

Gauge field evolution after inflation

We now turn to the description of the postinflationary evolution of the primordial gauge fields. We will discuss in turn the different stages until the beginning of the inverse cascade regime (see Sec. 6.1), until the electroweak phase transition (see Sec. 6.2), and until today (see Sec. 6.3).

6.1 From the end of inflation to the onset of the inverse cascade regime

As stressed several times before, we are going to work in the approximation of instant reheating.[1] That is, we make the simplifying assumption that, at the end of inflation, the vacuum energy density driving inflation is converted instantaneously into thermal radiation,

$$\rho_{\rm inf}\left(t_{\rm rh}\right) = 3\,H_{\rm rh}^2\,M_{\rm Pl}^2 \quad \rightarrow \quad \rho_{\rm rad}\left(t_{\rm rh}\right) = \frac{\pi^2}{30}\,g_*\,T_{\rm rh}^4\,, \tag{6.1}$$

where $g_* = 106.75$ denotes the effective number of relativistic DOFs in the standard model. We consequently neglect the period of inflaton oscillations after inflation as well as the gradual production of (charged) particles in inflaton decays. This assumption simplifies our analysis considerably — given the fact that the charged particles in the emerging plasma actually interfere with the evolution of the primordial gauge fields.[2] A reliable description of this complicated process however requires a dedicated

---

[1]Similarly, we also assume that there is no charged plasma even as a subdominant component of the universe until the end of inflation. The presence of such a charged plasma component already during the stage of inflation might prevent the hypermagnetic helicity from developing and, hence, change our estimate.

[2]The oscillations of the inflaton field would enhance the production of primordial gauge fields [106]. But, at the same time, the high electric conductivity of the charged plasma would suppress the hypermagnetic helicity [108].

numerical simulation that takes into account both nonperturbative particle production and MHD, which is not yet available and which is certainly beyond the scope of this work. The assumption of instant reheating moreover allows us to eliminate the reheating temperature $T_{\rm rh}$ as a free parameter in our scenario. According to Eq. (6.1), we can simply express $T_{\rm rh}$ in terms of the Hubble rate at the end of inflation, $H_{\rm rh}$,

$$T_{\rm rh} = \sqrt{M_* H_{\rm rh}} \simeq 2.7 \times 10^{15}\,\text{GeV} \left(\frac{H_{\rm rh}}{10^{13}\,\text{GeV}} \right)^{1/2} , \quad M_* = \left(\frac{90}{\pi^2\, g_*} \right)^{1/2} M_{\rm Pl}. \quad (6.2)$$

By employing this relation, we choose to discard all details of the reheating process. While this introduces an uncertainty to some degree, it also makes our analysis more model-independent.

To describe the behavior of the primordial gauge fields after reheating, we shall follow the discussion in [74, 98, 100] (see also [73, 82, 95]). Our first observation is that, once the plasma is in place, the hyper-EM field begins to interact with hypercharged particles in the thermal bath. This interaction makes the primordial hyperelectric fields vanishingly small, $\boldsymbol{E} \simeq 0$ (i.e., $\boldsymbol{E}$ becomes suppressed by the large electric conductivity), leaving us mainly with the hypermagnetic $\boldsymbol{B}$ field. In the following, we will assume that, initially, the backreaction from the charged particles has neither an impact on the overall strength of the hypermagnetic field, B_p, nor on its correlation length, λ_p. The starting point of our analysis are, therefore, our results for B_p and λ_p that we obtained in Sec. 5.3; see Eqs. (5.21) and (5.23),

$$B_p^{\rm rh} = (2\mathcal{I}_{BB})^{1/2} \frac{e^{\pi\xi_{\rm rh}}}{\xi_{\rm rh}^{5/2}} H_{\rm rh}^2 \simeq 1.7 \times 10^{-2}\, \frac{e^{\pi\xi_{\rm rh}}}{\xi_{\rm rh}^{5/2}} H_{\rm rh}^2, \quad \lambda_p^{\rm rh} = \xi_{\rm rh}\, \frac{\mathcal{I}_\lambda}{\mathcal{I}_{BB}}\, \frac{2\pi}{H_{\rm rh}} \simeq 3.7\, \frac{\xi_{\rm rh}}{H_{\rm rh}}\,. \quad (6.3)$$

We are now going to outline how these two quantities behave as functions of the radiation temperature T, as the universe expands. Our final results are summarized schematically in Fig. 6.1, which illustrates the time dependence of B_p and λ_p for different values of $\xi_{\rm rh}$ and $H_{\rm rh}$.

At early times, i.e., directly after reheating, we expect that both the field strength B_p as well as the correlation length λ_p simply redshift adiabatically [89],

$$B_p(T) = \left(\frac{R_{\rm rh}}{R(T)} \right)^2 B_p^{\rm rh}, \quad \lambda_p(T) = \left(\frac{R(T)}{R_{\rm rh}} \right) \lambda_p^{\rm rh}\,. \quad (6.4)$$

This expectation is justified by the fact that, initially, the correlation length λ_p is much longer than the eddy scale of the velocity fields of the charged plasma, $\lambda_T \simeq vt$, (see also the discussion in the next section) implying that the charged plasma cannot affect the evolution of the hypermagnetic field. During radiation domination and for a constant number of effective DOFs, the scale factor R increases in inverse proportion to the plasma temperature, $R \propto 1/T$. During the early phase of adiabatic expansion, B_p therefore drops like T^2, while λ_p grows like $1/T$.
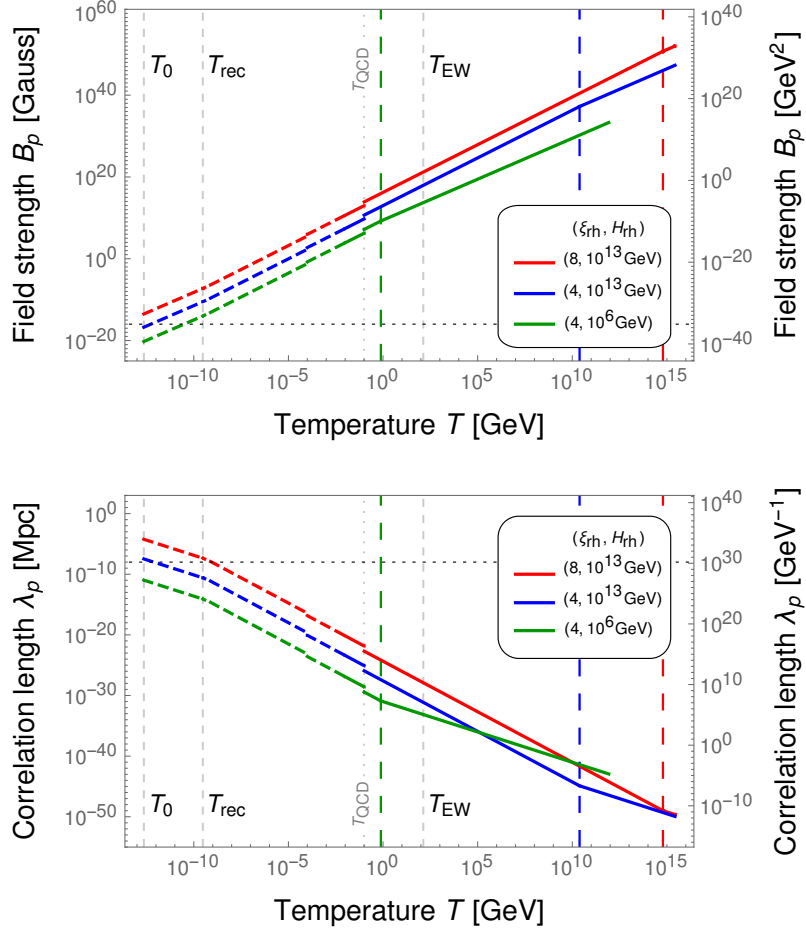
Figure 6.1: Physical field strength B_p (**upper panel**) and physical correlation length λ_p (**lower panel**) of the hypermagnetic $\boldsymbol{B}$ field as functions of the radiation temperature T for representative values of H and ξ at the end of inflation. The vertical dotted lines mark the respective temperatures at which the adiabatic regime transitions into the inverse cascade regime. Both plots account for the decrease in the effective number of DOFs in the course of the expansion. The kinks around $T \sim 100\,\text{MeV}$ correspond, e.g., to the QCD phase transition. For $T < 10\,\text{MeV}$, damping effects might become important (see [74, 98, 100]) and our description of the magnetic field evolution becomes less accurate. For this reason, we only draw dashed lines in the low-temperature regime.

6.2 From the onset of the inverse cascade regime to the electroweak crossover

In the course of the further evolution, the interaction of the $\boldsymbol{B}$ field and the charged plasma (described by the velocity field $\boldsymbol{v}$) results in a complicated co-evolution of both fields, governed by the MHD equations: The $\boldsymbol{B}$ field induces a $\boldsymbol{v}$ field and the $\boldsymbol{v}$ field back-reacts on the evolution of the $\boldsymbol{B}$ field, which likely results in turbulent field configurations. If the charged plasma develops a turbulence, the scale up to which the velocity field is capable of affecting the $\boldsymbol{B}$ field can be estimated in terms of the turbulence (or eddy) scale λ_T,

$$\lambda_T \simeq v\,t = \frac{v}{2H}\,, \quad v = |\boldsymbol{v}|\,. \tag{6.5}$$

As long as $\lambda_T \ll \lambda_p$, the $\boldsymbol{v}$ field affects the $\boldsymbol{B}$ field only on small scales and the evolution of B_p and λ_p remains unaffected. Both the turbulence scale λ_T and the correlation length λ_p grow with time. However, λ_T grows faster than λ_p, such that, after some finite time, the turbulence scale catches up with the correlation length, $\lambda_T \sim \lambda_p$. After that, the $\boldsymbol{B}$ field can no longer evolve adiabatically. Indeed, it has been observed in MHD simulations that a maximally helical magnetic field generates a turbulent plasma and that the kinetic energy of the plasma waves becomes comparable to (or equilibrated with) the energy stored in the hypermagnetic field [98, 100], $\rho_{\mathrm{kin}} \sim \rho_{BB}$. This means that the amplitude of the $\boldsymbol{v}$ field is comparable to the Alfvén velocity v_A. In the nonrelativistic limit, $v_A \ll 1$, the Alfvén velocity is given as [114],

$$v \sim v_A = \frac{v_A^0}{\sqrt{1 + \left(v_A^0\right)^2}} \sim v_A^0\,, \quad v_A^0 = \frac{B_p}{\sqrt{\rho_{\mathrm{ch}} + p_{\mathrm{ch}}}}\,, \quad \rho_{\mathrm{ch}} = \frac{\pi^2}{30}\,g_{*,\mathrm{ch}}\,T^4\,, \quad p_{\mathrm{ch}} = \frac{\rho_{\mathrm{ch}}}{3}\,, \tag{6.6}$$

with ρ_{ch} and p_{ch} denoting the energy density and pressure of the hypercharged particles in the plasma. $g_{*,\mathrm{ch}} = 82.75$ counts the effective number of relativistic DOFs carrying nonzero hypercharge in the standard model. In the following, we will not distinguish between v_A and v_A^0 and simply approximate $v_A \approx v_A^0$. Combining Eqs. (6.5) and (6.6) and assuming that the $\boldsymbol{B}$ and $\boldsymbol{v}$ fields are equilibrated even in the adiabatic regime, we find for λ_T in the adiabatic regime

$$\lambda_T \propto \frac{B_p}{\sqrt{\rho_{\mathrm{ch}}}\,H} \propto R^2 \propto \frac{1}{T^2} \tag{6.7}$$

Indeed, this corresponds to a faster growth than in the case of λ_p, which simply scales like $1/T$.

Once the turbulence scale has caught up with the correlation length, $\lambda_T \sim \lambda_p$, the hypermagnetic field enters into the inverse cascade regime [96–98]. From this point on, the growth of λ_p is simply driven by the turbulence scale λ_T, such that $\lambda_T \sim \lambda_p$

at all subsequent times,

$$\lambda_p \sim \lambda_T \propto \frac{B_p}{\sqrt{\rho_{\rm ch}}\,H} \quad \Rightarrow \quad \frac{\lambda_p}{B_p} \propto \frac{1}{\sqrt{\rho_{\rm ch}}\,H} \propto R^4 \propto \frac{1}{T^4}\,. \tag{6.8}$$

This relation is, however, not yet sufficient to fully estimate the scaling behavior of B_p and λ_p during the inverse cascade regime. In addition to Eq. (6.8), we need a second, independent relation between λ_T and B_p. At this point, it comes in handy that, as a consequence of the high hyperelectric conductivity of the charged plasma, the comoving helicity density h_c is approximately conserved at high temperatures; see, e.g., [88, 89] and references therein,[3]

$$h_c = \lim_{V \to \infty} \frac{1}{V} \int_V d^3\boldsymbol{x}\, \boldsymbol{A}_c \cdot \boldsymbol{B}_c \sim {\rm const}\,. \tag{6.9}$$

Here, the integral over the volume V represents nothing but a spatial average, $h_c = \langle \boldsymbol{A}_c \boldsymbol{B}_c \rangle$. Moreover, we emphasize that both vector fields, $\boldsymbol{A}_c \equiv \boldsymbol{A}$ and $\boldsymbol{B}_c = R^2 \boldsymbol{B}$, correspond to comoving quantities. We roughly estimate the typical size of $\boldsymbol{A}_c$ as $A_c \sim \lambda_c/(2\pi)\,B_c \propto R\,\lambda_p B_p$, such that

$$h_c = R^2 \langle \boldsymbol{A}\boldsymbol{B} \rangle \propto R^3 \lambda_p B_p^2 \sim {\rm const}\,. \tag{6.10}$$

Together with Eq. (6.8), this relation then yields the scaling behavior of B_p and λ_p,

$$B_p \propto \frac{1}{R^{7/3}} \propto T^{7/3}\,, \quad \lambda_p \propto R^{5/3} \propto \frac{1}{T^{5/3}}\,, \tag{6.11}$$

which coincides with the scaling laws of the inverse cascade found in MHD simulations [98, 100].

We stress that all of the relations in Eqs. (6.5), (6.6), (6.8), and (6.10) are simply rough estimates. A more careful treatment would require a full-fledged MHD simulation [74, 95], which is beyond the scope of this work. Moreover, the study of primordial magnetic fields in MHD simulations is still the subject of on-going work in the literature. In anticipation of new simulations, we shall therefore settle for the estimates above, leaving any refinement of our analysis for future work.

Next, let us determine the temperature at the onset of the inverse cascade regime. We find the transition temperature, $T = T_{\rm ic}$, simply by solving the condition $\lambda_T(T_{\rm ic}) = \lambda_p(T_{\rm ic})$ for $T_{\rm ic}$,

$$\frac{T_{\rm ic}}{T_{\rm rh}} = \frac{\mathcal{I}_{BB}^{3/2}}{4\sqrt{2}\,\pi\,\mathcal{I}_\lambda} \left(\frac{g_*}{g_{*,{\rm ch}}}\right)^{1/2} \frac{e^{\pi\xi_{\rm rh}}}{\xi_{\rm rh}^{7/2}} \frac{H_{\rm rh}}{M_{\rm Pl}} \simeq 1.3 \times 10^{-3}\, \frac{e^{\pi\xi_{\rm rh}}}{\xi_{\rm rh}^{7/2}} \frac{H_{\rm rh}}{M_{\rm Pl}}\,, \tag{6.12}$$

---

[3]Based on Ampère's and Ohm's laws, one can show that the time derivative of h_c is suppressed by the inverse of the hyperelectric conductivity, $\dot{h}_c \propto 1/\sigma$. The fact that h_c is conserved to good approximation is, therefore, a direct consequence of the large (but finite) conductivity of the standard model plasma, $\sigma \sim 10^2\,T$ [115, 116].

where we used that $T_{\mathrm{rh}} = \sqrt{M_* H_{\mathrm{rh}}}$. The Alfvén velocity v_A at this temperature is given as

$$v_A = \frac{\mathcal{I}_{BB}^{1/2}}{\sqrt{2}} \left(\frac{g_*}{g_{*,\mathrm{ch}}} \right)^{1/2} \frac{e^{\pi\xi_{\mathrm{rh}}}}{\xi_{\mathrm{rh}}^{5/2}} \frac{H_{\mathrm{rh}}}{M_{\mathrm{Pl}}} \simeq 9.7 \times 10^{-3} \frac{e^{\pi\xi_{\mathrm{rh}}}}{\xi_{\mathrm{rh}}^{5/2}} \frac{H_{\mathrm{rh}}}{M_{\mathrm{Pl}}}, \tag{6.13}$$

Furthermore, we are now in the position to calculate the field strength as well as the correlation length of the hypermagnetic field at $T = T_{\mathrm{ic}}$. Combining Eqs. (6.3), (6.4), and (6.12), we obtain

$$B_p^{\mathrm{ic}} = \left(\frac{T_{\mathrm{ic}}}{T_{\mathrm{rh}}} \right)^2 B_p^{\mathrm{rh}} = \frac{\mathcal{I}_{BB}^{7/2}}{16\sqrt{2}\,\pi^2\,\mathcal{I}_\lambda^2} \frac{g_*}{g_{*,\mathrm{ch}}} \frac{e^{3\pi\xi_{\mathrm{rh}}}}{\xi_{\mathrm{rh}}^{19/2}} \frac{H_{\mathrm{rh}}^4}{M_{\mathrm{Pl}}^2} \simeq 2.9 \times 10^{-8} \frac{e^{3\pi\xi_{\mathrm{rh}}}}{\xi_{\mathrm{rh}}^{19/2}} \frac{H_{\mathrm{rh}}^4}{M_{\mathrm{Pl}}^2}, \tag{6.14}$$

$$\lambda_p^{\mathrm{ic}} = \left(\frac{T_{\mathrm{rh}}}{T_{\mathrm{ic}}} \right) \lambda_p^{\mathrm{rh}} = \frac{8\sqrt{2}\,\pi^2\,\mathcal{I}_\lambda^2}{\mathcal{I}_{BB}^{5/2}} \left(\frac{g_{*,\mathrm{ch}}}{g_*} \right)^{1/2} \frac{\xi_{\mathrm{rh}}^{9/2}}{e^{\pi\xi_{\mathrm{rh}}}} \frac{M_{\mathrm{Pl}}}{H_{\mathrm{rh}}^2} \simeq 2.9 \times 10^3 \frac{\xi_{\mathrm{rh}}^{9/2}}{e^{\pi\xi_{\mathrm{rh}}}} \frac{M_{\mathrm{Pl}}}{H_{\mathrm{rh}}^2}.$$

At temperatures below T_{ic}, the field strength B_p behaves as follows; see Eq. (6.11),

$$B_p(T) = \left(\frac{T}{T_{\mathrm{ic}}} \right)^{7/3} B_p^{\mathrm{ic}} = \left(\frac{T}{T_{\mathrm{rh}}} \right)^{7/3} \left[16\,\pi\,\mathcal{I}_\lambda \left(\frac{g_{*,\mathrm{ch}}}{g_*} \right)^{1/2} \frac{e^{2\pi\xi_{\mathrm{rh}}}}{\xi_{\mathrm{rh}}^4} H_{\mathrm{rh}}^5 M_{\mathrm{Pl}} \right]^{1/3} \tag{6.15}$$

$$\simeq 0.16 \left(\frac{T}{T_{\mathrm{rh}}} \right)^{7/3} \left(\frac{e^{2\pi\xi_{\mathrm{rh}}}}{\xi_{\mathrm{rh}}^4} H_{\mathrm{rh}}^5 M_{\mathrm{Pl}} \right)^{1/3},$$

whereas for the correlation length λ_p, we find

$$\lambda_p(T) = \left(\frac{T_{\mathrm{ic}}}{T} \right)^{5/3} \lambda_p^{\mathrm{ic}} = \left(\frac{T_{\mathrm{rh}}}{T} \right)^{5/3} \left(\frac{\pi\,\mathcal{I}_\lambda}{4} \frac{g_*}{g_{*,\mathrm{ch}}} \frac{e^{2\pi\xi_{\mathrm{rh}}}}{\xi_{\mathrm{rh}}^4} \frac{1}{H_{\mathrm{rh}} M_{\mathrm{Pl}}^2} \right)^{1/3} \tag{6.16}$$

$$\simeq 4.5 \times 10^{-2} \left(\frac{T_{\mathrm{rh}}}{T} \right)^{5/3} \left(\frac{e^{2\pi\xi_{\mathrm{rh}}}}{\xi_{\mathrm{rh}}^4} \frac{1}{H_{\mathrm{rh}} M_{\mathrm{Pl}}^2} \right)^{1/3}.$$

Note that we assumed a constant effective number of DOFs in both Eq. (6.15) and Eq. (6.16).

6.3 From the electroweak crossover to the present epoch

The evolution of the field strength and correlation length at late times can be described by standard techniques with the assumption that the magnetic fields evolve according to the inverse cascade until recombination and evolve adiabatically again after that until today. In the usual ΛCDM model (without any additional stages of late-time entropy production or the like), we can readily relate the values of B_p and λ_p around
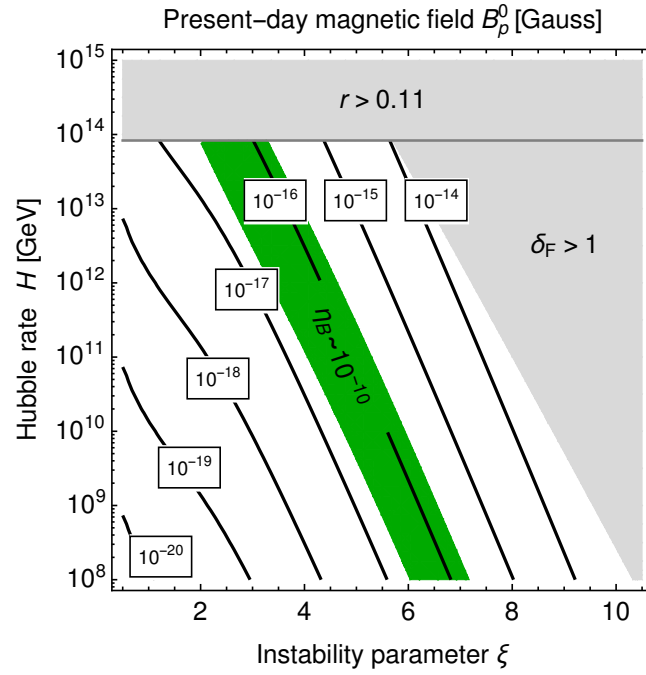
Figure 6.2: Present-day strength of the physical magnetic field, B_p^0, as a function of the instability parameter ξ and the Hubble rate H; see Eq. (6.18). Here, both ξ and H are understood to correspond to the respective values at the end of inflation, $\xi \equiv \xi_{\rm rh}$ and $H \equiv H_{\rm rh}$. The green band illustrates the region in parameter space where baryogenesis around the time of EWSB results in a baryon asymmetry η_B in accord with the observed value, $\eta_B^{\rm obs} \sim 10^{-10}$; see Eq. (7.11) and Fig. 7.1. The gray-shaded regions are the same as in Fig. 5.2.

the time of EWSB to their values in the present epoch,

$$B_p^0 \simeq 1.1 \times 10^{-14}\,\mathrm{G} \left(\frac{B_p^{\mathrm{ew}}}{10^{20}\,\mathrm{G}} \right) \left(\frac{100\,\mathrm{GeV}}{T_{\mathrm{ew}}} \right)^{7/3} , \tag{6.17}$$

$$\lambda_p^0 \simeq 0.40\,\mathrm{pc} \left(\frac{\lambda_p^{\mathrm{ew}}}{10^{-29}\,\mathrm{Mpc}} \right) \left(\frac{T_{\mathrm{ew}}}{100\,\mathrm{GeV}} \right)^{5/3} ,$$

which is consistent with the corresponding relations in [89, 90]. Here, the values of B_p^{ew} and λ_p^{ew} simply follow from evaluating our results in Eq. (6.15) and Eq. (6.16) at $T = T_{\mathrm{ew}} \sim 100\,\mathrm{GeV}$, i.e., the temperature at the time of EWSB.[4] We then obtain the following final expression for the present-day strength of the physical magnetic field,

$$B_p^0 \simeq 6.0 \times 10^{-18}\,\mathrm{G} \left[\mathcal{I}_\lambda \left(\frac{g_{*,\mathrm{ch}}}{g_*} \right)^{1/2} \frac{e^{2\pi\xi_{\mathrm{rh}}}}{\xi_{\mathrm{rh}}^4} \right]^{1/3} \left(\frac{H_{\mathrm{rh}}}{10^{13}\,\mathrm{GeV}} \right)^{1/2} \tag{6.18}$$

$$\simeq 2.5 \times 10^{-19}\,\mathrm{G} \left(\frac{e^{2\pi\xi_{\mathrm{rh}}}}{\xi_{\mathrm{rh}}^4} \right)^{1/3} \left(\frac{H_{\mathrm{rh}}}{10^{13}\,\mathrm{GeV}} \right)^{1/2} ,$$

which we plot as a function of ξ_{rh} and H_{rh} in Fig. 6.2. This relation illustrates how the explosive production of gauge fields during pseudoscalar inflation results in magnetic fields on astrophysical scales in the present epoch. Note that B_p^0 in Eq. (6.18) does not depend on the exact value of T_{ew}. Moreover, it only depends on $\mathcal{I}_\lambda$ and is independent of the integral function $\mathcal{I}_{BB}$. Meanwhile, we find that the present-day value of the correlation length, λ_p^0, satisfies exactly the relation which one expects for causally generated magnetic fields [100]; see also Eq. (4.4) and footnote 5,

$$\lambda_p^0 \simeq 0.28\,\mathrm{pc} \left(\frac{B_p^0}{10^{-14}\,\mathrm{G}} \right) \simeq \frac{1.0\,\mathrm{pc}}{(4\pi)^{1/2}} \left(\frac{B_p^0}{10^{-14}\,\mathrm{G}} \right) . \tag{6.19}$$

We stress that this result is based on the strict relation $v = v_A$; see Eq. (6.6). However, there are also MHD simulations suggesting that v might in fact be slightly suppressed compared to the Alfvén velocity, $v \simeq \mathcal{O}(0.1)\,v_A$ [98, 100]. Thus, our above estimates come with at least an $\mathcal{O}(10)$ uncertainty.[5] Nonetheless, we expect our expressions to catch the basic *qualitative* features of the magnetic field from pseudoscalar inflation, in particular, the relation between the inflationary parameters H and ξ on the one hand and the quantities B_p and λ_p on the other hand.

---

[4]During EWSB, the hypermagnetic $\boldsymbol{B}_Y$ field turns into the electromagnetic $\boldsymbol{B}_{\mathrm{EM}}$ field. The amplitudes $|\boldsymbol{B}_Y|$ and $|\boldsymbol{B}_{\mathrm{EM}}|$ are, however, continuously connected [91], which is why we do not distinguish between them here.

[5]Note that we also omitted possible damping effects at low temperatures, $T < 10\,\mathrm{MeV}$, due to processes such as neutrino and photon free streaming. However, despite these effects, it has been demonstrated that both the field strength and the correlation length eventually reach the same values as in the simple inverse-cascade estimate [100].

Chapter 7

Implications for baryon asymmetry and gravitational waves

The primordial gauge fields generated during inflation have important phenomenological consequences. Not only do they seed the intergalactic magnetic fields that permeate our Universe today (see Eq. (6.18)), they also lead to the generation of a nonzero baryon number around the time of EWSB (see Sec. 7.1) as well as to a signal in the stochastic GW background at high frequencies (see Sec. 7.2). We shall now discuss these two phenomena in turn.

7.1 Baryogenesis from pseudoscalar inflation

The gauge fields generated during inflation are maximally helical. This can be seen explicitly from our analysis in Sec. 5.1, where we showed that only modes in one helicity eigenstate are exponentially amplified during inflation, while the other helicity modes stay at the vacuum level; see Eq. (5.13). Moreover, we found that the sign of the final helicity depends on the sign of the inflaton velocity, $\text{sgn}\,\mathcal{H} = \text{sgn}\,\dot{a}$. In Sec. 5.1, we chose $\dot{a} > 0$, in order to achieve positive helicity.

Changes in the comoving helicity density h_c (see Eq. (6.9)) after inflation are suppressed by the hyperelectric conductivity of the thermal plasma, $\dot{h}_c \propto 1/\sigma$; see footnote 3. Therefore, given the large value of σ in the standard model, $\sigma \sim 10^2\,T$ [115, 116], h_c is *approximately* conserved after inflation; see Eq. (6.10). At the same time, it is important to remember that any change in the hypermagnetic helicity results in the production of baryon number B and lepton number L. This is reflected in Eq. (4.3), which follows from the chiral triangle anomaly in the standard model. Therefore, even slight changes in h_c, because of the finite conductivity σ, are physically relevant as soon as we turn our attention to the time evolution of B and L. This observation is

71

the basis for the scenario of *baryogenesis via decaying hypermagnetic helicity* [88–92]. In the following, we will illustrate how this scenario fits together with our analysis of primordial magnetogenesis in models of pseudoscalar inflation. In doing so, we will follow the discussion in [91] (see also [90]).

In analogy to h_c in Eq. (6.9), we may define the physical helicity density h_p as follows,

$$h_p = \frac{h_c}{R^3} = \lim_{V \to \infty} \frac{1}{V} \int_V d^3\boldsymbol{x} \, \boldsymbol{A}_p \cdot \boldsymbol{B}_p = \langle \boldsymbol{A}_p \boldsymbol{B}_p \rangle \ . \tag{7.1}$$

Here and only here, $\boldsymbol{A}_p$ is defined as $\boldsymbol{A}_p = \boldsymbol{A}/R$, whereas $\boldsymbol{B_p} \equiv \boldsymbol{B}$ is nothing but the ordinary physical hypermagnetic $\boldsymbol{B}$ field. Again, the angle brackets in Eq. (7.1) denote the volume average of the scalar product $\boldsymbol{A}_p\boldsymbol{B}_p$. One can show that the time derivative of the helicity density h_p is related to the (Abelian) Chern-Simons density of the hypercharge gauge field,

$$\frac{d}{dt} h_p = \frac{1}{2} \langle F_{\mu\nu} \tilde{F}^{\mu\nu} \rangle = -2 \langle \boldsymbol{E}\boldsymbol{B} \rangle \ . \tag{7.2}$$

According to the standard model chiral anomaly, the Chern-Simons density $F_{\mu\nu}\tilde{F}^{\mu\nu}$ contributes in turn to the divergence of the baryon and lepton number currents J_B^μ and J_L^μ,

$$\partial_\mu J_B^\mu = \partial_\mu J_L^\mu = N_g \left(\frac{g_W^2}{16\pi^2} W_{\mu\nu}^a \tilde{W}_a^{\mu\nu} - \frac{g_Y^2}{32\pi^2} F_{\mu\nu} \tilde{F}^{\mu\nu} \right) \ . \tag{7.3}$$

In combination with Eq. (7.2), the time integral of this equation results in the relation in Eq. (4.3).

For our purposes, the important conclusion from Eq. (4.3) is that a decaying hypermagnetic helicity, $\dot{h}_p \neq 0$, induces nonzero baryon and lepton number. To properly track the evolution of baryon number B as a function of time during this process, one needs to solve a coupled system of kinetic equations, which take into account all relevant effects; see [90, 91] for details. As it turns out, B is fixed after EWSB, i.e., at $T \sim 100\,\mathrm{GeV}$, since after EWSB, baryon and lepton number are no longer anomalously violated. In the kinetic equations, the generation of baryon number because of the time-dependent hypermagnetic helicity is characterized by a temperature-dependent source term, $S = f\mathcal{S}$, which factorizes into two contributions,

$$f\left(\theta_W, T\right) = -T \frac{d\theta_W}{dT} \sin\left(2\theta_W\right) , \quad \mathcal{S}\left(T\right) = \frac{H}{sT} \frac{h_p}{8\pi^2} \ . \tag{7.4}$$

Similarly as in the case of h_c (see Eq. (6.10)), we can estimate the magnitude of h_p as follows,

$$h_p \sim \frac{\lambda_p}{2\pi} B_p^2 \quad \Rightarrow \quad \mathcal{S} \sim \frac{H}{sT} \frac{\lambda_p B_p^2}{16\pi^3} \ , \tag{7.5}$$

where λ_p and B_p at $T \sim 100\,\text{GeV}$ are given in Eqs. (6.15) and (6.16).[1] Note that $\mathcal{S}$ is proportional to the amplitude of the hypermagnetic helicity, h_p. Meanwhile, f is a function of the weak mixing angle θ_W, which varies as a function of temperature during the electroweak crossover. For $d\theta_W/dT = 0$, the hypermagnetic helicity does not decay and hence the source $\mathcal{S}$ vanishes.

The production of baryon number because of the change in the weak mixing angle has to compete with the usual washout processes because of electroweak sphalerons. The effect of sphaleron washout is conveniently accounted for in the kinetic equations by a transport coefficient $\gamma_{\text{w,sph}}$. For a Higgs mass of $125\,\text{GeV}$, lattice simulations of the electroweak crossover yield [117],

$$\gamma_{\text{w,sph}} \simeq \exp\left[-147.7 + 107.9\left(\frac{T}{130\,\text{GeV}}\right)\right], \quad \text{for } T \lesssim 161\,\text{GeV}, \qquad (7.6)$$

where $T \simeq 130\,\text{GeV}$ is just the temperature at which the electroweak sphalerons freeze out. The resulting kinetic equations are quite complicated and need to be solved numerically. However, as shown in [91], the final baryon asymmetry is nicely reproduced by the following compact analytical expression,

$$\eta_B = \frac{n_B}{s} \simeq \frac{17}{37}\left[\left(g_W^2 + g_Y^2\right)\frac{f\left(\theta_W, T\right)\mathcal{S}}{\gamma_{\text{w,sph}}}\right]_{T=T_{\text{BAU}}}, \quad T_{\text{BAU}} = 135\,\text{GeV}. \qquad (7.7)$$

Here, the baryogenesis temperature T_{BAU} is chosen, so as to optimize the agreement between the analytical result and the outcome of the numerical calculation.

Combining Eqs. (6.15), (6.16), (7.5), (7.6), and (7.7) and using $g_W \simeq 0.64$ and $g_Y \simeq 0.35$ at the electroweak scale, we obtain the following expression for the final baryon asymmetry,

$$\eta_B \simeq 2.9 \times 10^{-3}\,\mathcal{I}_\lambda\left[\frac{f\left(\theta_W, T\right)}{\gamma_{\text{w,sph}}}\left(\frac{e^{2\pi\xi_{\text{rh}}}}{\xi_{\text{rh}}^4}\right)\left(\frac{H_{\text{rh}}^3 T^2}{M_{\text{Pl}}^5}\right)^{1/2}\right]_{T=T_{\text{BAU}}}. \qquad (7.8)$$

A reliable determination of the final baryon asymmetry requires a precise understanding of the function f, i.e., of the temperature dependence of the weak mixing angle. The latest lattice studies of the electroweak crossover, however, have a relatively large uncertainty, as far as the exact evolution of $\theta_W(T)$ is concerned [118]. Moreover, there is a relatively large discrepancy between the numerical results and the one-loop perturbative analytical estimate [119]. For this reason, we shall follow [91] and simply model θ_W in terms of a smooth step function,

$$\cos^2\theta_W = \cos^2\theta_W^0 + \frac{1 - \cos^2\theta_W^0}{2}\left[1 + \tanh\left(\frac{T - T_{\text{step}}}{\Delta T}\right)\right], \quad \cos^2\theta_W^0 = \frac{g_W^2}{g_W^2 + g_Y^2} \simeq 0.77, \tag{7.9}$$

---

[1]Here we consider the case where the hypermagnetic field enters the inverse cascade regime prior to EWSB.
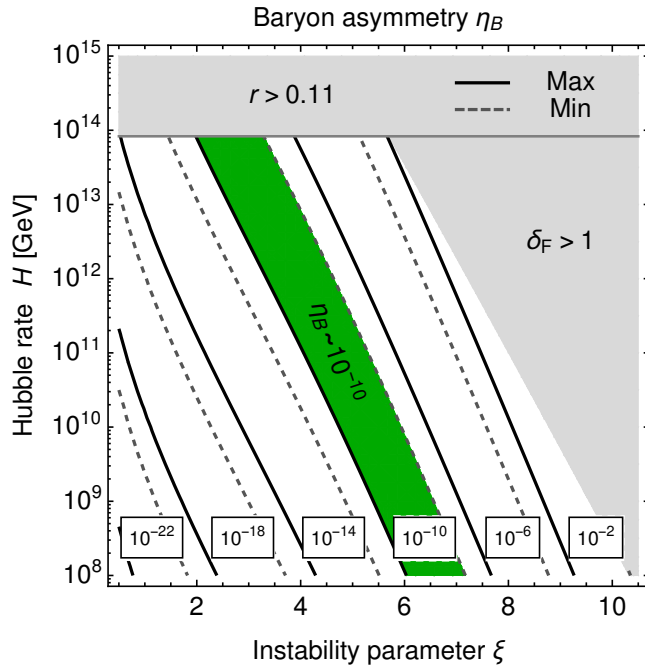
Figure 7.1: Baryon asymmetry $\eta_B = n_B/s$ as a function of the instability parameter ξ and the Hubble rate H; see Eq. (7.11). Here, both ξ and H are understood to correspond to the respective values at the end of inflation, $\xi \equiv \xi_{\rm rh}$ and $H \equiv H_{\rm rh}$. The black solid [gray dashed] contours correspond to the maximally [minimally] allowed value of the function f; see Eq. (7.10). The green band illustrates the region in parameter space where η_B is in accord with the observed value, $\eta_B^{\rm obs} \sim 10^{-10}$. The gray-shaded regions are the same as in Fig. 5.2.

which we believe to cover all realistic values of the function f including its uncertainties. Our phenomenological ansatz reflects the fact that, at $T \sim T_{\rm step}$, the weak mixing angle changes from its high-temperature value in the symmetric phase, $\cos^2 \theta_W = 1$, to its low-temperature value in the Higgs phase, $\cos^2 \theta_W = \cos^2 \theta_W^0$. The width of this transition in temperature space is characterized by the parameter ΔT. Realistic values of $T_{\rm step}$ and ΔT fall into the ranges $155\,{\rm GeV} \lesssim T_{\rm step} \lesssim 160\,{\rm GeV}$ and $5\,{\rm GeV} \lesssim \Delta T \lesssim 20\,{\rm GeV}$, respectively. Varying $T_{\rm step}$ and ΔT within these ranges, we find that the realistic values of f almost span three orders of magnitude,

$$5.6 \times 10^{-4} \lesssim f\left(\theta_W, T_{\rm BAU}\right) \lesssim 0.32 \,, \tag{7.10}$$

which translates into an uncertainty in the final baryon asymmetry,

$$\eta_B \simeq \left(1.9 \times 10^{-3} \cdots 1.1\right) \times 10^{-16} \left(\frac{e^{2\pi\xi_{\rm rh}}}{\xi_{\rm rh}^4}\right) \left(\frac{H_{\rm rh}}{10^{13}\,{\rm GeV}}\right)^{3/2} \,. \tag{7.11}$$

This expression for η_B is one of the main results of our paper. We show η_B as a function of $H_{\rm rh}$ and $\xi_{\rm rh}$ in Fig. 7.1. Evidently, the observed baryon asymmetry,

$\eta_B^{\mathrm{obs}} \sim 10^{-10}$ [3], can be reproduced in a large part of parameter space. In view of Fig. 7.1, several comments are in order:

(i) For most values of the Hubble rate at the end of inflation, H_{rh}, the instability parameter ξ_{rh} needs to take a value in the range $4 \lesssim \xi_{\mathrm{rh}} \lesssim 6$ to allow for successful baryogenesis. According to Eq. (5.28), this requires the suppression scale Λ to take a value in the following interval,

$$2.9 \times 10^{17}\,\mathrm{GeV} \lesssim \Lambda \lesssim 4.3 \times 10^{17}\,\mathrm{GeV}\,. \tag{7.12}$$

In other words, the requirement of successful baryogenesis roughly fixes the value of the suppression scale Λ in the axion-gauge-field coupling, $\Lambda \sim 3 \times 10^{17}\,\mathrm{GeV}$. This is within a factor of 10 of the Planck scale, which indicates that the axion needs to be coupled rather weakly.

(ii) With $\Lambda \sim 3 \times 10^{17}\,\mathrm{GeV}$ and given the location of the green band in Fig. 7.1, it is clear that successful baryogenesis is incompatible with large values of δ_{F} and δ_{KG}; see Fig. 5.2 and Eq. (5.19). This means that, in the case of successful baryogenesis, the gauge field production during inflation is never going to dominate the inflationary dynamics. Conversely, this can be rephrased by saying that inflationary scenarios that eventually do lead to $\delta_{\mathrm{F}} \sim 1$ unavoidably result in an overproduction of baryon number.[2] Of course, this problem can be trivially solved by re-interpreting the axion coupling to the hypercharge gauge fields as a coupling to the gauge fields of some other, hidden $U(1)$. But this solution comes at a high cost: If we replaced $U(1)_Y$ by some hidden $U(1)'$, we would have to give up on primordial magnetogenesis and baryogenesis via decaying hypermagnetic helicity as well. That is, we might still be able to generate a sizable signal in GWs (see Sec. 7.2); but we would loose all other virtues of our scenario.

(iii) The parameter region consistent with successful baryogenesis is also marked in Fig. 6.2. As can be seen from this figure, successful baryogenesis around the time of EWSB correlates with a particular strength of the large-scale magnetic fields in the present epoch, $B_p^0 \sim 10^{-16}\,\mathrm{GeV}$. Note that this is the value that we already anticipated in Eq. (4.4).

(iv) Our result in Fig. 7.1 presents an update of earlier studies in the literature [88,92]. In comparison to these earlier works, we find that successful baryogenesis apparently requires larger values of H_{rh} as well as larger values of ξ_{rh}. Otherwise, the produced asymmetry will fall short off the observed value by several orders of magnitude. The reason for this change in numbers is that we indirectly include several effects in our analysis that had previously been neglected. By employing the analytical expression in Eq. (7.7), we make sure to account for the gradual change of the weak

---

[2]This conclusion can be avoided if the reheating temperature after inflation is below the electroweak scale, $T_{\mathrm{rh}} \lesssim 100\,\mathrm{GeV}$. In this case, baryon number is not anomalously violated after inflation and the decaying *magnetic* (not hypermagnetic) helicity fails to generate a nonzero baryon asymmetry. Similarly, our conclusions regarding the overproduction of baryon number may change if the dynamics of reheating, which we did not account for in our analysis, should dramatically change our estimate of the initial hypermagnetic field strength in Eq. (6.3).

mixing angle during the electroweak crossover, the chiral magnetic effect, the standard model Yukawa interactions, etc. The combination of Eq. (7.7) with our results for B_p and λ_p at the time of EWSB (see Eqs. (6.15) and (6.16)) then enables us to assess the efficiency of baryogenesis more accurately. On the other hand, it must not be forgotten that also our analysis still suffers from quite large uncertainties. Future work needs to tackle in particular two issues: a better treatment of reheating after inflation as well as a better understanding of the evolution of the weak mixing angle during the electroweak phase transition. Moreover, to relate the efficiency of baryogenesis to the strength of the present-day intergalactic magnetic fields more precisely, more work on the evolution of magnetic fields at low temperature is needed.

7.2   High-frequency signal in gravitational waves

In Sec. 5.1, we discussed the equations of motion for the homogeneous background fields a and $A_\pm^k$ in an exact FLRW background; see Eqs. (5.2), (5.5) and (5.9). In addition to this, it is also essential to study the dynamics of the corresponding perturbations in the inflaton field as well as in the metric tensor. Here, a crucial observation is that the exponentially enhanced gauge field readily provides new source terms for the primordial scalar and tensor perturbations [48, 49]. As it turns out, the new contributions to the scalar power spectrum are mostly controlled by the backreaction parameter δ_{KG}; see, e.g., [69]. As long as we stay in the weak field regime, $\delta_{\mathrm{KG}} \ll 1$ (see Eq. (5.19)), the corrections to the scalar power spectrum are, therefore, more or less negligible for our purposes. The corrections to the tensor power spectrum, on the other hand, can become quite sizable from the point of view of observational prospects — and that even so in the weak field regime! In fact, primordial tensor perturbations from the epoch of inflation give rise to a spectrum of stochastic GWs in the present epoch over a broad range of frequencies. The amplification of the tensor power spectrum in models of pseudoscalar inflation, therefore, has important consequences for the expected signal of stochastic GWs from inflation. As shown in [46, 47], pseudoscalar inflation may even result in sizable GWs on small scales that are possibly within the reach of direct GW observations. As we will discuss in the following, the primordial GW signal on small scales ends up being dominated by the gauge contribution rather than the vacuum contribution in a large part of parameter space. This opens up the possibility to test our scenario, at least in principle, by means of future GW observations.

Let us now discuss the spectral GW energy density from inflation, $\Omega_{\mathrm{GW}}^0 h^2$, in more detail. We first argue that the GW spectrum is flat to first approximation. In the presence of the axion-gauge-field coupling in Eq. (4.2), the spectral energy density $\Omega_{\mathrm{GW}}^0 h^2$ receives two contributions,

$$\Omega_{\mathrm{GW}}^0 h^2 = \left[\Omega_{\mathrm{GW}}^0 h^2\right]_{\mathrm{vacuum}} + \left[\Omega_{\mathrm{GW}}^0 h^2\right]_{\mathrm{gauge}} . \tag{7.13}$$

Here, $\left[\Omega_{\mathrm{GW}}^0 h^2\right]_{\mathrm{vacuum}}$ denotes the vacuum contribution in standard single-field slow-roll inflation,

$$\left[\Omega_{\mathrm{GW}}^0 h^2\right]_{\mathrm{vacuum}} = \frac{\Omega_{\mathrm{rad}}^0 h^2}{12} \left(\frac{g_*}{g_*^0}\right) \left(\frac{g_{*,s}^0}{g_{*,s}}\right)^{4/3} \left(\frac{H}{\pi M_{\mathrm{Pl}}}\right)^2 , \qquad (7.14)$$

which scales with the square of Hubble rate during inflation. $\Omega_{\mathrm{rad}}^0 h^2 \simeq 2.5 \times 10^{-5}$ is the density parameter of radiation in the present epoch, while the combination of effective numbers of DOFs ($g_* = 106.75$, $g_*^0 = 2$, $g_{*,s} = 106.75$, $g_{*,s}^0 \simeq 3.91$) accounts for the redshift behavior of the GW signal since its production.[3] For typical values of H, Eq. (7.14) yields a rather weak GW signal,

$$\left[\Omega_{\mathrm{GW}}^0 h^2\right]_{\mathrm{vacuum}} \simeq 2.3 \times 10^{-22} \left(\frac{H}{10^{11}\,\mathrm{GeV}}\right)^2 . \qquad (7.15)$$

Recalling that the Hubble rate during inflation is related to the primordial tensor-to-scalar ratio, $H \simeq 7.9 \times 10^{13}\,\mathrm{GeV}\,(r/0.1)^{1/2}$, we point out that Eq. (7.15) is in fact equivalent to Eq. (4.1).

Meanwhile, one obtains for the contribution to $\Omega_{\mathrm{GW}}^0 h^2$ [48, 49] from the gauge fields,

$$\left[\Omega_{\mathrm{GW}}^0 h^2\right]_{\mathrm{gauge}} \simeq \left[\Omega_{\mathrm{GW}}^0 h^2\right]_{\mathrm{vacuum}} \left(\frac{H}{M_{\mathrm{Pl}}}\right)^2 (f_L + f_R)\, e^{4\pi\xi} , \qquad (7.16)$$

where f_L and f_R are two fit functions that need to be determined numerically,[4]

$$f_L = 10^{-7} \times \begin{cases} 2.6\,/\,\xi^{5.7} & ; \quad \xi \lesssim 3 \\ 4.3\,/\,\xi^{6.0} & ; \quad \xi \gtrsim 3 \end{cases} , \qquad f_R = \frac{9.2}{\xi^{6.0}} \times 10^{-10} . \qquad (7.17)$$

Fitting Eq. (7.16) as a function of H^4 and $e^{4\pi\xi}$ results in the following phenomenological expression, which reproduces the exact result very accurately in the entire parameter space of interest,

$$\left[\Omega_{\mathrm{GW}}^0 h^2\right]_{\mathrm{gauge}} \simeq 2.3 \times 10^{-22} \exp\left[0.91 \times 4\pi\,(\xi - 4.61)\right] \left(\frac{H}{10^{11}\,\mathrm{GeV}}\right)^4 . \qquad (7.18)$$

Note that, in Eqs. (7.15) and (7.18), we have chosen the reference values for H and ξ such that both contributions to the GW spectrum are of the same size. Moreover,

---

[3]More precisely, these factors are part of the so-called transfer function, which describes the redshift behavior of GW modes outside and inside the Hubble horizon; see, e.g., [120] and references therein. Strictly speaking, the functional form of Eq. (7.14) only applies to those modes which cross inside the Hubble horizon prior to matter-radiation equality. This is however the case for all GW modes that we are going to be interested in.

[4]In Sec. 5.2, we solved all relevant momentum integrals by ourselves; see Eq. (5.16). However, in our discussion of the primordial tensor perturbations, we will now rely on the numerical fit functions available in the literature.

Eqs. (7.15) and (7.18) also illustrate that, for $H = 10^{11}\,\mathrm{GeV}$ and $\xi > 4.61$, the gauge contribution to $\Omega_{\mathrm{GW}}^0 h^2$ exceeds the vacuum contribution. This demonstrates that the GW signal can indeed be dominated by the gauge contribution, although both backreaction parameters, δ_{F} and δ_{KG}, actually take small values; see Eq. (5.18). In fact, it is easy to show that the GW spectrum is always dominated by the gauge contribution as soon as H is larger than some critical, ξ-dependent value $H_{\mathrm{GW}}^{\mathrm{crit}}$,

$$H_{\mathrm{GW}}^{\mathrm{crit}} = (f_L + f_R)^{-1/2}\, e^{-2\pi\xi}\, M_{\mathrm{Pl}} \simeq 1.1 \times 10^{10}\,\mathrm{GeV}\, \exp\left[-0.88 \times 2\pi\,(\xi - 5)\right]\,. \quad (7.19)$$

As long as ξ and H are constant, both $\left[\Omega_{\mathrm{GW}}^0 h^2\right]_{\mathrm{vacuum}}$ and $\left[\Omega_{\mathrm{GW}}^0 h^2\right]_{\mathrm{gauge}}$ are independent of time t and frequency f. In this limit, GWs therefore exhibit a flat power spectrum.

Next, let us discuss the frequency dependence of this spectrum. We just saw that the GW spectrum is flat in the limit where ξ and H are constant. However, ξ and H are not *exactly* constant but slowly vary during inflation. This results in a frequency dependence of the GW spectrum, after all. A GW signal at frequency f corresponds to a primordial tensor perturbation with wavenumber $k = 2\pi R_0 f$, where R_0 denotes the present-day value of the scale factor. During inflation, the amplitude of this perturbation mode freezes out once it is sufficiently far outside the Hubble horizon, if there are no active sources on *super*-horizon scales. In standard slow-roll inflation without any additional coupling to gauge fields, this requirement is satisfied simply once the k mode exits the horizon at $k/R\,(t_k) = H\,(t_k)$ (where t_k is defined by this very relation). In this case, one finds the GW amplitude at frequency f by evaluating the spectral energy density $\Omega_{\mathrm{GW}} h^2$ for $R\,(t_k)\, H\,(t_k) = k = 2\pi R_0 f$. On the other hand, it is not *a priori* clear whether this statement also remains true if the inflaton couples to gauge fields. The axion-gauge-field coupling may, e.g., affect the evolution of the tensor modes even on *super*-horizon scales. However, for $\xi \sim \mathcal{O}\,(1)$, it turns out that the k mode of the gauge field as well as the tensor perturbations of the metric are amplified only around the time of horizon exit. We therefore conclude that the GW spectrum at wavenumber k is generated and fixed once the k mode exits the horizon. For this reason, we can simply evaluate ξ and H in Eq. (7.16) at the time of horizon exit,

$$\xi = \xi\,(t_k)\,, \quad H = H\,(t_k)\,, \quad R\,(t_k)\, H\,(t_k) = k = 2\pi R_0 f\,. \quad (7.20)$$

Since both ξ and H slightly vary with time during inflation, this procedure results in a *frequency-dependent* spectrum of stochastic GWs. The contribution from the gauge fields has an exponential dependence on ξ, which results in a peak in the GW spectrum when ξ is maximal.

The present frequency f of the GW mode with wavenumber $k = 2\pi R_0 f$ is related to the number of e-folds between the time of horizon exit and the end of inflation, N_e, as follows,

$$N_e\,(f) = \ln\left[\frac{1}{2\pi f}\left(\frac{\pi^2}{45}\frac{g_*\, g_{*,s}^0}{g_{*,s}}\right)^{1/3}\frac{T_0\, T_{\mathrm{rh}}^{1/3}\, H_{\mathrm{inf}}^{1/3}}{M_{\mathrm{Pl}}^{2/3}}\right]\,, \quad (7.21)$$
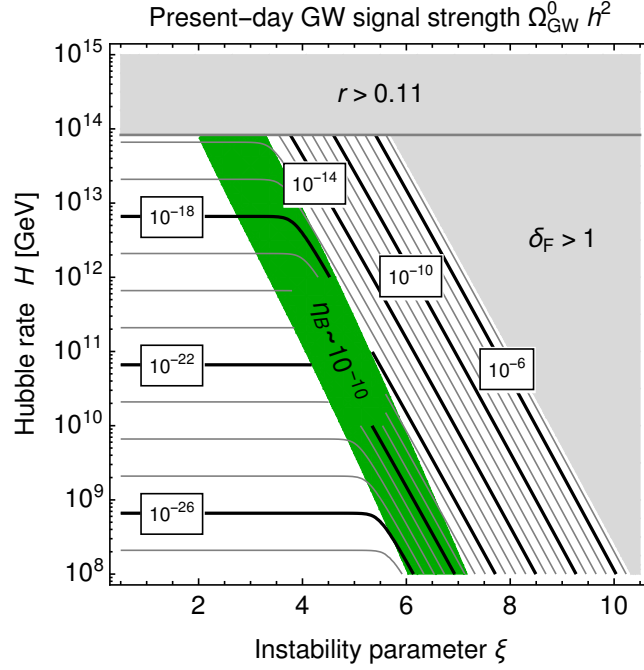
Figure 7.2: Present-day GW signal strength $\Omega_{\mathrm{GW}}^0 h^2$ as a function of the instability parameter ξ and the Hubble rate H; see Eqs. (7.13), (7.14), and (7.16). Here, ξ and H correspond to free parameters, which vary in the course of inflation. The green band is the same as in Figs. 6.2 and 7.1. The gray-shaded regions are the same as in Fig. 5.2.

where $H_{\mathrm{inf}} \approx H_{\mathrm{rh}}$ is the Hubble rate during inflation. In the approximation of instant reheating, $T_{\mathrm{rh}} = \sqrt{M_* H_{\mathrm{rh}}}$, this expression reduces to

$$N_e(f) \simeq 2.0 + \frac{1}{2} \ln\left(\frac{H_{\mathrm{rh}}}{10^{11}\,\mathrm{GeV}}\right) - \ln\left(\frac{f}{1\,\mathrm{MHz}}\right) . \qquad (7.22)$$

Then, we obtain the frequency-dependent GW spectrum as the following expression,

$$\Omega_{\mathrm{GW}} h^2(f) = \Omega_{\mathrm{GW}} h^2\left(\xi\left(N_e(f)\right), H\left(N_e(f)\right)\right) . \qquad (7.23)$$

The interplay between both contributions to the GW spectrum is depicted in Fig. 7.2, where we plot the total spectral energy density $\Omega_{\mathrm{GW}}^0 h^2$ as a function of ξ and H that slightly vary during inflation.[5] Each inflation model defines a trajectory γ in the ξ–H plane that may, e.g., be parametrized in terms of the number of e-folds until the end of inflation,

$$\gamma = \left\{\left(\xi\left(N_e\right), H\left(N_e\right)\right) \forall N_e\right\} . \qquad (7.24)$$

---

[5]During slow-roll inflation, ξ and H vary only very slowly, such that their time dependence does not have a strong impact on the gauge field evolution. This is the reason why we are able to solve Eq. (5.11) for constant ξ.

γ passes through various values of $\Omega_{\mathrm{GW}}^0 h^2$ during inflation. For each model, this results in a characteristic spectrum of stochastic GWs that could, in principle, be still observed today.

For many models of pseudoscalar inflation, ξ grows towards the end of inflation, as the inflaton velocity $\dot{a}$ becomes larger and larger. If this growth in ξ is strong enough, such that $H > H_{\mathrm{GW}}^{\mathrm{crit}}$ at some point (see Eq. (7.19)), the gauge contributions to $\Omega_{\mathrm{GW}} h^2$ will result in an exponentially steep increase in the GW spectrum. This mechanism of GW production will shut off as soon as inflation is over and our mechanism of gauge field production is no longer active. All in all, we therefore expect a characteristic feature in the GW spectrum associated with the explosive gauge field production at the end of inflation, i.e., around $N_e \simeq 0$. According to Eq. (7.22), we estimate that this peak should occur at frequencies in the MHz range or at even higher frequencies,

$$ N_e \left(f_{\mathrm{peak}} \right) \simeq 0 \quad \Rightarrow \quad f_{\mathrm{peak}} \simeq 7.1\,\mathrm{MHz} \left(\frac{H_{\mathrm{rh}}}{10^{11}\,\mathrm{GeV}} \right)^{1/2} . \qquad (7.25) $$

To estimate the strength of the peak in the GW spectrum, we simply need to evaluate $\Omega_{\mathrm{GW}} h^2$ in Eq. (7.13) for $\xi = \xi_{\mathrm{rh}}$ and $H = H_{\mathrm{rh}}$. Or alternatively, we may trade the dependence on ξ_{rh} and H_{rh} for the present-day strength of the magnetic field, B_p^0, as well as the peak frequency, f_{peak}. Making use of Eqs. (6.18), (7.13), and (7.25), we then find the following numerical relation,

$$ \left[\Omega_{\mathrm{GW}}^0 h^2 \right]_{\mathrm{peak}} \simeq 3.2 \times 10^{-20} \left(\frac{B_p^0}{10^{-16}\,\mathrm{GeV}} \right)^{6.13} \left(\frac{f_{\mathrm{peak}}}{10\,\mathrm{MHz}} \right)^{1.87} , \qquad (7.26) $$

which is another main result of our paper. In order to eliminate the ξ dependence in $\Omega_{\mathrm{GW}} h^2$, we numerically solved Eq. (6.18) for ξ. Based on the relation in Eq. (7.26), we plot B_p^0 as a function of f_{peak} and $\left[\Omega_{\mathrm{GW}}^0 h^2 \right]_{\mathrm{peak}}$ in Fig. 7.3. In view of Eq. (7.26) and Fig. 7.3, several comments are in order:

(i) In scenarios consistent with successful baryogenesis, the gauge field production at the end of inflation is typically accompanied by a rather weak signal in GWs at high frequencies. The detection of this peak is certainly out of reach of present-day technology. On the other hand, it is an unavoidable consequence of primordial magnetogenesis in our scenario. In the future, the detection of such a GW peak may therefore serve as a smoking-gun signal of primordial magnetogenesis at the end of pseudoscalar inflation. This in turn would lend support to the idea of baryogenesis from decaying hypermagnetic helicity. In particular, one could assess whether the strength of the observed GW signal turns out to be consistent with an inflaton coupling to the hypercharge gauge field — or whether this assumption would lead to baryon overproduction.

(ii) Along the diagonal line in Fig. 7.3, the GW spectrum at the end of inflation is dominated by the (irreducible) vacuum contribution. The part of parameter space below this line is therefore not accessible. Meanwhile, the vertical distance between
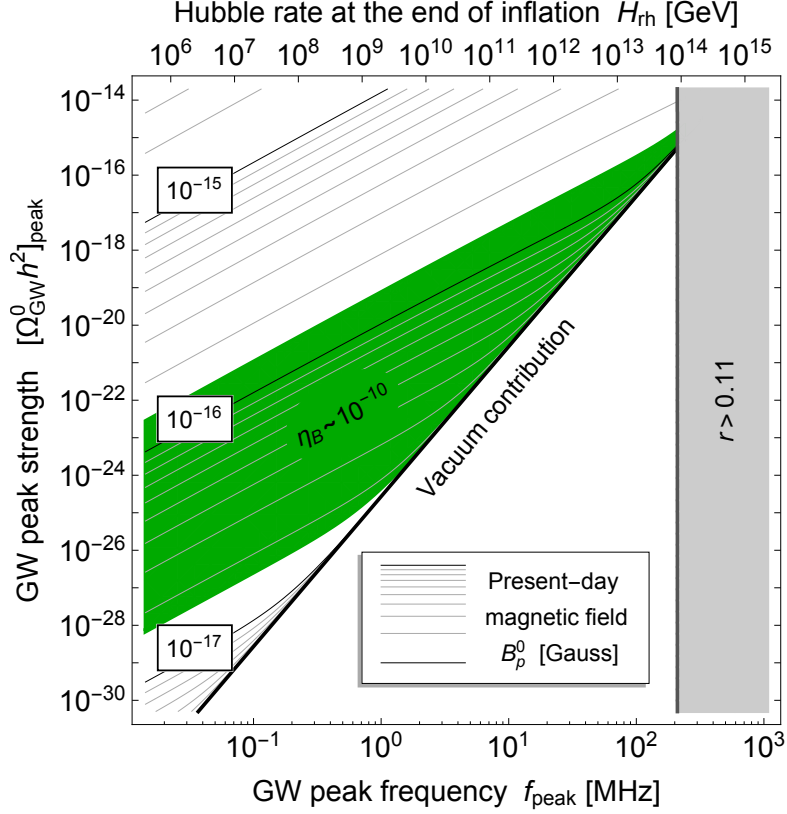
Figure 7.3: Present-day magnetic field strength B_p^0 as a function of the peak frequency f_{peak} and the strength of the peak in the GW spectrum associated with the gauge field production at the end of inflation, $\left[\Omega_{\text{GW}}^0 h^2\right]_{\text{peak}}$; see Eq. (7.26). In the approximation of instant reheating, f_{peak} is directly related to the Hubble rate at the end of inflation; see Eq. (7.25). The green band illustrates the region in parameter space where $\eta_B \sim 10^{-10}$; see Eq. (7.11).

this line and any point above indicates the extent to which the peak in the GW spectrum sticks out of the usual vacuum background.

(iii) We stress once more that, at the quantitative level, Eq. (7.26) and Fig. 7.3 may still receive a number of corrections. After all, every quantity in our analysis $(B_p^0, \eta_B, \Omega_{\text{GW}} h^2)$ comes with potentially large uncertainties. Nonetheless, we believe that Eq. (7.26) and Fig. 7.3 convey the correct idea at the qualitative level. Our results illustrate that pseudoscalar inflation leads to a highly nontrivial relation between initially completely independent phenomena: the present-day strength of the intergalactic magnetic field, the baryon asymmetry of the universe, and the stochastic background of GWs. This realization is one of our main achievements in this paper.

Chapter 8

Explicit scenarios based on natural inflation

All quantities that we were interested in so far (B_p^0, λ_p^0, η_B, and $\Omega_{\mathrm{GW}}^0 h^2$) solely depend on the values of ξ and H at the end of inflation. This observation allowed us to perform a completely model-independent analysis up to this point. We did not specify the form of the inflaton potential $V(a)$ and discarded all details of the reheating process. Instead, we simply employed a model-independent parametrization in terms of ξ_{rh} and H_{rh}. This means that all of our results up to this point apply to any model of pseudoscalar inflation that is anomalously coupled to the standard model hypercharge sector. Now, however, we shall illustrate our results by means of concrete examples, in order to see how realistic models of inflation give rise to the phenomenology described in the previous sections. To this end, we shall now study the evolution of ξ and H during inflation in concrete models and illustrate how they approach certain values towards the end of inflation. In other words: up to now, we were only interested in certain points in the ξ–H parameter plane; now we turn to the *inflationary trajectories* in this parameter plane.

Given the Lagrangian in Eq. (5.1), the inflaton field a is naturally identified as an axion, *i.e.*, the PNGB of a spontaneously broken global symmetry G_{global}. If this symmetry is anomalous under the standard model hypercharge gauge group $U(1)_Y$, the axion a will couple to the standard model hypercharge gauge field just as in Eq. (4.2). Moreover, if G_{global} is *in addition* anomalous under some strongly coupled gauge symmetry G_{strong}, nonperturbative effects in the G_{strong} gauge sector will generate a scalar potential for a of the following form,

$$V(a) = m_a^2 f_a^2 \left[1 - \cos\left(\frac{a}{f_a}\right) \right] . \tag{8.1}$$

Here, m_a and f_a denote the axion mass as well as the axion decay constant. The overall scale of the axion potential is set by the confinement scale in the strongly coupled sector, $m_a^2 f_a^2 \sim \Lambda_{\mathrm{strong}}^4$. In the following, we can treat both m_a and f_a as

free parameters. The scalar potential in Eq. (8.1) is nothing but the scalar potential of natural inflation [50, 51]. This is a trivial statement given the fact that natural inflation denotes the very idea that inflation is driven by the PNGB of some spontaneously broken and anomalous global symmetry. In the following, we shall study the inflationary trajectory for natural inflation in the ξ–H plane.

For any value of the inflaton field during slow-roll inflation, one can determine (ξ, H) from Eqs. (5.2) and (5.5). Once we replace $\dot{a}$ by $2\Lambda H\xi$, see Eq. (5.10), and neglect $\ddot{a}$, we have

$$3M_{\mathrm{Pl}}^2 H^2 - \frac{1}{2}\left(2\Lambda H\xi\right)^2 - V - \frac{1}{2}\left[\,\rho_{EE}\left(\xi, H\right) + \rho_{BB}\left(\xi, H\right)\,\right] = 0\,, \qquad (8.2)$$

$$6\Lambda H^2\xi + \frac{dV}{da} - \frac{1}{\Lambda}\,\rho_{EB}\left(\xi, H\right) = 0\,.$$

For a given pair of values for $\left(V, \frac{dV}{da}\right)$ as well as for given Λ, we can numerically solve Eq. (8.2) for (ξ, H). The slow-roll parameter ε including the contribution of the gauge field is [64]

$$\varepsilon = -\frac{\dot{H}}{H^2} = \frac{1}{2M_{\mathrm{Pl}}^2 H^2}\left[\dot{a}^2 + \frac{2}{3}\left(\rho_{EE} + \rho_{BB}\right)\right]\,, \qquad (8.3)$$

which can be computed once (ξ, H) has been determined. For each field value, we are therefore able to compute the corresponding value of ε. With the aid of Eq. (8.3), we can hence numerically determine the end point of inflation, where $\varepsilon = 1$. The number of e-folds N_e is given by

$$N_e = \int_{a_{\mathrm{end}}}^{a} da\,\frac{dN_e}{da}\,, \qquad (8.4)$$

where a_{end} is the field value at the end of inflation and the integrand is a simple function of ξ,

$$\frac{dN_e}{da} = -\frac{H}{\dot{a}} = -\frac{1}{2\Lambda\xi}. \qquad (8.5)$$

In summary, for each inflaton field value, we can compute the quadruplet $(\xi, H, \varepsilon, N_e)$, which enables us to draw an inflationary trajectory for any given model in the ξ–H parameter plane.

Now let us compute some explicit examples. Our variant of the natural inflation model is characterized by three parameters: the two parameters (m_a, f_a) in the potential, see Eq. (8.1), as well as the suppression scale Λ in the Chern-Simons interaction. We take the following values:[1]

$$\text{Model A:} \qquad m_a^2 = 4.1 \times 10^{-11}\,M_{\mathrm{Pl}}^2, \quad f_a = 7.0\,M_{\mathrm{Pl}}, \quad \Lambda^{-1} = 5.6\,M_{\mathrm{Pl}}^{-1}\,. \qquad (8.6)$$

---

[1]The parameters f_a and Λ ought to be related to each other in the UV completion of our model. But in this study, we do not specify any UV physics, which is why we treat f_a and Λ as independent parameters.
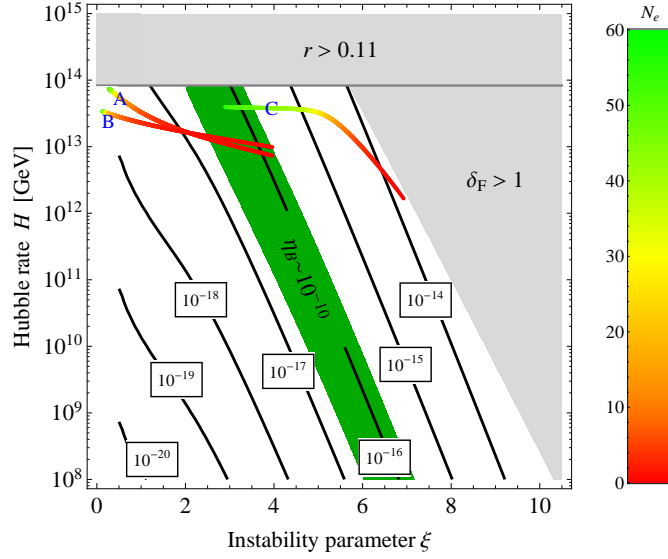
Figure 8.1: Trajectories of several inflation models in the ξ–H parameter plane. Trajectory A corresponds to natural inflation, see Eqs. (8.1) and (8.6), while trajectories B and C correspond to Starobinsky inflation, see Eq. (8.13), in the case of small and large axion-gauge-fields coupling, respectively. Numerical details are listed in Tab. 8.1. Successful baryogenesis is accomplished for any inflationary trajectory that ends in the green band, i.e., if the point $(\xi, H)_{\mathrm{end}} = (\xi_{\mathrm{rh}}, H_{\mathrm{rh}}) = \left(\xi(N_e = 0), H(N_e = 0)\right)$ lies in the green band; see Fig. 6.2 and Eq. (7.11).

Here, to distinguish it from other models that will be discussed, we refer to it as model A. Note that, to ensure successful baryogenesis, Λ cannot be chosen arbitrarily; see Eq. (7.12). Besides, to make the model compatible with the CMB observations, we need to chose particular values for the two parameters m_a and f_a. The parameters in Eq. (8.6) have been tuned in such a way that the model is compatible with all CMB observations and the baryon number asymmetry.

Following the procedure introduced above, we numerically compute (ξ, H) by solving Eq. (8.2) for each field value in the relevant part of the potential with a step width of $\Delta a = 0.01\, M_{\mathrm{Pl}}$. Then we compute the slow-roll parameter ε to determine the end of inflation, which is at

$$\text{Model A:} \qquad a_{\mathrm{end}} = -0.94\, M_{\mathrm{Pl}}\,. \tag{8.7}$$

For all field values during inflation, $a < a_{\mathrm{end}}$, the number of e-folds N_e is computed according to Eq. (8.4). Together, these points form the trajectory corresponding to model A in Fig. 8.1.

Model	A	B	C
Λ^{-1}	$5.6\,M_{\mathrm{Pl}}^{-1}$	$5.6\,M_{\mathrm{Pl}}^{-1}$	$75\,M_{\mathrm{Pl}}^{-1}$
$V(a)$	Eq. (8.1)	Eq. (8.13)	Eq. (8.13)
$\begin{bmatrix} m_a^2 \\ f_a \end{bmatrix}$ or $\begin{bmatrix} V_0 \\ \gamma_{\mathrm{s}} \end{bmatrix}$	$\begin{bmatrix} 4.1 \times 10^{-11}\,M_{\mathrm{Pl}}^2 \\ 7.0\,M_{\mathrm{Pl}} \end{bmatrix}$	$\begin{bmatrix} 6.7 \times 10^{-10}\,M_{\mathrm{Pl}}^4 \\ 0.30\,M_{\mathrm{Pl}}^{-1} \end{bmatrix}$	$\begin{bmatrix} 1.0 \times 10^{-9}\,M_{\mathrm{Pl}}^4 \\ 0.30\,M_{\mathrm{Pl}}^{-1} \end{bmatrix}$
$\begin{bmatrix} a \\ \dot{a} \\ H \\ \xi \end{bmatrix}_{N_e=0}$	$\begin{bmatrix} -0.94\,M_{\mathrm{Pl}} \\ 4.3 \times 10^{-6}\,M_{\mathrm{Pl}}^2 \\ 3.0 \times 10^{-6}\,M_{\mathrm{Pl}} \\ 4.0 \end{bmatrix}$	$\begin{bmatrix} -0.83\,M_{\mathrm{Pl}} \\ 5.7 \times 10^{-6}\,M_{\mathrm{Pl}}^2 \\ 4.0 \times 10^{-6}\,M_{\mathrm{Pl}} \\ 4.0 \end{bmatrix}$	$\begin{bmatrix} -0.09\,M_{\mathrm{Pl}} \\ 1.3 \times 10^{-7}\,M_{\mathrm{Pl}}^2 \\ 6.9 \times 10^{-7}\,M_{\mathrm{Pl}} \\ 6.9 \end{bmatrix}$
$\begin{bmatrix} a \\ \dot{a} \\ H \\ \xi \end{bmatrix}_{N_e=55}$	$\begin{bmatrix} -13\,M_{\mathrm{Pl}} \\ 3.0 \times 10^{-6}\,M_{\mathrm{Pl}}^2 \\ 3.0 \times 10^{-5}\,M_{\mathrm{Pl}} \\ 0.28 \end{bmatrix}$	$\begin{bmatrix} -8.7\,M_{\mathrm{Pl}} \\ 6.7 \times 10^{-7}\,M_{\mathrm{Pl}}^2 \\ 1.4 \times 10^{-5}\,M_{\mathrm{Pl}} \\ 0.13 \end{bmatrix}$	$\begin{bmatrix} -7.2\,M_{\mathrm{Pl}} \\ 1.3 \times 10^{-6}\,M_{\mathrm{Pl}}^2 \\ 1.6 \times 10^{-5}\,M_{\mathrm{Pl}} \\ 2.9 \end{bmatrix}$
$\begin{bmatrix} P_s \\ n_s \\ r \end{bmatrix}_{N_e=55}$	$\begin{bmatrix} 2.3 \times 10^{-9} \\ 0.96 \\ 0.08 \end{bmatrix}$	$\begin{bmatrix} 2.1 \times 10^{-9} \\ 0.97 \\ 0.02 \end{bmatrix}$	$\begin{bmatrix} 2.2 \times 10^{-9} \\ 0.94 \\ 0.05 \end{bmatrix}$

Table 8.1: Various parameters and numerical results for the three models A, B, and C.

The scalar power spectrum is evaluated according to

$$P_s = \left(\frac{H^2}{2\pi\dot{a}}\right)^2 \left(\frac{k}{k_{\mathrm{CMB}}}\right)^{n_s-1}, \tag{8.8}$$

where $k_{\mathrm{CMB}} = 0.05\,\mathrm{Mpc}^{-1}$ is the CMB pivot scale; and H and $\dot{a}$ are evaluated at the time when the pivot scale exits the horizon. We neglect the contribution from the gauge fields, since it is negligibly small in the region of interest. This should be compatible with the CMB normalization [40]:

$$P_s^{\mathrm{obs}} = (2.21 \pm 0.07) \times 10^{-9}. \tag{8.9}$$

The CMB pivot scale exits the horizon at $N_e^{\mathrm{CMB}} \simeq 55$, where we obtain

$$\text{Model A:} \quad a = -13.4\,M_{\mathrm{Pl}}, \quad \dot{a} = 3.0 \times 10^{-6}\,M_{\mathrm{Pl}}^2,$$

$$H = 3.0 \times 10^{-5}\,M_{\mathrm{Pl}}, \quad \xi = 0.28. \tag{8.10}$$

With these numerical results, we can evaluate the scalar power spectrum:

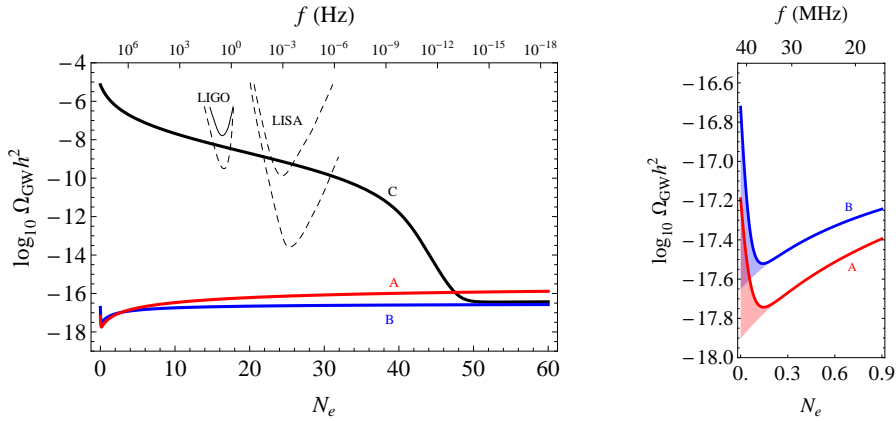$$\text{Model A:} \quad P_s = 2.3 \times 10^{-9}, \tag{8.11}$$

Figure 8.2: GW spectra of several models compared to the current (solid lines) and future (dashed lines) constraints from advanced LIGO and LISA. The red, blue and black curves corresponds to models A, B, and C, respectively. Model A: natural inflation; model B/C: Starobinsky inflation with a small/large axion-gauge-field coupling; see Tab. 8.1 for the numerical details. The red and blue shadows in the right panel represent the gauge contributions. To relate the number of e-folds N_e and the frequency f we have used Eq. (7.22) with $H_{\rm rh} = 10^{12.5}$ GeV, which is approximately correct for the models A, B, and C.

which is compatible with Eq. (8.9). Since the gauge field contribution is very weak at $N_e = N_e^{\rm CMB}$, the spectral index n_s and the tensor-to-scalar ratio r can be evaluated in the conventional way:

$$\text{Model A:} \qquad n_s = 1 + 2\,\eta - 6\,\varepsilon \simeq 0.96\,, \quad r = 16\,\varepsilon \simeq 0.08\,. \tag{8.12}$$

which agrees with the current PLANCK constraints [40]. All of the above numerical results are summarized in Tab. 8.1.

We can further compute the GW spectrum according to Eq. (7.13), including both the vacuum and gauge contributions. This is shown by the red curve in Fig. 8.2, where the red shadow denotes the gauge contribution. In Fig. 8.2, we also present the current constraints from advanced LIGO and future sensitivities from advanced LIGO and LISA. It turns out that the GW energy density $\Omega_{\rm GW}^0 h^2$ produced in model A is far below the reach of current or upcoming GW interferometers.

It has been shown [46] however that, with a strongly coupled axion, some models could reach the sensitivity of current or upcoming GW interferometers. For the Starobinsky model [11], e.g.,

$$V_{\rm Starobinsky}(a) = V_0 \left(1 - e^{\gamma_{\rm s} a}\right)^2\,, \quad a < 0\,, \tag{8.13}$$

with $(V_0, \gamma_{\rm s}) = (1.0 \times 10^{-9}\, M_{\rm Pl}^4, 0.3\, M_{\rm Pl}^{-1})$ and an axion-gauge-field coupling $\Lambda^{-1} = 75\, M_{\rm Pl}^{-1}$ (which is more than 10 times larger than the case we just discussed), $\Omega_{\rm GW}^0 h^2$ can reach the future sensitivities of advanced LIGO and LISA, as shown by the black curve in Fig. 8.2. Such a large GW energy is due to a very strong axion-gauge-field

coupling, which transfers almost the entire energy carried by the inflaton into the gauge field and induces much larger tensor perturbations. But strong axion-gauge-field couplings will always lead to baryon overproduction, as discussed model-independently in Sec. 7; see Eq. (7.12). Indeed, Fig. 8.1 shows that the trajectory of this model (we refer to it as model C; for numerical details, see Tab. 8.1) ends at a point far away from the region for successful baryogenesis (the green band). Actually, this point is very close to the bound $\delta_{\mathrm{F}} = 1$, which corresponds to the situation that the entire energy of the universe is stored in the gauge field. If we reduce the axion-gauge-field coupling of model C to the same value as in model A, then the model (now referred to as model B) leads to successful baryogenesis; see Fig. 8.1. But it has small $\Omega_{\mathrm{GW}}^0 h^2$, approximately of the same order of magnitude as model A.

It is interesting to note that the GW spectra of model A and B both peak at the very end of inflation, where the gauge contributions become dominant (at $0 \lesssim N_e \lesssim 0.3$, corresponding to $f \sim 40$ MHz, see the right panel of Fig. 8.2). This is an important feature of these models compared to models without the inflaton-gauge-field coupling. Although these peaks are out of reach of conventional GW interferometers, once detected by some other new technology in the future, they may serve as a smoking-gun signal for baryogenesis via primordial magnetic fields.

Chapter 9

Conclusions

In this paper, we revisited the implications of a Chern-Simons-like inflaton coupling to the standard model hypercharge gauge field, $\mathcal{L} \supset a/\left(4\Lambda\right)F\tilde{F}$, in general models of pseudoscalar inflation. We focused in particular on two phenomenological aspects: (i) the production of primordial gauge fields towards the end of inflation (i.e., primordial magnetogenesis) and its consequences for baryogenesis from decaying (hyper)magnetic fields at the time of EWSB; and (ii) the associated production of primordial tensor perturbations and their impact on the present-day spectrum of stochastic gravitational waves. Our main results can be summarized as follows:

1. Primordial magnetogenesis at the end of pseudoscalar inflation can result in sizable present-day magnetic fields with a correlation length on astrophysical scales; see Eqs. (6.18) and (6.19). These fields then contribute to the intergalactic magnetic fields we observe today. The main uncertainties in our estimate are: (i) the impact of reheating on the gauge field production after the end of inflation and (ii) the impact of damping effects at temperatures below $10\,\mathrm{MeV}$. In particular, we point out that the presence of a strong hyper-EM field during reheating may open up new channels of particle production, such as pair production via the Schwinger effect. This effect has recently been studied by the authors of Ref. [121], who referred to it as *Schwinger reheating*. Moreover, it is important to understand how the emerging charged plasma back-reacts on the primordial gauge field. A better treatment of this complicated process requires a dedicated numerical simulation that takes into account both nonperturbative particle production as well as MHD effects. Such a study is beyond the scope of this paper; but we certainly encourage further efforts into this direction.

2. The primordial gauge fields generated towards the end of pseudoscalar inflation are maximally helical and can, thus, source the generation of nonzero baryon number around the time of the electroweak crossover via the chiral anomaly in the standard model. We updated previous studies of this mechanism of primordial baryogenesis, which led us to the conclusion that successful baryogenesis is

indeed possible in a large part of parameter space, see Eq. (7.11). We found that the pseudoscalar inflaton must be *weakly* coupled to the hypercharge gauge field, since the primordial gauge fields will otherwise result in an overproduction of baryon number. To be more precise, successful baryogenesis requires an instability parameter ξ of around $\xi \sim 5$ at the end of inflation, which translates into a suppression scale Λ of around $\Lambda \sim 3 \times 10^{17}$ GeV. Again, a main uncertainty of our estimate is the strength of the primordial hypermagnetic field at the time of EWSB. Besides that, the poor knowledge of the temperature dependence of the weak mixing angle during the crossover, $\theta_W(T)$, induces further uncertainties. A better understanding of baryogenesis via decaying helicity, therefore, requires a more careful determination of $\theta_W(T)$.

3. The gauge field production at the end of inflation is accompanied by the production of stochastic gravitational waves. We are able to show that the production of gauge fields consistent with successful baryogenesis at later times typically results a weak GW signal at frequencies in the MHz range or even above; see Eq. (7.26) and Fig. 7.3. GWs at such high frequencies are extremely hard to detect; see [122, 123] for a past measurement, [124] for an on-going experiment as well as [125, 126] for proposals of future techniques. However, if the signal predicted in our scenario should eventually be measured by future experiments, it would serve as a smoking gun for the explosive gauge field production at the end of inflation (and hence provide evidence for baryogenesis via decaying magnetic fields during the electroweak crossover). On the other hand, we are able to conclude that any stronger GW signal would imply the overproduction of baryon number. In this case, one would either have to give up on an inflaton coupling to the standard model hypercharge gauge field or one would have to assume low reheating temperature, such that $T_{\rm rh} \lesssim T_{\rm ew}$.

Our analysis illustrates how models of pseudoscalar inflation result in a highly non-trivial interrelation of several, *a priori* unrelated phenomena: the present-day large-scale magnetic field, the baryon asymmetry of the universe, and features in the spectrum of stochastic GWs. In the present paper, we mainly focused on the qualitative aspects of this interplay of phenomena and more work is needed to arrive at more reliable and more precise quantitative predictions. In particular, the impacts of non-perturbative effects [110, 111] and possible thermalization [112] on the gauge field production during (including the last of) the slow-roll stage of inflation for larger ξ as well as those at the inflaton oscillation/reheating stage [106–108] must be understood more deeply for the precise evaluation of the production of the magnetic fields and the GWs. Such an effort requires progress on several fronts. But it also promises to lead to a better understanding of an intriguing cosmological scenario that comes with rich phenomenology deriving from a single additional operator in the effective Lagrangian: $\mathcal{L} \supset a/(4\Lambda)\, F\tilde{F}$.

Acknowledgements

I would like to thank everyone that made this work possible and enjoyable. First, Manfred Lindner for allowing me to work at his group in the MPIK, and, in particular, Kai Schmitz, who introduced me to the topic and allowed me to experience firsthand what research is like; his help was an essential step towards accomplishing this thesis. Moreover, I am grateful for all discussions with Xunjie Xu, Kohei Kamada and Kai, as well as with Valerie Domcke, and for all I learnt from them. Last but not least, I would like to thank my family, friends and colleagues for all the support which made my master's degree not only possible but also a memorable experience. Special thanks to Kevin, Veronica, Gabriel and, above all, my parents.

Bibliography

[1] D. Jiménez, K. Kamada, K. Schmitz and X. J. Xu, *Baryon Asymmetry and Gravitational Waves from Pseudoscalar Inflation*, JCAP **1712** (2017) no. 12, 011, 1707.07943 [HEP-PH].

[2] D. Baumann, Lecture notes on *Cosmology*, University of Cambridge (2014).

[3] P. A. R. Ade *et al.* [Planck Collaboration], *Planck 2015 results. XIII. Cosmological parameters*, Astron. Astrophys. **594**, A13 (2016), 1502.01589 [ASTRO-PH.CO].

[4] C. W. Misner, K. S. Thorne, J. A. Wheeler, *Gravitation*, Freeman, New York (1973).

[5] C. Patrignani *et al.* [Particle Data Group], *Review of Particle Physics*, Chin. Phys. C **40** (2016) no. 10, 100001.

[6] W. H. Kinney, *TASI Lectures on Inflation*, 0902.1529 [ASTRO-PH.CO].

[7] A. H. Guth, *The Inflationary Universe: A Possible Solution to the Horizon and Flatness Problems*, Phys. Rev. D **23**, 347 (1981).

[8] K. Sato, *First Order Phase Transition of a Vacuum and Expansion of the Universe*, Mon. Not. Roy. Astron. Soc. **195**, 467 (1981).

[9] A. D. Linde, *A New Inflationary Universe Scenario: A Possible Solution of the Horizon, Flatness, Homogeneity, Isotropy and Primordial Monopole Problems*, Phys. Lett. B **108**, 389 (1982).

[10] A. Albrecht and P. J. Steinhardt, *Cosmology for Grand Unified Theories with Radiatively Induced Symmetry Breaking*, Phys. Rev. Lett. **48**, 1220 (1982).

[11] A. A. Starobinsky, *A New Type of Isotropic Cosmological Models Without Singularity*, Phys. Lett. B **91**, 99 (1980).

[12] A. R. Liddle and S. M. Leach, *How long before the end of inflation were observable perturbations produced?*, Phys. Rev. D **68** (2003) 103503, 0305263 [ASTRO-PH].

[13] W. H. Kinney and A. Riotto, *Theoretical uncertainties in inflationary predictions*, JCAP **0603** (2006) 011, 0511127 [ASTRO-PH].

[14] A. A. Starobinsky, *Spectrum of relict gravitational radiation and the early state of the universe*, JETP Lett. **30**, 682 (1979), Pisma Zh. Eksp. Teor. Fiz. **30**, 719 (1979).

[15] V. F. Mukhanov and G. V. Chibisov, *Quantum Fluctuations and a Nonsingular Universe*, JETP Lett. **33** (1981) 532 [Pisma Zh. Eksp. Teor. Fiz. **33** (1981) 549].

[16] S. W. Hawking, *The Development of Irregularities in a Single Bubble Inflationary Universe*, Phys. Lett. **115B** (1982) 295.

[17] S. W. Hawking and I. G. Moss, *Fluctuations in the Inflationary Universe*, Nucl. Phys. B **224** (1983) 180.

[18] A. A. Starobinsky, *Dynamics of Phase Transition in the New Inflationary Universe Scenario and Generation of Perturbations*, Phys. Lett. **117B** (1982) 175.

[19] A. H. Guth and S. Y. Pi, *Fluctuations in the New Inflationary Universe*, Phys. Rev. Lett. **49** (1982) 1110.

[20] J. M. Bardeen, P. J. Steinhardt and M. S. Turner, *Spontaneous Creation of Almost Scale - Free Density Perturbations in an Inflationary Universe*, Phys. Rev. D **28** (1983) 679.

[21] D. Baumann, *Inflation*, TASI 2009, 0907.5424 [HEP-TH].

[22] K. A. Malik and D. Wands, *Cosmological perturbations*, Phys. Rept. **475** (2009) 1, 0809.4944 [ASTRO-PH].

[23] J. M. Bardeen, *Gauge Invariant Cosmological Perturbations*, Phys. Rev. D **22** (1980) 1882.

[24] D. Wands, K. A. Malik, D. H. Lyth and A. R. Liddle, *A New approach to the evolution of cosmological perturbations on large scales*, Phys. Rev. D **62** (2000) 043527 0003278 [ASTRO-PH].

[25] V. Acquaviva, N. Bartolo, S. Matarrese and A. Riotto, Nucl. Phys. B **667** (2003) 119, 0209156 [ASTRO-PH].

[26] J. M. Maldacena, *Non-Gaussian features of primordial fluctuations in single field inflationary models*, JHEP **0305** (2003) 013, 0210603 [ASTRO-PH].

[27] D. H. Lyth, *What would we learn by detecting a gravitational wave signal in the cosmic microwave background anisotropy?*, Phys. Rev. Lett. **78** (1997) 1861 9606387 [HEP-PH].

[28] T. Jacobson, *Introduction to quantum fields in curved space-time and the Hawking effect*, CECS School on Quantum Gravity, Valdivia, Chile (2002), 0308048 [GR-QC].

[29] N. D. Birrell and P. C. W. Davies, *Quantum Fields in Curved Space*, vol. 7, Cambridge University Press, Cambridge, UK (1982).

[30] A. D. Sakharov, *Violation of CP Invariance, C Asymmetry, and Baryon Asymmetry of the Universe*, Pisma Zh. Eksp. Teor. Fiz. **5** (1967) 32 [JETP Lett. **5** (1967) 24] [Sov. Phys. Usp. **34** (1991) 392] [Usp. Fiz. Nauk **161** (1991) 61].

[31] L. Canetti, M. Drewes and M. Shaposhnikov, *Matter and Antimatter in the Universe*, New J. Phys. **14** (2012) 095012, 1204.4186 [HEP-PH].

[32] B. P. Abbott *et al.* [LIGO Scientific and Virgo Collaborations], *Observation of Gravitational Waves from a Binary Black Hole Merger*, Phys. Rev. Lett. **116**, 061102 (2016), 1602.03837 [GR-QC].

[33] B. P. Abbott *et al.* [LIGO Scientific and Virgo Collaborations], *GW151226: Observation of Gravitational Waves from a 22-Solar-Mass Binary Black Hole Coalescence*, Phys. Rev. Lett. **116**, 241103 (2016), 1606.04855 [GR-QC].

[34] B. P. Abbott *et al.* [LIGO Scientific and VIRGO Collaborations], *GW170104: Observation of a 50-Solar-Mass Binary Black Hole Coalescence at Redshift 0.2*, Phys. Rev. Lett. **118**, 221101 (2017), 1706.01812 [GR-QC].

[35] M. Maggiore, *Gravitational wave experiments and early universe cosmology*, Phys. Rept. **331**, 283 (2000), GR-QC/9909001.

[36] V. A. Rubakov, M. V. Sazhin and A. V. Veryaskin, *Graviton Creation in the Inflationary Universe and the Grand Unification Scale*, Phys. Lett. **115B**, 189 (1982).

[37] M. Guzzetti, C., N. Bartolo, Liguori, M. and S. Matarrese, *Gravitational waves from inflation*, Riv. Nuovo Cim. **39**, 399 (2016), 1605.01615 [ASTRO-PH.CO].

[38] K. Nakayama, S. Saito, Y. Suwa and J. Yokoyama, *Space laser interferometers can determine the thermal history of the early Universe*, Phys. Rev. D **77**, 124001 (2008), 0802.2452 [HEP-PH].

[39] K. Nakayama, S. Saito, Y. Suwa and J. Yokoyama, *Probing reheating temperature of the universe with gravitational wave background*, JCAP **0806**, 020 (2008), 0804.1827 [ASTRO-PH].

[40] P. A. R. Ade *et al.* [Planck Collaboration], *Planck 2015 results. XX. Constraints on inflation*, Astron. Astrophys. **594**, A20 (2016), 1502.02114 [ASTRO-PH.CO].

[41] B. P. Abbott *et al.* [LIGO Scientific and Virgo Collaborations], *Upper Limits on the Stochastic Gravitational-Wave Background from Advanced LIGO's First Observing Run*, Phys. Rev. Lett. **118**, 121101 (2017), 1612.02029 [GR-QC].

[42] N. Seto, S. Kawamura and T. Nakamura, *Possibility of direct measurement of the acceleration of the universe using 0.1-Hz band laser interferometer gravitational wave antenna in space*, Phys. Rev. Lett. **87**, 221103 (2001), astro-ph/0108011.

[43] S. Kawamura *et al.*, *The Japanese space gravitational wave antenna DECIGO*, Class. Quant. Grav. **23**, S125 (2006).

[44] J. Crowder and N. J. Cornish, *Beyond LISA: Exploring future gravitational wave missions*, Phys. Rev. D **72**, 083005 (2005), gr-qc/0506015.

[45] G. M. Harry, P. Fritschel, D. A. Shaddock, W. Folkner and E. S. Phinney, *Laser interferometry for the big bang observer*, Class. Quant. Grav. **23**, 4887 (2006), Erratum ibid. **23**, 7361 (2006).

[46] V. Domcke, M. Pieroni and P. Binétruy, *Primordial gravitational waves for universality classes of pseudoscalar inflation*, JCAP **1606**, 031 (2016), 1603.01287 [astro-ph.CO].

[47] J. Garcia-Bellido, M. Peloso and C. Unal, *Gravitational waves at interferometer scales and primordial black holes in axion inflation*, JCAP **1612**, 031 (2016), 1610.03763 [astro-ph.CO].

[48] J. L. Cook and L. Sorbo, *Particle production during inflation and gravitational waves detectable by ground-based interferometers*, Phys. Rev. D **85**, 023534 (2012), Erratum ibid. D **86**, 069901 (2012), 1109.0022 [astro-ph.CO].

[49] M. M. Anber and L. Sorbo, *Non-Gaussianities and chiral gravitational waves in natural steep inflation*, Phys. Rev. D **85**, 123537 (2012), 1203.5849 [astro-ph.CO].

[50] K. Freese, J. A. Frieman and A. V. Olinto, *Natural inflation with pseudo-Nambu-Goldstone bosons*, Phys. Rev. Lett. **65**, 3233 (1990).

[51] F. C. Adams, J. R. Bond, K. Freese, J. A. Frieman and A. V. Olinto, *Natural inflation: Particle physics models, power law spectra for large scale structure, and constraints from COBE*, Phys. Rev. D **47**, 426 (1993), hep-ph/9207245.

[52] S. Weinberg, *A New Light Boson?*, Phys. Rev. Lett. **40**, 223 (1978).

[53] F. Wilczek, *Problem of Strong p and t Invariance in the Presence of Instantons*, Phys. Rev. Lett. **40**, 279 (1978).

[54] R. D. Peccei and H. R. Quinn, *CP Conservation in the Presence of Instantons*, Phys. Rev. Lett. **38**, 1440 (1977).

[55] R. D. Peccei and H. R. Quinn, *Constraints Imposed by CP Conservation in the Presence of Instantons*, Phys. Rev. D **16**, 1791 (1977).

[56] P. Svrcek and E. Witten, *Axions In String Theory*, JHEP **0606**, 051 (2006), hep-th/0605206.

[57] M. B. Green and J. H. Schwarz, *Anomaly Cancellation in Supersymmetric D=10 Gauge Theory and Superstring Theory*, Phys. Lett. **149B**, 117 (1984).

[58] I. Obata, *Chiral primordial blue tensor spectra from the axion-gauge couplings*, 1612.08817 [astro-ph.CO].

[59] M. S. Turner and L. M. Widrow, *Inflation Produced, Large Scale Magnetic Fields*, Phys. Rev. D **37**, 2743 (1988).

[60] W. D. Garretson, G. B. Field and S. M. Carroll, *Primordial magnetic fields from pseudoGoldstone bosons*, Phys. Rev. D **46**, 5346 (1992), hep-ph/9209238.

[61] M. M. Anber and L. Sorbo, *N-flationary magnetic fields*, JCAP **0610**, 018 (2006), astro-ph/0606534.

[62] R. Durrer, L. Hollenstein and R. K. Jain, *Can slow roll inflation induce relevant helical magnetic fields?*, JCAP **1103**, 037 (2011), 1005.5322 [astro-ph.CO].

[63] P. D. Meerburg and E. Pajer, *Observational Constraints on Gauge Field Production in Axion Inflation*, JCAP **1302**, 017 (2013), 1203.6076 [astro-ph.CO].

[64] M. M. Anber and L. Sorbo, *Naturally inflating on steep potentials through electromagnetic dissipation*, Phys. Rev. D **81**, 043534 (2010), 0908.4089 [hep-th].

[65] N. Barnaby, R. Namba and M. Peloso, *Phenomenology of a Pseudo-Scalar Inflaton: Naturally Large Nongaussianity*, JCAP **1104**, 009 (2011), 1102.4333 [astro-ph.CO].

[66] N. Barnaby, E. Pajer and M. Peloso, *Gauge Field Production in Axion Inflation: Consequences for Monodromy, non-Gaussianity in the CMB, and Gravitational Waves at Interferometers*, Phys. Rev. D **85**, 023525 (2012), 1110.3327 [astro-ph.CO].

[67] N. Barnaby and M. Peloso, *Large Nongaussianity in Axion Inflation*, Phys. Rev. Lett. **106**, 181301 (2011), 1011.1500 [hep-ph].

[68] L. Sorbo, *Parity violation in the Cosmic Microwave Background from a pseudoscalar inflaton*, JCAP **1106**, 003 (2011), 1101.1525 [astro-ph.CO].

[69] A. Linde, S. Mooij and E. Pajer, *Gauge field production in supergravity inflation: Local non-Gaussianity and primordial black holes*, Phys. Rev. D **87**, 103506 (2013), 1212.1693 [hep-th].

[70] E. Bugaev and P. Klimai, *Axion inflation with gauge field production and primordial black holes*, Phys. Rev. D **90**, 103501 (2014), 1312.7435 [astro-ph.CO].

[71] E. Erfani, *Primordial Black Holes Formation from Particle Production during Inflation*, JCAP **1604**, 020 (2016), 1511.08470 [astro-ph.CO].

[72] J. Garcia-Bellido, M. Peloso and C. Unal, *Gravitational Wave signatures of inflationary models from Primordial Black Hole Dark Matter*, 1707.02441 [ASTRO-PH.CO].

[73] L. M. Widrow, D. Ryu, D. R. G. Schleicher, K. Subramanian, C. G. Tsagas and R. A. Treumann, *The First Magnetic Fields*, Space Sci. Rev. **166**, 37 (2012), 1109.4052 [ASTRO-PH.CO].

[74] R. Durrer and A. Neronov, *Cosmological Magnetic Fields: Their Generation, Evolution and Observation*, Astron. Astrophys. Rev. **21**, 62 (2013), 1303.7121 [ASTRO-PH.CO].

[75] A. Neronov and I. Vovk, *Evidence for strong extragalactic magnetic fields from Fermi observations of TeV blazars*, Science **328**, 73 (2010), 1006.3504 [ASTRO-PH.HE].

[76] F. Tavecchio, G. Ghisellini, L. Foschini, G. Bonnoli, G. Ghirlanda and P. Coppi, *The intergalactic magnetic field constrained by Fermi/LAT observations of the TeV blazar 1ES 0229+200*, Mon. Not. Roy. Astron. Soc. **406**, L70 (2010), 1004.1329 [ASTRO-PH.CO].

[77] K. Dolag, M. Kachelriess, S. Ostapchenko and R. Tomas, *Lower limit on the strength and filling factor of extragalactic magnetic fields*, Astrophys. J. **727**, L4 (2011), 1009.1782 [ASTRO-PH.HE].

[78] W. Essey, S. Ando and A. Kusenko, *Determination of intergalactic magnetic fields from gamma ray data*, Astropart. Phys. **35**, 135 (2011), 1012.5313 [ASTRO-PH.HE].

[79] A. M. Taylor, I. Vovk and A. Neronov, *Extragalactic magnetic fields constraints from simultaneous GeV-TeV observations of blazars*, Astron. Astrophys. **529**, A144 (2011), 1101.0932 [ASTRO-PH.HE].

[80] K. Takahashi, M. Mori, K. Ichiki, S. Inoue and H. Takami, *Lower Bounds on Magnetic Fields in Intergalactic Voids from Long-term GeV-TeV Light Curves of the Blazar Mrk 421*, Astrophys. J. **771**, L42 (2013), 1303.3069 [ASTRO-PH.CO].

[81] J. D. Finke, L. C. Reyes, M. Georganopoulos, K. Reynolds, M. Ajello, S. J. Fegan and K. McCann, *Constraints on the Intergalactic Magnetic Field with Gamma-Ray Observations of Blazars*, Astrophys. J. **814**, no. 1, 20 (2015), 1510.02485 [ASTRO-PH.HE].

[82] A. Kandus, K. E. Kunze and C. G. Tsagas, *Primordial magnetogenesis*, Phys. Rept. **505**, 1 (2011), 1007.3891 [ASTRO-PH.CO].

[83] M. Giovannini and M. E. Shaposhnikov, *Primordial magnetic fields, anomalous isocurvature fluctuations and big bang nucleosynthesis*, Phys. Rev. Lett. **80**, 22 (1998), HEP-PH/9708303.

[84] M. Giovannini and M. E. Shaposhnikov, *Primordial hypermagnetic fields and triangle anomaly*, Phys. Rev. D **57**, 2186 (1998), hep-ph/9710234.

[85] K. Bamba, *Baryon asymmetry from hypermagnetic helicity in dilaton hypercharge electromagnetism*, Phys. Rev. D **74**, 123504 (2006), hep-ph/0611152.

[86] S. H. S. Alexander, M. E. Peskin and M. M. Sheikh-Jabbari, *Leptogenesis from gravity waves in models of inflation*, Phys. Rev. Lett. **96**, 081301 (2006), hep-th/0403069.

[87] A. Maleknejad, *Gravitational leptogenesis in axion inflation with $SU(2)$ gauge field*, JCAP **1612**, 027 (2016), 1604.06520 [hep-ph].

[88] M. M. Anber and E. Sabancilar, *Hypermagnetic Fields and Baryon Asymmetry from Pseudoscalar Inflation*, Phys. Rev. D **92**, 101501 (2015), 1507.00744 [hep-th].

[89] T. Fujita and K. Kamada, *Large-scale magnetic fields can explain the baryon asymmetry of the Universe*, Phys. Rev. D **93**, 083520 (2016), 1602.02109 [hep-ph].

[90] K. Kamada and A. J. Long, *Baryogenesis from decaying magnetic helicity*, Phys. Rev. D **94**, 063501 (2016), 1606.08891 [astro-ph.CO].

[91] K. Kamada and A. J. Long, *Evolution of the Baryon Asymmetry through the Electroweak Crossover in the Presence of a Helical Magnetic Field*, Phys. Rev. D **94**, 123509 (2016), 1610.03074 [hep-ph].

[92] Y. Cado and E. Sabancilar, *Asymmetric Dark Matter and Baryogenesis from Pseudoscalar Inflation*, 1611.02293 [hep-ph].

[93] V. B. Semikoz, A. Y. Smirnov and D. D. Sokoloff, *Generation of hypermagnetic helicity and leptogenesis in the early Universe*, Phys. Rev. D **93**, 103003 (2016), 1604.02273 [hep-ph].

[94] S. Rostam Zadeh and S. S. Gousheh, *Effects of the $U_Y(1)$ Chern-Simons term and its baryonic contribution on matter asymmetries and hypermagnetic fields*, Phys. Rev. D **95**, 056001 (2017), 1607.00650 [hep-ph].

[95] A. Brandenburg and K. Subramanian, *Astrophysical magnetic fields and nonlinear dynamo theory*, Phys. Rept. **417**, 1 (2005), astro-ph/0405052.

[96] U. Frisch, A. Pouquet, J. Leorat and A. Mazure, *Possibility of an inverse cascade of magnetic helicity in magnetohydrodynamic turbulence*, J. Fluid Mech. **68**, 769 (1975).

[97] A. Pouquet, U. Frisch and J. Leorat, *Strong MHD helical turbulence and the nonlinear dynamo effect*, J. Fluid Mech. **77**, 321 (1976).

[98] T. Kahniashvili, A. G. Tevzadze, A. Brandenburg and A. Neronov, *Evolution of Primordial Magnetic Fields from Phase Transitions*, Phys. Rev. D **87**, 083007 (2013), 1212.0596 [astro-ph.CO].

[99] A. Vilenkin, *Equilibrium Parity Violating Current In A Magnetic Field*, Phys. Rev. D **22**, 3080 (1980).

[100] R. Banerjee and K. Jedamzik, *The Evolution of cosmic magnetic fields: From the very early universe, to recombination, to the present*, Phys. Rev. D **70**, 123003 (2004), astro-ph/0410032.

[101] P. Adshead and M. Wyman, *Chromo-Natural Inflation: Natural inflation on a steep potential with classical non-Abelian gauge fields*, Phys. Rev. Lett. **108**, 261302 (2012), 1202.2366 [hep-th].

[102] E. Dimastrogiovanni, M. Fasiello and A. J. Tolley, *Low-Energy Effective Field Theory for Chromo-Natural Inflation*, JCAP **1302**, 046 (2013), 1211.1396 [hep-th].

[103] E. Dimastrogiovanni and M. Peloso, *Stability analysis of chromo-natural inflation and possible evasion of Lyth's bound*, Phys. Rev. D **87**, 103501 (2013), 1212.5184 [astro-ph.CO].

[104] P. Adshead, E. Martinec and M. Wyman, *Perturbations in Chromo-Natural Inflation*, JHEP **1309**, 087 (2013), 1305.2930 [hep-th].

[105] E. Dimastrogiovanni, M. Fasiello and T. Fujita, *Primordial Gravitational Waves from Axion-Gauge Fields Dynamics*, JCAP **1701**, 019 (2017), 1608.04216 [astro-ph.CO].

[106] P. Adshead, J. T. Giblin, T. R. Scully and E. I. Sfakianakis, *Magnetogenesis from axion inflation*, JCAP **1610**, 039 (2016), 1606.08474 [astro-ph.CO].

[107] P. Adshead, J. T. Giblin, T. R. Scully and E. I. Sfakianakis, *Gauge-preheating and the end of axion inflation*, JCAP **1512**, 034 (2015), 1502.06506 [astro-ph.CO].

[108] T. Fujita, R. Namba, Y. Tada, N. Takeda and H. Tashiro, *Consistent generation of magnetic fields in axion inflation models*, JCAP **1505**, 054 (2015), 1503.05802 [astro-ph.CO].

[109] P. Fileviez Perez and H. H. Patel, *The Electroweak Vacuum Angle*, Phys. Lett. B **732**, 241 (2014), 1402.6340 [hep-ph].

[110] R. Z. Ferreira, J. Ganc, J. Noreña and M. S. Sloth, *On the validity of the perturbative description of axions during inflation*, JCAP **1604**, 039 (2016), Erratum:[JCAP **1610**, E01 (2016)], 1512.06116 [astro-ph.CO].

[111] M. Peloso, L. Sorbo and C. Unal, *Rolling axions during inflation: perturbativity and signatures*, JCAP **1609**, no. 09, 001 (2016), 1606.00459 [ASTRO-PH.CO].

[112] R. Z. Ferreira and A. Notari, *Thermalized Axion Inflation*, 1706.00373 [ASTRO-PH.CO].

[113] M. Abramowitz and I. Stegun, *Handbook of Mathematical Functions with Formulas, Graphs, and Mathematical Tables*, Dover, New York (1972).

[114] M. Gedalin, *Linear waves in relativistic anisotropic magnetohydrodynamics*, Phys. Rev. E **47**, 4354 (1993).

[115] G. Baym and H. Heiselberg, *The Electrical conductivity in the early universe*, Phys. Rev. D **56**, 5254 (1997), ASTRO-PH/9704214.

[116] P. B. Arnold, G. D. Moore and L. G. Yaffe, *Transport coefficients in high temperature gauge theories. 1. Leading log results*, JHEP **0011**, 001 (2000), HEP-PH/0010177.

[117] M. D'Onofrio, K. Rummukainen and A. Tranberg, *Sphaleron Rate in the Minimal Standard Model*, Phys. Rev. Lett. **113**, 141602 (2014), 1404.3565 [HEP-PH].

[118] M. D'Onofrio and K. Rummukainen, *Standard model cross-over on the lattice*, Phys. Rev. D **93**, 025003 (2016), 1508.07161 [HEP-PH].

[119] K. Kajantie, M. Laine, K. Rummukainen and M. E. Shaposhnikov, *A Nonperturbative analysis of the finite T phase transition in SU(2) × U(1) electroweak theory*, Nucl. Phys. B **493**, 413 (1997), HEP-LAT/9612006.

[120] W. Buchmuller, V. Domcke, K. Kamada and K. Schmitz, *The Gravitational Wave Spectrum from Cosmological B−L Breaking*, JCAP **1310**, 003 (2013), 1305.3392 [HEP-PH].

[121] W. Tangarife, K. Tobioka, L. Ubaldi and T. Volansky, *Dynamics of Relaxed Inflation*, 1706.03072 [HEP-PH].

[122] A. Nishizawa *et al.*, *Laser-interferometric Detectors for Gravitational Wave Background at 100 MHz: Detector Design and Sensitivity*, Phys. Rev. D **77**, 022002 (2008), 0710.1944 [GR-QC].

[123] T. Akutsu *et al.*, *Search for a stochastic background of 100-MHz gravitational waves with laser interferometers*, Phys. Rev. Lett. **101**, 101101 (2008), 0803.4094 [GR-QC].

[124] A. S. Chou *et al.* [Holometer Collaboration], *MHz Gravitational Wave Constraints with Decameter Michelson Interferometers*, Phys. Rev. D **95**, 063002 (2017), 1611.05560 [ASTRO-PH.IM].

[125] A. M. Cruise, *The potential for very high-frequency gravitational wave detection*, Class. Quant. Grav. **29**, 095003 (2012).

[126] A. Arvanitaki and A. A. Geraci, *Detecting high-frequency gravitational waves with optically-levitated sensors*, Phys. Rev. Lett. **110**, 071105 (2013), 1207.5320 [GR-QC].

Erklärung:

Ich versichere, dass ich diese Arbeit selbstständig verfasst habe und keine anderen als die angegebenen Quellen und Hilfsmittel benutzt habe.

Heidelberg, den 15. August 2017   . . . .